Sander Bierens
4439465

Design of a prilling device with controlled breakup of a particulate suspension jet into droplets

TU Delft

Design of a prilling device with controlled breakup of a particulate suspension jet into droplets

By

A.J. Bierens
4439465

in partial fulfilment of the requirements for the degree of

Master of Science
in Mechanical Engineering

at the Delft University of Technology,
to be defended publicly on Thursday October 6, 2022 at 10:30 AM.

Supervisor:	Ir. Y.E. Kamis	TU Delft
Thesis committee:	Dr. Ir. W-P Breugem,	TU Delft
	Dr. H.B. Eral,	TU Delft
	Ir. T. Nieboer	Kreber BV

This thesis is confidential and cannot be made public until December 31, 2023.

An electronic version of this thesis is available at http://repository.tudelft.nl/.

Abstract

Prilling is the industrial process in which thin jets of a molten substance break up into drops and the subsequent solidification of the droplets into solids due to cooling when they fall down in the prilling tower. Prilling is widely used for efficient production of a variety of materials such as, e.g., fertilizer grains, laundry detergent, and substances for drugs and foods.

While in most prilling applications the jet can be considered as a pure liquid, in some cases the molten substance may contain suspended particles. The present study is motivated by prilling of fertilizers composed of Urea or Ammonium Nitrate (AN) containing polyhalite particles. To date, the effects of suspended particles on jet breakup, drop formation and crystallization are not well-understood. In the first part of this report a literature review is given on prilling and the current understanding of the effect of suspended particles on this. It has been found in literature that a large concentration of suspended particles will increase the viscosity of the suspension but also promote breakup of the jet. Besides, the size of the particles also influences the viscosity and jet breakup, resulting in a decrease in the amount of smaller formed secondary droplets at larger suspended particle sizes, hence increasing monodispersity.

The objectives of this MSc research project are to assess under what conditions high-quality fertilizer grains can be optimally prilled from polyhalite suspensions in molten urea or ammonium nitrate. An experimental setup was designed to assess how molten liquid jets of Urea or AN with suspended polyhalite particles can be optimally prilled for producing high-quality fertilizer grains. This design consists of melting and mixing the batch of materials, from where it will pump the particulate suspension through a vertical tube with a screw pump to a nozzle. Here, a jet will be formed. This will breakup into droplets, which will fall in an oil batch to increase cooling and hence fasten the solidification process. Unfortunately, the current design was always dripping and not able to form a jet due clogging and the formation of hard lumps, which decreased the flow rate. The droplets were however collected and analyzed.

It was found in this thesis that a larger concentration of P4 particles in urea will increase the viscosity. When the particles are grinded more, the viscosity increased as well, however a direct relationship between particle size and viscosity has yet to be determined. The particles were also unequally distributed over the prills, because P4 tends to stick together. To obtain the best quality prills, it is recommended to use relatively large P4 particles in combination with larger nozzles of >1mm to decrease the desired prilling force and prevent clogging. Also melting the suspension beforehand with intensely mixing the suspension will increase the prilling performance.

List of Symbols

Symbol	Description	Unit
A	Projection area	m^2
c_p	Specific heat capacity	J kg^{-1} K^{-1}
f	Frequency	s^{-1}
g	Gravitational acceleration	m s^{-2}
d_p	Diameter of a particle	m
D_e	Diameter of smallest circumscribed circle	m
D_i	Diameter of largest inscribed circle	m
g	Gravitational acceleration	m s^{-2}
h_c	Heat transfer coefficient	W/m^2 K
k	Thermal conductivity	W m^{-1} K^{-1}
k_b	Boltzmann constant	m^2 kg s^{-2} K^{-1}
K	Relative consistency index	mPa s^n
l_{int}	Characteristic lengthscale	m
l_{min}	Smallest particle projection length	m
l_{max}	Largest particle projection length	m
L	Characteristic length (jet radius)	m
$\dot{m}$	Mass flow rate	kg s^{-1}
$\dot{Q}$	Heatflow	W
Q	Volumetric flow rate	m^3 s^{-1}
R	Radius	m
t	Time	s
T	Temperature	K
s_0	Radial position of the orifice on the rotating bucket	m
U	Velocity	m s^{-1}
v_0	Initial velocity	m s^{-1}
v_{nozzle}	Velocity of the jet	m s^{-1}
x	Reduced wavenumber	-

Greek symbol	Description	Unit
α	Thermal diffusivity	m^2 s^{-1}
γ	Surface tension	N m^{-1}
$\dot{\gamma}$	Shear rate	1 s^{-1}
θ_c	Dimensionless center temperature	-
λ	Wavelength	m
μ	Dynamic viscosity	kg m^{-1} s^{-1}
ρ	Density	kg m^{-3}
τ	Shear stress	Pa
τ_{adv}	Advection timescale	s
τ_{IC}	Capillary-inertial timescale	s
τ_{int}	Intrinsic timescale	s
τ_{vd}	Viscous diffusion timescale	s
ϕ_m	Maximum packing fraction	-
Ω	Angular velocity	rad s^{-1}

Content

1 Introduction

In 2008, the food prices increased radically, which even raised the question at the UN how to feed the world in the future [1]. It is predicted that in 2050, there will be 9.3 billion people on this planet, which will lead to an estimated increase of 70-100% in the production of crops worldwide [2]. Two options are available: search for more land to grow more crops, or increase the yield per already cultivated land. Increasing the amount of cultivated land is not desirable, because this can lead to a decrease in the amount of precious forest [3]. Therefore, in order to save forest and also increase the production of food to feed the world, fertilizers will become quite important [4].

For a long time, people were finding ways in order to increase the yield of their field. In the Middle Ages, people tried using a three-field system in order to grow their crops. Two field will contain different crops, which will require different nutrients. The third field was left alone, in order to recover from the previously seeded crops [5]. What they didn't know was that this was caused by the depletion of different nutrients, caused by the crops.

Crops require different nutrients. The most important nutrients are nitrogen, phosphorus and potassium. However, also calcium, magnesium and sulfur are needed for a plant to grow [6]. Nitrogen is one of the key elements in plant growth: all plants require this nutrient for their cells, proteins and hormones. Phosphorus will help transfer energy from the sun to the plants, stimulating plant growth. Potassium helps the defense mechanism of the plant, increasing disease resistance and can improve the fruit quality [6]. Not every soil does contain enough of these elements. Therefore, fertilizers can help plants to fulfil their need for different nutrients.

Farmers can use different kind of fertilizers and combine them in order to optimize the soil for their crops. As mentioned before, the soil would require a lot of elements in order to be good for plants. Therefore, it would become very interesting if different fertilizers can be mixed, to contain all the nutrients and minerals a plant needs to grow.

Currently, fertilizers are commonly made by means of prilling. During this process, a molten liquid containing for example urea, is pumped up into a large tower. At the top of the tower, this liquid is pumped through nozzles or a perforated rotating bucket containing small holes. This will result in the formation of liquid jets which will fall downwards. During the fall, the jets will breakup into small droplets which will cool down and therefore solidify. The solidified droplets are collected and can be used as fertilizer.

Next to prilling, also other techniques are used to produce fertilizers. About 50 years ago, granulation was introduced to make bigger fertilizers with a higher strength, but at the cost of a lower purity and a much more complex design, increasing costs. Therefore, prilling is still a very suitable technique when cheaper and a pure product is needed [7]. This process also allows for more control in the size of the fertilizer grains.

In this thesis, a combination of different elements in one fertilizer will be investigated by means of prilling. The focus will be most on the use of ammonium nitrate or urea in combination with solid particles of polyhalite. Polyhalite is a hydrated sulphate mineral, consisting of K, Ca and Mg [8], mined under the North Sea at low energy costs [9]. The mineral can be mixed with urea or ammonium nitrate to form a fertilizer containing all major nutrients a plant needs to grow [10]. This however poses new challenges to the prilling process for the production of such multinutrient fertilizer pellets.

The goals of this MSc research project are: (1) to assess how urea and ammonium nitrate suspensions containing polyhalite particles can be optimally prilled for producing high-quality fertilizer grains, and (2) to design and test an experimental setup for this.

This report is organized as follows. First a literature review is given in section 2 and 3. Next to that, the design process and experimental results will be presented in section 4 and 5, followed by a discussion and conclusion in section 6.

2 Theory

2.1 Prilling

One of the most common ways to produce a fertilizer is by prilling. Prilling is a technique invented by William Watts in 1782, in order to produce lead shot for shotguns [11]. Here, Watts took a pan, drilled some holes in the bottom of the pan, melted some lead and fed it through the holes when standing on the church's tower. The molten lead would fall down from the tower and would form spherical balls of lead. When reaching the ground, the lead would be completely solidified, thus forming spherical balls, as can be seen in Figure 1.

This process is still used for a number of different applications in order to produce spherical products. Fertilizers, for example, are made this way because this method is relatively cheap and results in a monodisperse size distribution of pure prills[7].

Figure 1: Example of some prilled chemicals. Composition is unknown. [11]

2.1.1 Working principle

Prilling is a spray crystallization process [12]: here, a liquid will be sprayed from a large tower with a maximum height of 100m and will be cooled on its way downwards. At a certain moment, the droplets are cooled below their melting point, which will induce crystallization. A big advantage of this technique is that it is possible to create a relatively monodisperse amount of spherical crystals, with relatively low costs at a high production capacity [12]. These crystals (or prills) can be used for example in the fertilizer industry.

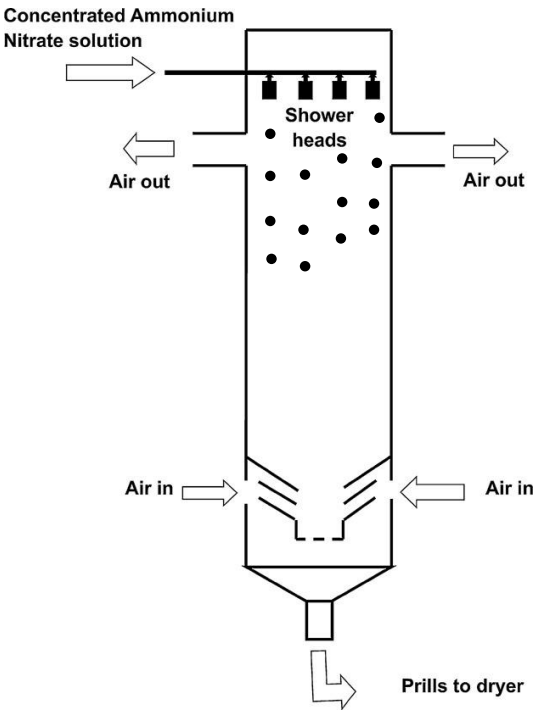

Figure 2: schematic overview of a showerhead prilling machine. [13]

First, the substance that has to be prilled (for example, ammonium nitrate) is melted, usually at a temperature which is 10-20 ^{o}C higher than the melting point [12]. The molten material is transported to the prilling bucket, where it will be sprayed into the prilling tower. Preferably, the material is to remain above the melting point during transport and jetting to prevent clogging.

When reaching the top of the prilling tower, the liquid is pumped into a nozzle or a rotating bucket, as can be seen in Figure 2. Due to pressure or centrifugal forces, depending on the equipment, the fluid is sprayed. The jet that is formed will soon breakup into droplet because of the Rayleigh-Plateau instability, where a liquid column, which is subjected to a disturbance becomes unstable because of surface tension forces, hence breaking up into droplets [14]. The viscosity, surface tension, density and jet radius of the liquid set the conditions for this Rayleigh-Plateau instability and how the droplets are formed, resulting in a relatively monodisperse distribution of droplet sizes [12],[15]. However, often a formation of a second droplet will take place, which is usually smaller. This droplet is called a satellite droplet, which is most times undesirable because it can lead to higher emissions [16] and dust explosions [12]. The formation of satellite droplets can be seen in Figure 6.

Now the droplet has formed, it will fall through the tower. During this fall, air, nitrogen or another gas is blown upwards through the tower. This result in an extra heat exchange between the droplet and the medium around it, which will cool down the droplet [17]. At a certain moment, the droplet will reach a temperature which is lower than its melting point. Now, crystallization will take place, starting at the outer shell of the droplet, moving inwards through the drop during the fall [17]. At the bottom of the tower, the crystallized droplets (prills) will be collected. It is not required that the prill is completely solidified in order to survive the fall; in fact, with new techniques, which will be discussed later, a solidification of 20-30% can be enough to survive the fall [17],[18]. The bigger the tower, the bigger the prills that can be produced, because a bigger tower will lead to more solidification of the droplets, which increases the strength and thus increase its chance of surviving the impact.

2.1.2 Jet Breakup

In order to control the process and tuning the prill dimensions, it is important to know how breakup of a jet works. Breakup of a jet is quite a complex phenomenon, depending on a lot of parameters. For example, one of the most important parameters to understand jet breakup, are liquid mass density, viscosity and surface tension [15]. Higher viscosity will prevent breakup of a jet; if this is high enough, breakup will even never take place, resulting in a very long and thin string of this viscous fluid (like honey). Surface tension on the other hand has the opposite effect on jet breakup: a high surface tension will lead to bigger jet instability, resulting in a faster breakup [15]. It has been found that breakup will require about 20% of the surface energy; half of this part will stay in the droplet, provoking oscillations, and the other half gets trapped in the jet side, which moves to the upstream direction [19]. To give insight in the different breakup mechanisms, various timescales can be introduced which have been obtained by dimension-analysis. If it is assumed that the 3 dimensions, mass (M), time (T) and length (L) of breakup can be described with density, surface tension, viscosity, characteristic length (which will be the jet radius in this analysis) and velocity of the jet, three different timescales can be obtained:

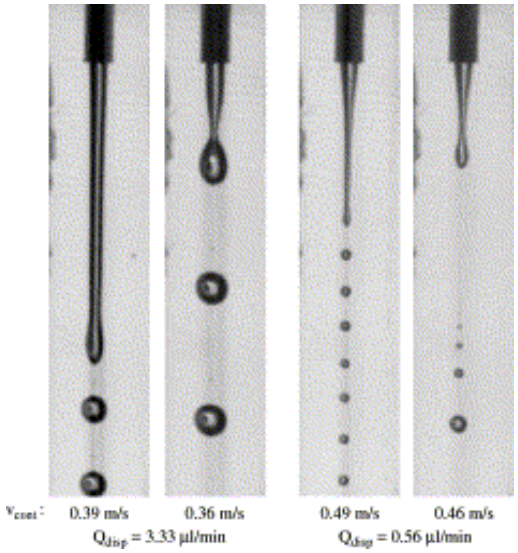

Figure 3: jet breakup at different flowrates [79].

$$\tau_{IC} = \sqrt{\frac{\rho L^3}{\gamma}} \qquad (1)$$

$$\tau_{adv} = \frac{L}{U} \qquad (2)$$

$$\tau_{vd} = \frac{L^2 \rho}{\mu} \qquad (3)$$

Here, μ is the dynamic viscosity in [Pa s], ρ the density in [kg/m^3], L the characteristic length, which is the (initial) radius of the jet in [m], U in [m/s] is the velocity of the jet and γ is the surface tension coefficient [N/m]. In equation (1), the capillary-inertial timescale or characteristic timescale of capillarity-driven motion is presented, equation (2) represents the timescale for advection and equation (3) shows the timescale for axial viscous diffusion.
When examining only the physical parameters of the fluid, an intrinsic time (equation (4)) and length scale (equation (5)) can be obtained [15]:

$$\tau_{int} = \frac{\mu^3}{\rho \gamma^2} \qquad (4)$$

$$l_{int} = \frac{\mu^2}{\rho \gamma} \qquad (5)$$

Some dimensionless numbers are important concerning jet breakup. The Ohnesorge number (Oh) will show the effect of viscosity on the dispersion relation [15]. For high Oh numbers, viscosity will dominate, resulting in a longer breakup time, or no breakup at all. This also reveals that the

dimensionless numbers such as the Ohnesorge and Weber number can be interpreted as a ratio of timescales, which has been shown in equation (6) and (7).

$$Oh = \frac{\mu}{\sqrt{\rho L \gamma}} = \sqrt{\frac{l_{int}}{L}} = \frac{\tau_{IC}}{\tau_{vd}} \quad (6)$$

According to [20], increasing the Oh number, which can be found in equation (6), at moderate We number will result in long, thin ligaments of fluid formed between the primary drops, but will shatter into many satellite droplets. Another important dimensionless number is the Weber number (We). This number measures the ratio of kinetic energy of a drop relative to its surface tension [15]. It measures how much a disturbance can grow from one swell to the next. A small Weber number can be connected to a dripping regime, while a large We number and thus high flow rate will result in a continuous jet [21], which means that jet formation can be connected to flow rate. A visualization can be found in Figure 3. A mathematical description can be found in equation (7).

$$We = \frac{\rho L U^2}{\gamma} = \left(\frac{\tau_{IC}}{\tau_{adv}}\right)^2 \quad (7)$$

If however the jet velocity is small, the flow won't turn into a jet. Instead, this flow can fall back into the dripping regime. Here, gravity plays an important role. This can be described with the Bond or Eötvös number [15] in equation (8)

$$E_O = Bo = \frac{\rho g L^2}{\gamma} \quad (8)$$

In this equation, g is the gravitational constant in [m/s^2]. It is not expected that this number becomes important in this thesis, because a dripping regime leads to a very monodisperse distribution of prills, but the production rate when dripping is too small compared to the breaking up of jets to be interesting for industry [22]. To obtain high monodispersity in droplet size at maximum flowrate, it is recommended to operate in the Rayleigh jet breakup regime [13]. At a certain moment, waves will be formed in the jet, resulting in areas with a larger and smaller diameter of the jet. In this aforementioned Rayleigh regime, the Laplace pressure in the wave trough of the jet is larger than the Laplace pressure in the wave crest, which will happen at a wavelength of more than 2π-times the undisturbed radius of the jet [15]. This will result in a breakup of the jet into droplets.

The breakup of a jet is governed by the Rayleigh-Plateau instability where the perturbations are expressed as normal modes, with a perturbation amplitude and frequency [15]. Those are the dimensionless perturbation amplitude "A" and the reduced wavenumber, "x".
These parameters can be obtained with equation (9) and (10):

$$v_{nozzle} = v_0 + A\left(\frac{\gamma}{\rho L}\right)^{1/2} sin(2\pi f t) \quad (9)$$

$$x = 2\pi L / \lambda \quad (10)$$

V is the velocity of the jet, L the unperturbed radius, f the driving frequency and t the time in seconds. At a resonance (Rayleigh) wavenumber x_R, perturbations grow fastest with shortest breakup length. If "x" becomes bigger than 1, breakup becomes much more irregular[15].

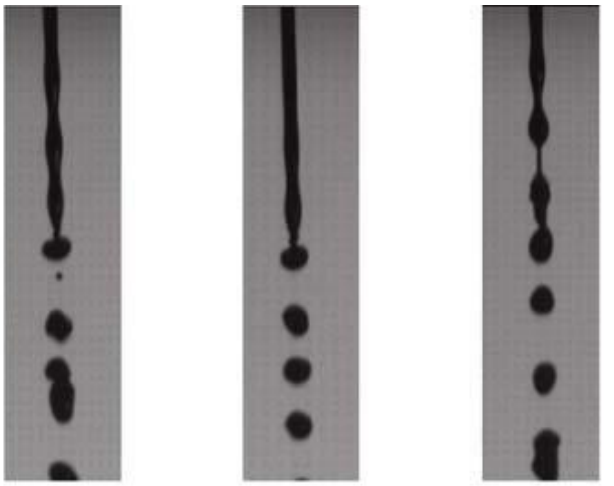

Figure 4: formation of jet breakup under different disturbance frequencies [80].

The jet is stable to the perturbations whose wavelength is smaller than the jet circumference [15]. The perturbations however will grow and at a certain moment, this will result in a breakup of a droplet from the jet. Instability can be induced by vibrations [23], applying an electric field or an extra outer fluid-flow around the jet [15]. Next to this, applying vibrations to the system will also help prevent blockage of the orifices due to the presence of impurities [13]. An example of the relation between applied vibrations versus breakup can be found in Figure 4.
Jet breakup, as mentioned above, can be controlled by imposing the droplets to different frequencies. Small frequencies will result in a jet decay that is characterized with the formation of a main droplet combined with a satellite droplet, which have almost identical dimensions. When increasing the frequency, there will be much more breakup of the jet. Now, the thin filament which connects the satellite droplet to its main counterpart will break down, resulting in the formation of small secondary satellites. This effect also decreases the diameters of the main droplets [23].

Next to the dimensionless numbers mentioned above, other dimensionless numbers are also important in explaining jet breakup, sometimes more specific for a rotating bucket in a prilling tower. In a study of *Decent* [24], the effect of the Froude number (Fr), Rossby number (Rb) and the Weber number have been studied. The Froude and Rossby number explains how respectively gravity and rotation affect the fluid motion. They are described in equation (11) and (12):

$$Fr = \frac{U}{\sqrt{s_0 g}} = \sqrt{\frac{We}{Bo}} \qquad (11)$$

$$Rb = \frac{U}{\Omega s_0} \qquad (12)$$

Take in mind that according to *S.P Decent* [24], s_0 is the same in both equations and equal to the location of the orifice at the radial position on the bucket. The Rossby number is quite similar to the Froude number where only gravitational acceleration (g) is replaced with the radial acceleration ($\Omega^2 L$). According to a study [24], perturbations (and therefore instability) will grow by increasing the Froude number (with fixed Rb and We). Increasing Rb will sometimes lead to a bigger growth rate of perturbations. However, increasing We will lead to a decrease in growth rate, but also results in the formation of more satellite droplets [20]. Both the numbers will give a comparison between the body forces and inertia, which will indicate if the perturbations will grow over time.

2.1.3 Non-Newtonian fluids

During this thesis, a suspension (which exhibits non-Newtonian behavior) will be used during prilling. Most low-molecular weight substances will show Newtonian flow characteristics [25]. Newtonian fluids have a shear stress which is proportional to the shear rate. This is described by Newton's law of viscous friction, as can be seen in equation (13) [26].

$$\tau = \mu \frac{\mathrm{du}}{\mathrm{dy}} \qquad (13)$$

Here, τ is the shear stress, μ is the viscosity and du/dy is the shear rate. Due to the constant viscosity, shear stress in Newtonian fluids is linear proportional to the shear rate.

The way non-Newtonian fluids react on stress or shear rate can be different: some fluids will show shear thinning, which means the viscosity will decrease at high shear rates:

$$\mu = K \left(\frac{\mathrm{du}}{\mathrm{dy}}\right)^{n-1} \qquad (14)$$

Here, K is the consistency index. This results in $n < 1$ in equation (14) [26] for shear-thinning fluids. Other fluids will show shear thickening ($n > 1$), which will lead to an increase of viscosity when increasing the shear rate [27]. There is also a final group of non-Newtonian fluids which will show visco-plastic behavior, sometimes in combination with shear-thinning [25]. The shear thickening and thinning behavior will reach a plateau at low shear rates, where viscosity will be independent of shear rate. This is however not seen in suspensions, which also exhibits non-Newtonian behavior. According to *van der Borght* [28], the suspensions of polyhalite with ammonium nitrate or urea will show the same dependence of shear rate on viscosity, in a shear thinning manner. In her results, it seems like both suspensions will stabilize at a certain shear rate of almost 10^3 s^{-1} and at a viscosity of 10^2 mPa· s for ammonium nitrate, which can be found in Figure 5. This seems strange as suspensions usually don't reach a plateau according to *Deshpande* [25]. It can be interesting to investigate the behavior of this suspension above a shear rate of 10^3 s^{-1}, to analyze if it is actually reaching a plateau or if it is just due to some fluctuations in the measurements.

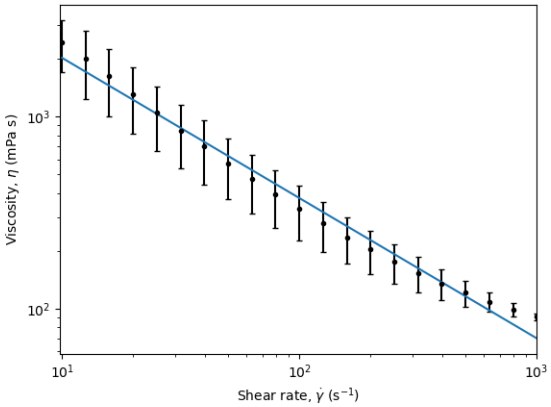

Figure 5: shear thinning behavior of polyhalite in ammonium nitrate at a temperature of 185 °C. At a shear rate of 600 s^{-1}, it seems like the suspension is reaching a plateau [28] *and doesn't follow the fit anymore.*

Sometimes, the shape of particles in suspensions can also lead to different behavior. There is evidence that some (shear thinning) suspensions of rigid rods thicken under extension. However, some suspensions with spherical particles show not only shear thinning but also extensional thinning [15]. Shear thinning suspensions will result in localized breakup, reducing the chance of producing satellite droplets.

2.1.4 Jet breakup of suspensions

In this study, we focus on using a particulate suspension. This introduces other ways a jet can breakup. Particles in a suspension will increase its effective viscosity [29], meaning that this will delay jet breakup. However, during experiments, scientists found that the jet breakup length has been shorten considerably with a suspension compared to a pure fluid [29], [30]. The more particles are added to the suspension, the higher the viscosity, but the lower the jet length (see Figure 6). Furthermore, larger particles accelerate breakup as well [29]. According to a previous study [31], particles will rearrange during thinning because they are getting pushed out of the thinning structure, resulting in less dense areas or even areas in the thin filament which is particle-free. This can be seen in Figure 7. Thinning will become localized and at a certain moment only small parts of the thread will continue to thin [30],[15]. It was shown that particles in the suspension can promote the growth of several secondary necks during the formation of the jet. This also results in a local difference in viscosity, accelerating thinning. *McIlroy* suggests that an increasing size of the particles or volume fraction tends to have a stabilizing effect, hence decreasing the number of satellite droplets that are formed [31],[15]. During experiments of *van Deen* [30], there was sometimes a bubble trapped in the thread of their experiments. This leads to exactly the same thinning dynamics as with a particle [30], which could suggest research on the droplet-breakup of other multiphase systems could also apply on suspensions. In order to analyze if this statement is correct, other literature has been evaluated as well. For instance, according to Dubey [32], the viscosity of an emulsion will increase when the droplet size of the dispersed phase will decrease. This is also the case with suspensions, according to [33]. Here, the scientists found a relationship between particle size of a suspension and its viscosity: the viscosity decreases with increasing particle size, which is the same for emulsions. This statement is only valid for suspensions with a low liquid viscosity, where a small effect has been measured of the particle sizes on the suspension viscosity. On very viscous liquids, the effect of particle size is rather small [34]. Next to the relationships mentioned above, the surface tension of emulsions was significantly higher compared to their continuous phases [32]. If there is much clogging in the equipment due to the particles present in the suspension, prilling an emulsion containing the same nutritious elements and same droplet dimensions could be considered to prevent clogging without changing the design much.

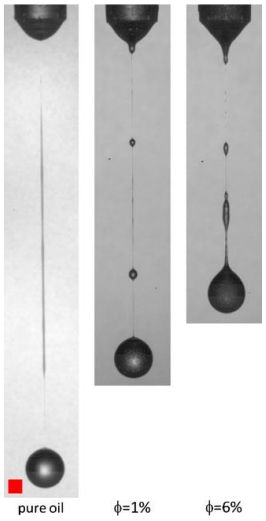

Figure 6: : jet breakup of a suspension, containing different fractions of particles [27]*. The small secondary droplets are satellite droplets*

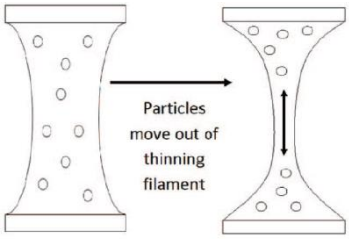

Figure 7: thinning of a particulate bridge [28].

2.1.5 Crystallization

Just after the pinch-off, the droplet will fall due to gravity. It will face an upward stream of a cold medium (for example, nitrogen). The droplet will be cooled, which will result in a temperature lower than the melting point, hence initiating solidification. When this point has been reached, the outer layer of the droplet will crystallize first. During the fall, the crystallization process will move from the outer layer to the inside [12]. Because a liquid will have a different density than a solid structure, stresses will build up during solidification. Eventually, a small cavity will be formed in the prills, because of the excess stress, which can be seen in Figure 8. Prills can be bigger than expected because ammonium nitrate will decompose into (gaseous) ammonia at temperatures of around 180 °C [35]. This will slightly inflate the size of particles due to ammonia bubbles which are formed and trapped inside the prill [13],[16].

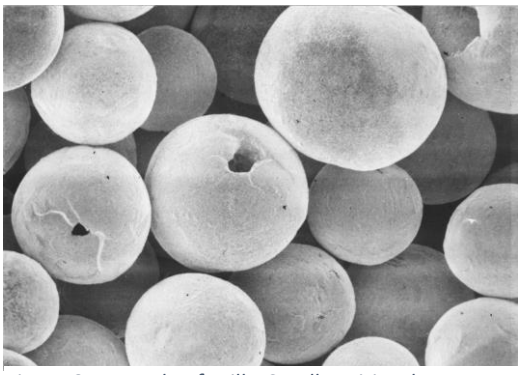

Figure 8: example of prills. Small cavities due to excess stresses can be found [9].

In order to determine prill quality and dimensions, a method is required to analyze particle shape and dimensions. *Bagheri* made such a method to calculate the size and shape of particles [36]. In this method, shape can be described by analyzing the volume, surface area and sphericity of a particle. The PA (Projection Area) protocol analyzes two specific projections with maximum and minimum amount of areas on the particle. The size can be described by analyzing the smallest length on the minimum area projection and analyzing the smallest and biggest dimension in the maximum area projection. This method is illustrated in Figure 9. There are more protocols that can calculate these parameters, such as the Standard (STD) and Minimum Bounding Box (MBB) protocol. The PA method however is much easier to use, leading to lower operator errors and is the best compromise between analysis time and accuracy.

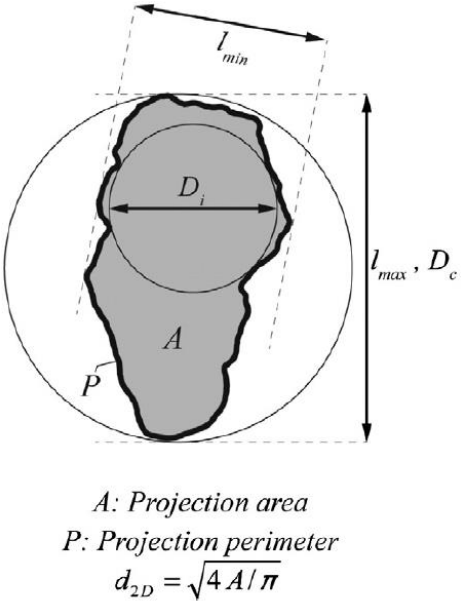

Figure 9: the PA method, which shows the maximum projection area. l_{min} is the smallest length, l_{max} the largest [33].

There is however another method to determine the shape of the particles, such as the Cox roundness. According to [28], the Cox roundness takes into account much more parameters compared to Riley, has a better correlation with roundness and leads to a smaller shape distribution in specific P4 particles. Therefore, this method will be used in this thesis. The Cox roundness can be determined with equation (15) [37]**:**

$$\phi_{Cox} = \frac{4\pi A}{P^2} \qquad (15)$$

Here, A is the projection area and P is the perimeter of the particle. The closer the Cox roundness is to 1, the rounder the object is.

2.1.6 Equipment

There are different design choices for prilling equipment. All designs require a high tower, which can be up to 100m high [12]. In a prilling tower, crystallization can happen in a cocurrent or countercurrent air flow in the tower [11]. Cocurrent flow will result in a quick solidification process because the droplets are in contact with colder air. Countercurrent flow however will lead to a higher air temperature that reaches the droplets but also will increase the residence time due to the upward flow, which will decrease the acceleration of the droplets [12]. At the bottom, prills will be collected and transported with a vibratory or belt conveyer. The machine that makes the droplets exists also in different shapes. Two different designs are most used: prilling where the jet is formed out of a nozzle (showerhead), or a rotating perforated bucket. The showerhead, or pressure nozzles will form droplets if the velocity is small enough, or jets if there is more pressure, which will eventually breakup into droplets. The jet length increases when the velocity is increased, up to a certain critical velocity. Usually, droplets produced from this device have a diameter of approximately 2 times the nozzle diameter, with a large, monodispersed size distribution at viscosities of 10^{-3} – 10^{-1} $N{\cdot}s{\cdot}m^{-2}$. The other method, with perforated buckets will lead to a larger product output. An example of a prilling bucket can be seen in Figure 11. However, van den Berg and Hallie [12] reported that the diameter of these droplets is much smaller than the droplets produced from a stationary nozzle. The diameter doesn't depend much on the rotational speed of the bucket, unlike the capacity, which will increase by increasing the rotational speed. For a prilling bucket, one can assume a droplet-diameter of approximately 1.5 – 2 times the orifice diameter at the same viscosities previously mentioned for a stationary nozzle. The performance of a bucket can be improved by placing pressure blades with holes inside the rotating bucket. Normally, all fluid will be pressed to the walls, which will decrease outlet velocity of the flow.

Figure 10: Prilling buckets [8].

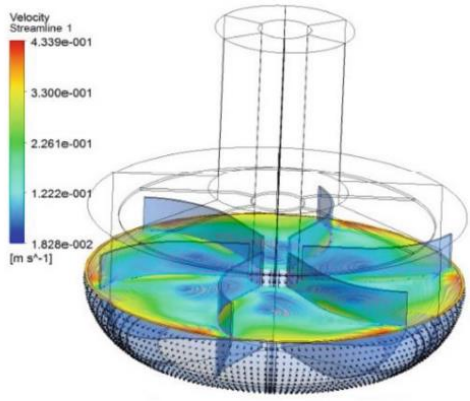

Figure 11: rotating bucket design with static forward-bent blades, which will improve the outflow velocity [31].

By placing an ideal amount of 6 forward-bent blades inside a bucket, the outflow velocity will be increased by 37%, thus increasing productivity and reducing the probability of plugging, caused by impurities [38]. In a design without pressure blades, the fluid is pressed against the wall of the bucket. If there is a hole on that location, fluid will be discharged. However, if it fails to enter the hole, it is just pressed against the wall and will move along with it without entering a hole. By placing pressure blades, the fluid will directed to another hole which allows it to leave the bucket. An example of such a design can be found Figure 11. Thus, this design makes it also possible to disperse melts containing solid additives, which will be investigated in this thesis.

During prilling, there will be some emittance of fine particles and air pollutants, due to the formation of ammonia during solidification and formation of satellite droplets during jetting and crystallization. Next to an increase in higher emissions, this also results in a loss of production capacity. In order to reduce that, there are some design choices one has to think of. It was found that, for example in a showerhead prilling tower, that the formation of a quiescent zone around the showerhead was crucial in order to minimize the formation of fine powder and disintegration of particles. Also, the air

flow inside the tower will influence emission rates. Higher air velocity will result in more collisions of the falling prills, which results in the formation of fine particles [16].

There are however also other ways to prevent emission. In another design, researchers combined a fluidized bed with a prilling tower. If a solid shell has been formed and the prill has just a solidification of 20%, the prill will survive the fall into the fluidized bed. In the fluidized bed, cooling can continue. This will lead to a decrease in the formation of fine powder, and makes it possible to reduce the height of the prilling tower with 50% [18].

2.2 Fertilizers

2.2.1 Ammonium nitrate

One of the most common used fertilizers used in agriculture is ammonium nitrate (NH_4NO_3), because of its simplicity of production and low cost [39]. One advantage of ammonium nitrate (AN) is that it can be sprayed on the soil surface without risking the loss of nitrogen to the atmosphere, which can happen with urea. [40]. However, AN has a smaller nitrogen content compared to urea (34 wt% compared to 46 wt% of urea). AN can also be mixed with other compounds, to make more complex fertilizers or explosives [41]. It is a crystalline powder varying in color from brown to almost white, and is a strong oxidizer, which is also the reason that it can be used for the production of explosives. Since AN is often contaminated by impurities, storage and handling should be taken with care as this can initiate auto-ignition and explosion due to the catalytic effects of the impurities on the decomposition of AN [42].

AN is stable at room temperature and has a melting point of 169.6 °C. At temperatures of 200 °C or higher, thermal decomposition will happen, which can result in a runaway reaction [41], [42]. Other studies however have showed that there is already some small decomposition of AN starting at 150 °C, with the formation of NO [35]. At temperatures of 180 °C or higher, HNO_3 and NH_3 will be formed. Decomposition reaction of AN is a complex process, depending on many parameters like heating rate, pressure and the presence of other materials. All decomposition reactions of AN can be found in Table 1, and its properties in Table 2.

#	Reaction	Δh_r	T_{ad} (K)	Notes
Rxn 1	$NH_4NO_3 \rightleftarrows HNO_3 + NH_3$	+179.9		150°C-500°C[a]; the reverse-direction reaction of the normal AN production reaction
Rxn 2	$NH_4NO_3 \rightarrow N_2O + 2H_2O$	−42.3	593	Main deton. reac. (Veley; Izato) 200°C-280°C (Rozman)
Rxn 3	$4NH_4NO_3 \rightarrow 3N_2 + N_2O_4 + 8H_2O$	−121.1		≥230°C
Rxn 4	$NH_4NO_3 \rightarrow N_2 + 2H_2O + ½O_2$	−123.9	1223	<200°C and >280°C (Rozman); 130°C-150°C (Manelis); main deton. reac. (Jones)
Rxn 5	$NH_4NO_3 \rightarrow NO + ½N_2 + 2H_2O$	−32.6	533	200°C-230°C (Chaturvedi); other deton. reac. (Jones)
Rxn 6	$3NH_4NO_3 \rightarrow 2N_2 + N_2O_3 + 6H_2O$	−95.0		
Rxn 7	$5NH_4NO_3 \rightarrow 2HNO_3 + 4N_2 + 9H_2O$	−129.1		130°C-150°C (Manelis)
Rxn 8	$8NH_4NO_3 \rightarrow 16H_2O + 2NO_2 + 4NO + 5N_2$	−70.0	833	≥300°C
Rxn 9	$4NH_4NO_3 \rightarrow 3N_2 + 2NO_2 + 8H_2O$	−377.1	1133	Main deton. reac. (Médard)
Rxn 10	$4NH_4NO_3 \rightarrow 2NH_3 + 3NO_2 + NO + N_2 + 5H_2O$	+82.2		
Rxn 11	$2NH_4NO_3 + C \rightarrow 2N_2 + 4H_2O + CO_2$	−320.7	2388	7% carbon (stoich.)
Rxn 12	$3NH_4NO_3 + CH_2 \rightarrow 2N_2 + 7H_2O + CO_2$			5.4% fuel oil (stoich.)
Rxn 13	$12NH_4NO_3 + C_6H_{10}O_5 \rightarrow 12N_2 + 29H_2O + 6CO_2$	−341.2		14% cellulose (stoich.)

[a]Reaction requires the presence of H_2O to occur.

Table 1: decomposition reactions of AN. During this thesis, it is expected reaction 1 is most important due to the temperature regimes of prilling AN (which will happen between 170 °C and 200 °C. [35]

Property	Value	Unit
ρ_{solid}	1720	kg m^{-3}
$c_{p,liq}$	1509	J kg^{-1} K^{-1}
μ	7	mPa s

Table 2: properties of AN [43], [44]. *Not all values could be found since much information is restricted due to the explosive property of this substance.*

2.2.2 Urea

Urea, which is the worlds most used fertilizer [45], is a white crystal containing 46% nitrogen [46], which can be seen in Figure 12. It is much safer than AN because there is no fire or explosion hazard during use. However, a disadvantage of urea is that nitrogen can be lost to the atmosphere if it remains on the soils' surface during warm weather for an extended period of time. It is recommended to incorporate this fertilizer into the soil to prevent nitrogen loss, or to blend it with water. Some properties of urea can be found in Table 3.

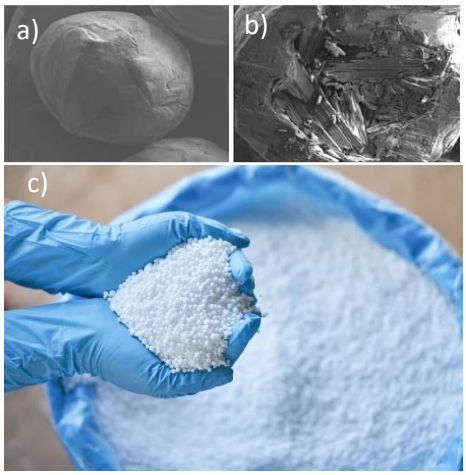

Figure 12: images of urea. a) a SEM image of a prill of pure urea, b) showing its internal structure and c) shows an example of prilled urea [81], [82].

Urea ($CO(NH_2)_2$) will melt at a temperature of 133 °C [47]. With increasing temperature, starting from its melting point, urea will start to vaporize and decompose into small amounts of ammonia and isocyanic acid (HNCO) at low temperatures. The latter will lead to the formation of biuret ($C_2H_5N_3O_2$), cyanuric acid ($C_3H_3N_3O_3$) and ammelide ($C_3H_4N_4O_2$ [47]. The decomposition of urea is classified into four temperature regions. The first region is described above, starting from 133 °C until 190 °C. From this temperature on until 250 °C, urea decomposition will be in its second temperature region, which is dedicated to biuret decomposition and some side reactions which will form cyanuric acid and ammelide. Urea will start to decompose from 152 °C [48]:

$$CO(NH_2)_2(m) + heat \rightarrow NH_4^+NCO^- \rightarrow NH_3(g) + HNCO(g) \qquad (16)$$

From 225 °C, the melt will turn in a sticky solid matrix [47]. In the third temperature region, ranging from 250 °C to 360 °C, cyanuric acid will decompose and there will be small amounts of ammelide, ammeline ($C_3H_5N_5O$) and melamine ($C_3H_6N_6$) formation. The fourth and hence last temperature region will be marked by the decomposition of ammelide, ammeline and melamine, at temperatures above 360 °C.

In hot days, urea can become a problem in prilling towers, when ambient air is used as a cooling stream. During these days, it can become hot in the prilling tower, which can lead to the formation of lamps and cakes of prills [49]. This is mainly caused by prills which aren't completely solidified on the bottom of the tower, hence influencing the product quality.

Property	Value	Unit
ρ_{solid}	1335	kg m^{-3}
ρ_{liq}	1247	kg m^{-3}
k_{sol}	1.19	W m^{-1} K^{-1}
k_{liq}	0.83	W m^{-1} K^{-1}
$c_{p,solid}$	1748	J kg^{-1} K^{-1}
$c_{p,liq}$	2250	J kg^{-1} K^{-1}
μ	3.018	mPa s

Table 3: some properties of urea [12], [50].

2.2.3 Polyhalite

Polyhalite ($K_2CA_2Mg(SO_4)_4{\cdot}2H_2O$ is a hydrated sulfate, which can be found all over the world, but is just recently mined, starting in the UK [51]. Figure 13 shows an example of mined polyhalite. The purity of this mined product is very high, containing about 95% pure polyhalite. The impurities mainly consist of NaCl.

Figure 13: image of mined polyhalite [55].

This mineral is a suitable fertilizer, providing the soil with four different nutrients. Polyhalite also releases its nutrients on a much slower rate compared to other fertilizers. It provides the soil with potassium (K), calcium (Ca), magnesium (Mg) and sulfur (S), which are very important nutrient elements [52]. Next to this, *van der Borght* [28] investigated the possibility to use this mineral in the prilling process, as an extra supply of nutrients to the soil. Because it will provide the soil with different nutrients than urea or ammonium nitrate, it can be interesting to use this nutrient as an addition, providing the soil with its most important nutrients to help crop growth [6].

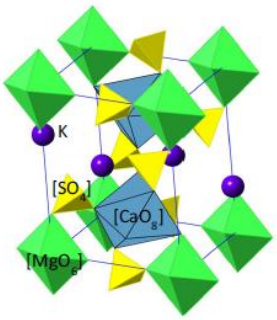

Figure 14: crystal structure of polyhalite [45].

At 233 °C, polyhalite will start to decompose into water vapor, anhydrite ($CaSO_4$) and two different langbeinite-type phases. The latter will lead to complex variations in crystallinity when increasing the temperature. It eventually will combine in a single-phase triple salt at 646 °C [52]. During this thesis, it is expected that this will not result into problems since this exceeds the temperatures that will be used in this thesis.

Polyhalite is a very small single crystal. Therefore, it was rather difficult to determine its crystal structure, only to be successful in 1970 [53]. The crystal structure can be found in Figure 14 and some of its properties in Table 4.

Property	Value	Unit
ρ	2790	kg m^{-3}
k	1.4	W m^{-1} K^{-1}
c_p	890	J kg^{-1} K^{-1}

Table 4: some properties of P4 [54], [55].

3 Summary literature study

In this literature research, different papers have been analyzed to find more information about prilling a suspension. It was found that suspensions with higher volume fraction increase viscosity, but also accelerate breakup. This breakup will occur locally, on areas where the viscosity is lower due to the rearrangement of particles. This will result in a reduction of the amount of satellite droplets that have been formed. It is interesting to see that emulsions and suspensions react the same way on breakup, thus indicating that this research can also be used for prilling emulsions. However, more research on this would be required.

It is expected that prilling a suspension can lead to problems like clogging or an uneven distribution of particles in the different prills. More insight in this effect will help finding solutions to prevent this.

Breakup is one important parameter to investigate because this effect will determine the size and its distribution of the prills. This can be tuned by applying external forces and vibrations on the system, which can promote certain breakups. To improve the quality, monodispersity and specifications of the prills, it is recommended to investigate how and in which way the prill dimensions can be tuned.

Also interesting to know is that the prills can have a bigger size than expected because of the inflation due to the formation of ammonia, which also will lead to cavities in combination with density differences of liquids and solids. A cavity in the prill will reduce its strength, therefore it can be interesting to find a way to reduce the size of the cavity. One such a way could be by initiating extra crystallization in the center of the prill, which will prevent excess stress during solidification in the center but distributes it more around the prill. It can be interesting to see if the added particles will work as seeds, and how to increase this effect in order to produce prills of a higher quality.

The liquids that will be used in this research are not the easiest ones. They will require high temperatures where decomposition will take place almost as soon as the liquids are melted. For this application, it is important to acquire a constant and even temperature of the liquid in the bucket, in particular for AN. If the temperature is a few degrees Celsius too low, solidification will happen before jetting, resulting in clogging. If the temperature is just too high, it will decompose, resulting in inflated prills and even dangerous situations in certain cases.

At last, prilling towers are very huge, which also lead to emissions of ammonia and fine powder. This can be reduced by choosing the right designs, for example by using a fluidized bed at the bottom of a smaller prilling tower or by creating a quiescent zone at the top of the tower at the prilling equipment. Smaller towers and lower emission rates will not only lead to less polution, but also increases the production rate.

4 Design process

In order to do experiments and improve the prilling process of a molten suspension, there were some requirements to make this successful. First, the prilling setup has to be a scaled-up version of the setup of *van der Borght* [28], to increase the prilling time and thus increasing the amount of measurements during prilling. This means that first a basic design has to be made which can be improved easily: the setup has to be modular. Finally, the setup has to be able to prill an urea or AN suspension containing polyhalite particles. Since the nozzle has a diameter between 0.5 and 1mm, this will result in prills with a diameter between 1 and 2mm [12]. This size was desired by *Kreber*. The two objectives for this setup to be successful are that it is able to form a jet and is able to produce prills which are suitable for further investigation.

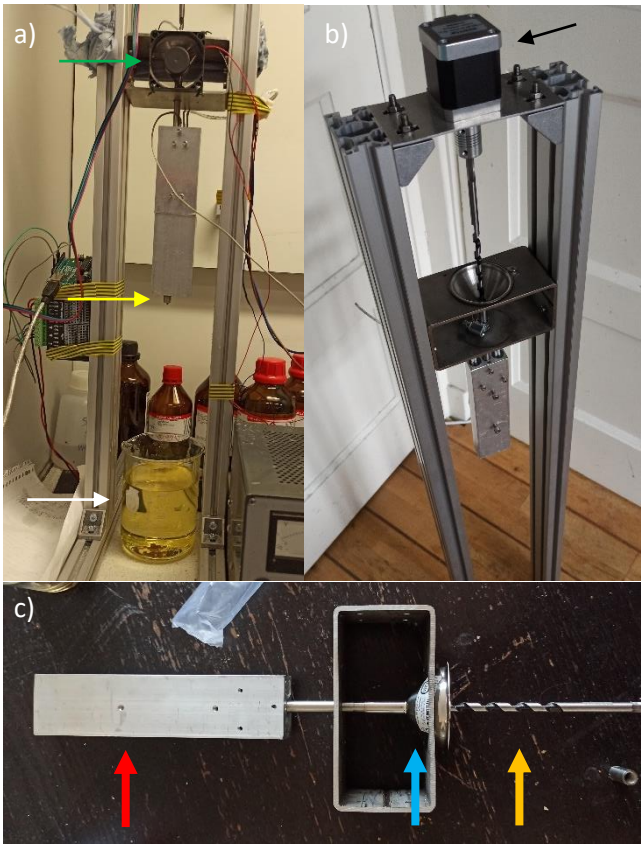

Figure 15: the continuous prilling setup. Figure a) shows the setup in action with the oil bath (white arrow), the nozzle (yellow arrow) and the ventilator (green arrow). Figure b) shows the setup before use with the stepper motor (black arrow). Figure c) shows the different important parts of the device: the red arrow shows the heater, the blue one the funnel and the orange arrow shows the screw. In

Next to this, two choices can be made: produce a batch-process setup or a (semi) continuous one. After some analyzes, the choice fell on a semi-continuous process: this process was much more simple with far less (critical) parts, and is next to that easy to scale up, which is useful if the industry wants to implements the findings. It was tried to design a piston that could mix and heat the suspension, but this turned out to be too difficult: the sealing would experience rotational and axial movements, urea fumes and would be operating between room and melting temperature of the chosen suspension. No suitable sealing could be found that was able to withstand all these regimes. Therefore, it is recommended to let the device only mix and prill the suspension or to heat and prill, since this will decrease a lot of the problems. The device that was now build needs mixing beforehand, but an iteration could make it even more simple by melting beforehand.

The first iteration of this setup is as has been mentioned before, very simple. It consists of a funnel, where the pre-mixed powder containing P4 and urea is loaded. When scaling up this design for industry, the powder can be transported continuously to the funnel. For the experiments however, it remains a batch process, since batches of the premixed suspension has to be added to the funnel. A screw is mounted above it, which will take the powder from the funnel through a stainless-steel tube. Stainless-steel has been chosen because this material can handle high temperatures and doesn't react with ammonia, urea or ammoniumnitrate. At the lower side of the tube, a heating block will be placed with 2 heaters of 400W, in order to melt the powder which is transported through the screw. The heating block consists of aluminum, because of its good heat conduction properties. The suspension won't be in contact with this block. At the bottom, the powder will reach high enough temperatures to melt and can afterwards be pumped through a nozzle with variable

diameter, resulting in different droplet sizes. With the largest flow rate, the setup can prill for at least 40 seconds when the funnel is not continuously refilled. This can be increased. The design can be seen in Figure 15 and in Appendix D: Experimental setup.

A few parameters have to be taken care of. First, urea and mostly AN will decompose at temperatures just above their melting points. So, the temperature difference between the heated wall of the tube and the center can't be too large. Next to that, it is required that all urea or AN is melted when it reaches the bottom of the tube, at a velocity which will result in a jet. According to [56], jetting will occur at a critical Weber number of 6,25. In this Weber number, the nozzle diameter has been considered instead of its radius ($We = \frac{\rho D U^2}{\gamma}$). Depending on the diameter of the nozzle, one could find the corresponding velocity, which will be around 0,47 m/s for a nozzle diameter of 1,1mm and 0,7 m/s for a nozzle diameter of 0,5mm. With this result an estimate of the velocity through the tube can be made by conservation of mass (the mass that is flowing into the system is equal to the mass flowing out of the system). The prill sizes can be determined with the following formula [12]:

$$d_p = 1.88\left(1 + 3\frac{\mu}{\sqrt{\rho\sigma d_{nozzle}}}\right)^{1/6} d_{nozzle} \qquad (17)$$

Here, d_{nozzle} is the diameter of the nozzle and d_p the droplet diameter.

Now the velocity of the fluid is known, one could estimate the required heat that is needed to heat up and melt the suspension. During the calculations, urea was considered as its c_p value and required heat of fusion is much higher than that of AN, which will lead to a bigger amount of energy required to heat and melt the suspension. The following formula was used to calculate the required heat in Watt:

$$\dot{Q} = (1 - wt\%) \cdot \dot{m} \cdot \left[c_{p,liq.ur}(T_e - T_m) + E_{melt} + c_{p,sol.ur}(T_m - T_i)\right] + wt\% \cdot \dot{m} \cdot c_{p,p4}(T_e - T_i) \qquad (18)$$

Here, *wt%* is the total mass of polyhalite particles in the suspension in % of the total mass of the suspension, $\dot{m}$ is the mass flow of the suspension in kg/s, c_p is the specific heat capacity in J/kg K of liquid urea, solid urea or polyhalite (P4), T_e the exit temperature of the suspension, T_m the melting temperature in Kelvin, E_{melt} the required latent heat of fusion in J/kg, and T_i the initial temperature of the mixture.
Take in mind that this result gives an indication of the minimum required heat to melt the mixture. There will be a maximum temperature at the wall to prevent decomposition from happening. Now a heat transfer coefficient (in W/m^2 K) can be calculated, using the following formula [57]:

$$h_c = \frac{\dot{Q}}{A(T_e - T_i)} \qquad (19)$$

Here, A is the heated area in m^2. This heat transfer coefficient can be used to calculate the Biot number:

$$Bi = \frac{h_c \cdot R}{k} \qquad (20)$$

With R the radius of the heated tube in m and k the thermal conductivity in W m^{-1} K^{-1}. The thermal conductivity can be expressed with the Maxwell's expression of conductivity [58]. The thermal conductivity of solid urea has been taken to determine this expression:

$$\frac{k_{sus}}{k_{ur}} = 1 + \frac{3\phi}{\frac{k_{p4} + 2k_{ur}}{k_{p4} - k_{ur}} - \phi} \qquad (21)$$

Here, ϕ is the volume fraction of P4 in the suspension. Take note that this expression is most suitable for composites with a low volume fraction of particles, but is used here only as an indication. The Biot number gives an indication how the temperature differs at the center compared to its surface. If this number is smaller than 0.1, the temperature at the center will not differ more than 5% compared to its surface [57]. This number can also be used to calculate the temperature at the center of the solid suspension after a certain amount of time. For this, we also need to calculate the Fourier number. The Fourier number calculates the ratio between conduction rate and energy storage rate of the substance. This number can provide how long it will take to reach a certain temperature at a given time:

$$Fo = \frac{\alpha t}{R^2} \qquad (22)$$

Here, α is the thermal diffusivity in m^2/s and t the time that has been passed in seconds. In this thesis, t can be determined by taking the length of the heater divided by the bulk velocity of the suspension, and $\alpha = \frac{k_{sus}}{\rho_{sus} c_{p,sus}}$, where $c_{p,sus} = (1 - wt)c_{p,ur} + wt\ c_{p,p4}$. To obtain the temperature at the center, a calculation has been made for how long one part of the moving suspension has been heated. This required amount of time has been used to calculate the Fourier number. Because our Fourier number is larger than 0.2, the following formulas can be used to calculate the temperature at the center of the mixture [57]:

$$\theta_c = A_l e^{-\lambda_l^2 Fo} \qquad (23)$$

$$\theta_c = \frac{T_c - T_e}{T_i - T_e} \qquad (24)$$

Here, θ_c is the dimensionless center temperature, T_c is the temperature at the center, λ_l^2 and A_l are some constants. Note that the wall temperature will be controlled and is kept at a constant temperature of 145 °C. The corresponding values of these constants can be found on *page 183* of *Mills* [57].

One of the objectives here is that the center of the suspension has to be molten. For urea, this temperature corresponds to about 133 °C. With this temperature, an estimate can be made for how long the suspension has to be heated in order to completely melt it. This will take for an urea 35wt% P4 suspension about 11 seconds. Now the height of the heating block can be determined. Take in mind that this is the temperature at the center of the suspension without assuming mixing but assuming the hole is purely filled with the powder.

Now another problem will arise: if the tube is heated, the heat will move up through the tube towards the funnel. The temperature at the funnel can't exceed 70 °C: during some tests, it was seen that the powder will start clumping together at these temperatures, resulting in big and hard clumps.

Therefore, active cooling is necessary because otherwise the temperature of the funnel will exceed 80 °C when AN is prilled (at temperatures of around 180 °C). According to *Mills* [57], forced convection by air will result in enough cooling. To calculate this, first the Reynolds number has to be obtained:

$$Re_D = \frac{\rho U D}{\mu} \qquad (25)$$

With D the outer diameter of the cooled tube. The Reynolds number of the selected ventilator is 1454. Since this is $Re_D < 10^4$, the following formula can be used to calculate the average Nusselt number (which can be found in *Mills formula 4.71a* [57]):

$$\overline{Nu_D} = 0.3 + \frac{0.62 Re_D^{1/2} Pr^{1/3}}{[1 + (0.4/Pr)^{2/3}]^{1/4}} \qquad (26)$$

Here, Pr is the Prandtl number, which is the ratio of kinematic viscosity to thermal diffusivity, which is constant for air at room temperature (Pr = 0.69). The Nusselt number is the ratio between convective and conductive heat transfer in the boundary layer of the moving gas. Now the heat transfer coefficient can be calculated:

$$hc = \frac{\overline{Nu_D}\, k_{air}}{D} \qquad (27)$$

A ventilator has been found that can cool the tube with a heat transfer coefficient of 60 W/m^{2}K (with a flow velocity of 35.7 m^3/hr), which will result in a temperature at the funnel of around 47 °C according to a simple simulation in *ANSYS Steady-State thermal* [59]. Here, radiation and convection has been taken into account with an emissivity of stainless steel of 0.3 [57]. On the bottom side, the tube has a constant temperature of 180 °C. When prilling the urea suspension, temperatures will be 148 °C maximum at the bottom. All the calculations named above can be found in Appendix F.1, and an overview of the parts can be found in Appendix E: Parts overview experimental setup.

The temperature of the heater is constantly controlled with a digital on/off PID Cooking Controller. This device is calibrated and will constantly measure the temperature of the thermocouple, which is attached to the heater. The controller will continuously switch the heater on and off, which will result in a temperature of 145 +/- 3 degrees Celsius. The rotational velocity of the screw will be controlled with an Arduino. The code for this can be found in Appendix G: Arduino script.

5 Main investigation

5.1 Polyhalite - microscopy

In order to determine the size and shape of P4, microscopy can be used in combination with the forementioned protocols in section 2.1.5 to determine its size and shape, which is expected to influence the viscosity and surface tension of the suspensions. To determine this effect, P4 is grinded by hand for different periods of time, in order to make obtain different particle sizes and shapes. The P4 is provided by Kreber, and is sieved to 50 micron according to the company. To reduce the size even more, P4 will be grinded for 1 minute, 2 minutes, 5 minutes and 10 minutes with a mortar by hand. Afterwards, the P4 will be suspended in silicon oil and will be analyzed under the microscope to see if grinding has reached its desired effect. It is expected that the longer the P4 is grinded, the smaller and rounder the particles will be. Also, it is expected that due to its smaller size, Brownian motion will take place [60], since here thermal forces will dominate the hydrodynamic forces. The Polyhalite will be submerged in silicon oil. The reason for this is to decrease the amount of clogging of the P4 particles, since it sticks together without being submerged in another fluid, and to see if Brownian motion will be present at room temperature.

For the microscopy analysis, a Nikon eclipse TI-E inverted microscope has been used with magnifications of 20x and 40x. An inverted microscope is a (visible) light microscope that has its components placed in inverted order, which means the light source will be placed above the specimen and the objective under it, which will make it possible to analyze different specimen in their original container and in bigger quantities compared to a standard microscope [61]. The microscope was already calibrated to measure the size and shape of the particles. It will provide the length scale, which is given in micron per pixel. After analyzing the samples, the pictures will be analyzed with ImageJ [62]. Here, the given length scale can be imported, and by drawing lines the diameter of the particles can be measured. To give however more accurate results, an attempt was made to let the computer automatically recognize the size and shape of all particles. However the particles were most times clustered together, probably due to van der Waals forces or static-electrical forces [63]. Since the particle sizes were also different, this resulted in different focal heights and therefore an image with sharp and blurry parts. Therefore, it was impossible to automatically recognize the particles with the computer, because the program couldn't recognize the particles in most cases. See

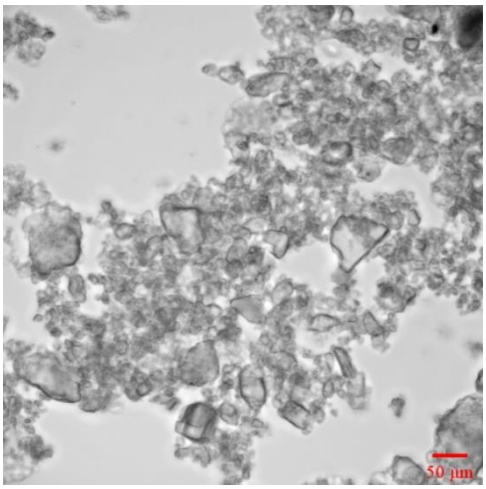

Figure 16: image of not-grinded P4, 20X magnification

Appendix C: P4 microscopy for the images that have been used to determine the P4 sizes and Appendix F.2 for the Matlab script of the calculations.

5.1.1.1 Size

As has been mentioned before, the particles have been analyzed by hand. The size was determined by measuring the diameter of the smallest circumscribed circle around the particles. Around 500-600 particles have been analyzed per batch to get an accurate representation of their dimensions. When analyzing the particles through the microscope, the clustered particles seemed to have a wider distribution in particle size compared to the single ones, which seemed most times much smaller. The samples were prepared and the not-grinded P4, 1 minute, 2 minutes, 5 minutes and 10 minutes

grinded P4 were analyzed and compared. It was found that grinding did have an effect on particle sizes. However, there was not much difference between the grinding times. The mean size of the particles remained almost the same after 1 minute grinding, even as the minimum and maximum sizes. After grinding, the mean size of the particles dropped to about half of its original size. The size of the smallest particles found dropped to around one third of the smallest particle size of the not grinded sample. The same happened to the maximum found particle size. The results of these measurements can be found in Table 5. Still, the mean size of the particles is just too high to detect Brownian motion. The smaller particles do fall in the Brownian motion regime of a maximum of 1µm [60] , but this wasn't detected during the microscopy analysis since this was performed at room temperature, which is too low.
Because the mean sizes have dropped, it is expected that the viscosity of urea with grinded P4 will be higher compared to non-grinded P4, but since the mean diameters between the different grinded samples are almost the same, it is not expected that a big difference can be found in their viscosities.

P4 grinded in minutes	Minimum P4 size [µm]	Maximum P4 size [µm]	Mean P4 size [µm]	Standard deviation [µm]
Not grinded	1.36	102.8	8.50	8.05
1 minute grinded	0.522	28.9	4.73	3.10
2 minutes grinded	0.889	35.4	5.41	4.38
5 minutes grinded	0.330	30.0	5.85	4.45
10 minutes grinded	0.495	35.6	5.85	4.43

Table 5: P4 particle sizes before and after grinding with a mortar.

5.1.1.2 *Shape*

Next to the size of the particles, the shape is also an important factor to study. To determine the shape, the Cox approximation of roundness has been used, which can be found in equation (15). For this determination, around 60 particles have been analyzed for their roundness. The results can be found in Table 6**.**

P4 grinded in minutes	Mean roundness	Standard deviation
Not grinded	0.768	0.120
1 minute grinded	0.680	0.156
2 minutes grinded	0.706	0.157
5 minutes grinded	0.686	0.132
10 minutes grinded	0.716	0.160

Table 6: roundness of the different P4 samples.

According to the data from Table 6, the roundness decreases sligthly when the particles are grinded. Also the standard deviation increases when the particles are grinded for a longer time, indicating that particles have more different shapes. Since the differences are minimal, it isn't expected that this influences the further experiments much.

5.2 Viscosity

The viscosity of a suspension depends on a lot of factors and determines the force that is needed to be able to prill. Therefore, it is important to know how the viscosity behaves in this particular suspension. The viscosity of a suspension depends on shape and size of the particles, the concentration and the temperature [64]. In this thesis, the influence of grinding and concentration of the P4 particles in the urea suspension have been analyzed. The samples that have been analyzed do contain only pure urea, urea with 10wt% P4 and urea with 35wt% P4. The suspensions also contain different P4 particles: one batch contains no grinded P4, the others are grinded for 1 minute, 2 minutes, 5 minutes and 10 minutes. The viscosity has been determined with an Anton Paar Rheometer.

It is expected that a higher concentration of P4 particles into the suspension leads to a higher viscosity. Next to that, it is expected that grinding do have a small effect on the viscosity, where longer grinding times lead to smaller particles thus increasing the apparent viscosity due to the presence of more particles at constant volume fraction, hence increasing the degree of interactions between the particles [33]. However, it is expected that this result is minimal to none because from the microscopy measurements it was found that the mean size and shape of the P4 particles didn't differ much after just grinding for 1 minute or longer.

Beforehand, batches of the different grinding times and concentrations have been prepared with a scale, which has a precision of ~0.01 grams**.** After obtaining the right concentrations, the powder is mixed by hand and with a vibrating mixing device**.** Now, the rheometer can be prepared by following the measuring procedure. First, it will calibrate the height of the parallel plate. After that, the mixture was added on the flat plate of the rheometer at room temperature, whereafter it will start heating to 140 °C. When reaching this temperature, it will wait for half a minute to guarantee the suspension has been fully melted. Now the measurements will start, measuring the viscosity at a shear rate from 9.90 to 100 s^{-1} and back. This procedure is repeated again for each sample, resulting in 4 viscosity measurements or sweeps per different shear rates.

It is important to determine the viscosity of the liquids for prilling. The liquid has to be sprayed out of a nozzle with a relatively small diameter. A larger pressure would be required: when the viscosity has been increased, it will take much more force to press the liquid out of the nozzle. In fact, it may be impossible to prill. According to [34], there is a certain critical solid fraction where the viscosity would go to infinity. This depends a bit on the size and suspended liquid, it is generally defined as one of the following two points for monodisperse hard spheres: 0.58, which corresponds to the glass transition and 0.64, which corresponds to the random close packing of the particles [65]. The glass transition is described as the point where a particle is only able to relax within a cage formed by its nearest neighbours. This limits diffusion and flow [66].

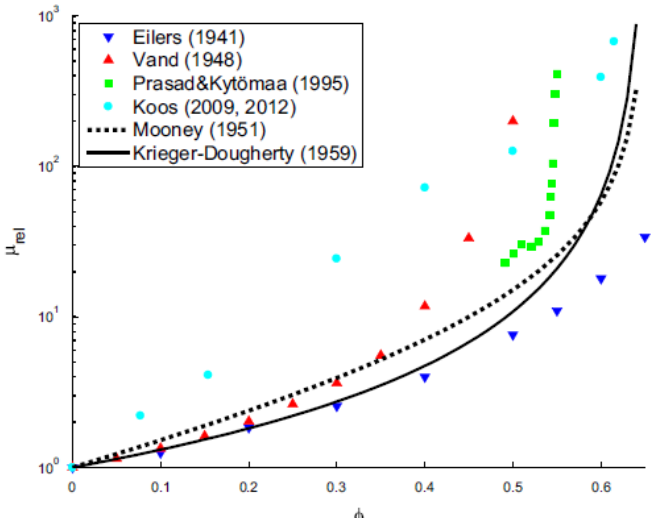

Figure 17: viscosity (vertical axis) dependence on the volume fraction (horizontal axis) of the suspended particles, compared with different models [52].

Some experimental data combined with different viscosity of suspension models from literature can be found in Figure 17**.**

Currently, our mass fraction of P4 in urea is 10% and 35%. However, this is translated to a solid volume fraction of P4 in urea of 0.19 and 0.53 respectively. The latter comes close to the predicted maximum solid fraction of suspensions, hence radically increasing viscosity of the slurry. It is therefore expected that it is impossible to increase the amount of P4 in the molten suspension much more because this will probably lead to an enormous amount of required prilling pressure. The data acquisition and processing can be found in Appendix F.3.

5.2.1 Results of the measurements

After initiating the experiments, it was observed that the viscosity dropped after each sweep, regardless of the sample. When heating up the sample, decomposition of urea already starts [47]. One of the main products that are formed here is ammonia, which is in its gas phase. The other byproducts are solid at the given temperature. Probably, ammonia gas will be trapped under the parallel plate of the rheometer. This decreases the contact area between the molten suspension and the plate, which will decrease the force required to rotate, hence decreasing the measured viscosity. It is also possible that the particles will settle over time, resulting in a thin liquid layer of urea over a bed of P4 particles. This will result in a smaller viscosity since only the effects of pure urea are measured. To verify this, a settling time scale can be obtained by using the settling velocity [67], using equation (28).

$$\tau = \frac{L_{gap}}{u_{set}} = \frac{18 L_{gap} \mu}{\left(\rho_{p4} - \rho_{ur}\right) g d_{particle}^2} \qquad (28)$$

Here, u_{set} is the settling velocity, L_{gap} the gap height and $d_{particle}$ the diameter of the suspended particles. Since the mean particle size is between 4-6 micron, this will result in a settling time of about 20 to 90 seconds. This corresponds to the used measurement window, which indicates that this is probably the main cause of the decreasing viscosity. Note that the larger particles with a diameter of about 30 microns will sink almost immediately to the bottom, while the smaller particles will have a settling time of more than an hour.

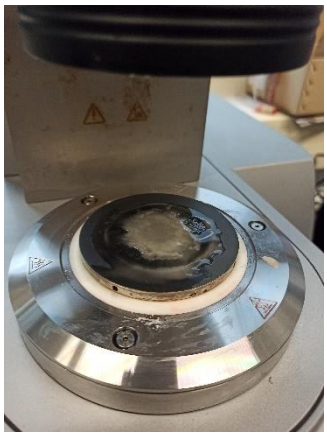

Figure 18: urea with 35wt% P4 in the rheometer

One could also think about the effect of centrifugal forces on the measured viscosity. This is however less logical since there is no evidence that the particles have moved to the edge, as can be seen in Figure 18. The white outer edge that is visible here is a remnant after cleaning and was not formed during the measurements. Next to that, this will only increase the measured viscosity: the presence of the particles will locally increase the viscosity. Since they move to the edge, this will result in a larger required torque to rotate leading to a too large measured viscosity.

Now, the plots of the effect on grinding on the viscosity will be presented here. As can be seen in Figure 19, grinding the P4 particles did have an effect on the viscosity. Note that there are only four viscosity measurements per different shear rate, which will increase the measured error. For example, the viscosity at a shear rate of 10 s^{-1} for the suspension urea with 10wt% P4 which has been grinded for 2 minutes seems quite high. However, the standard deviation of this measurement is almost 11mPa s, which means the viscosity can be even higher than the 10 minute grinded sample, but also lower than the 5 minute grinded sample. Matlab [68] was used to determine the standard

deviation by analyzing the four viscosity measurements per desired shear rate. There is a big uncertainty. For higher shear rates, the standard deviation drops to a value between 1.5 and 0.3 mPa s. Viscosity measurements at higher shear rates are therefore more reliable compared to results at lower shear rates. For this specific set of measurements, the measurements for the not grinded sample, the 5 minute and the 10 minute grinded samples are most reliable, with an average standard deviation between 0.86 mPa s and 2.9 mPa s.

For the samples that contain urea with 35wt% P4, the samples that are grinded for 1 minute, 5 and 10 minutes are on average the most reliable, with an average standard deviation of 1.4 mPa s to 1.8 mPa s. However, also here, the measurements at a shear rate of around 10 s^{-1} have a standard deviation between 3 and 12 mPa s, where the latter corresponds to the 2 minute grinded sample. Take note that the shear rates presented here are representative for the shear rates inside the heated tube (around ~20 s^{-1}) but not at the nozzle (around ~5000 s^{-1}). This shear rate was determined by calculating the shear rate in a pipe-flow for non-Newtonian fluids [69], with Q as the volume flow:

$$\dot{\gamma} = \frac{Q}{\pi r^3 \left(3 + \frac{1}{n}\right)} \qquad (29)$$

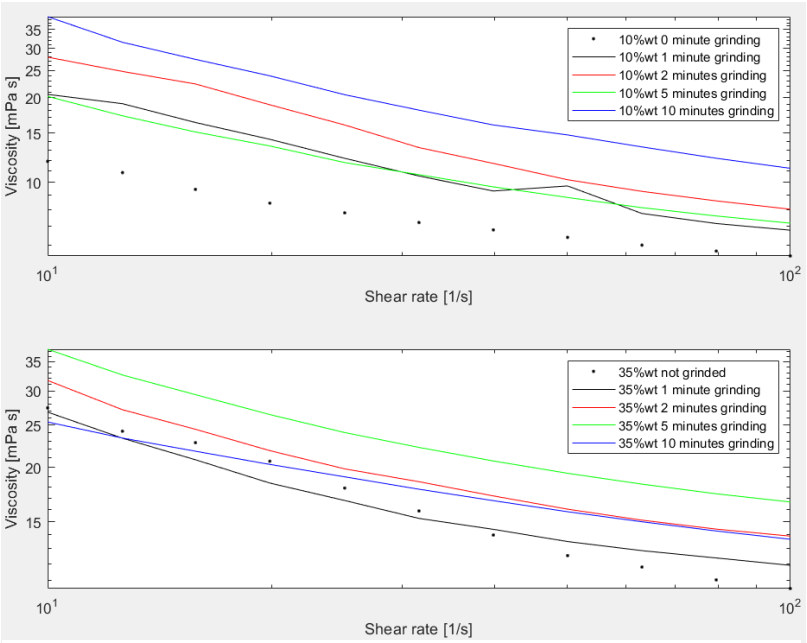

Figure 19: viscosity measurements of the different samples at different grinding times. Four measurements were performed on one sample per batch.

As can be seen in Figure 19, the effect of grinding has a rather big influence on the viscosity of the measurements. This is however not unexpected. According to *Konijn* [34], the sizes of the particles in the suspension have an influence on the viscosity of a suspension with a low liquid viscosity unlike suspensions with a high liquid viscosity, where the particle size has a rather small effect on the viscosity. The reason for this is not quite clear, but can have something to do with particle elasticity in the fluid due to adhesive forces between the particles and the viscosity of the base fluid. For the sample containing 10wt% P4 particles, the viscosity of the suspension which was grinded most intensely is almost twice as big as the viscosity of the non-grinded sample containing the same amount of P4. The effect of grinding is less for the suspension containing a higher concentration of P4 particles. Here, the viscosity of the 5 minute grinded sample is 'only' 1.5 times bigger compared to the not-grinded sample. Also, the results are much closer to each other. The amount of grinding didn't influence the viscosity much compared to the suspension containing urea and 10wt% P4.

These results are a bit remarkable. By grinding, it is possible to reach a viscosity of an urea suspension containing 10wt% P4 which is almost as high as the viscosity of a suspension containing 35wt% P4. This can be seen clearly later on in Figure 24. One could conclude from this that in order

to prill more easily, the P4 particles have to be as big as possible. This does of course increase the amount of clogging, but it reduces the pressure required to form a jet.

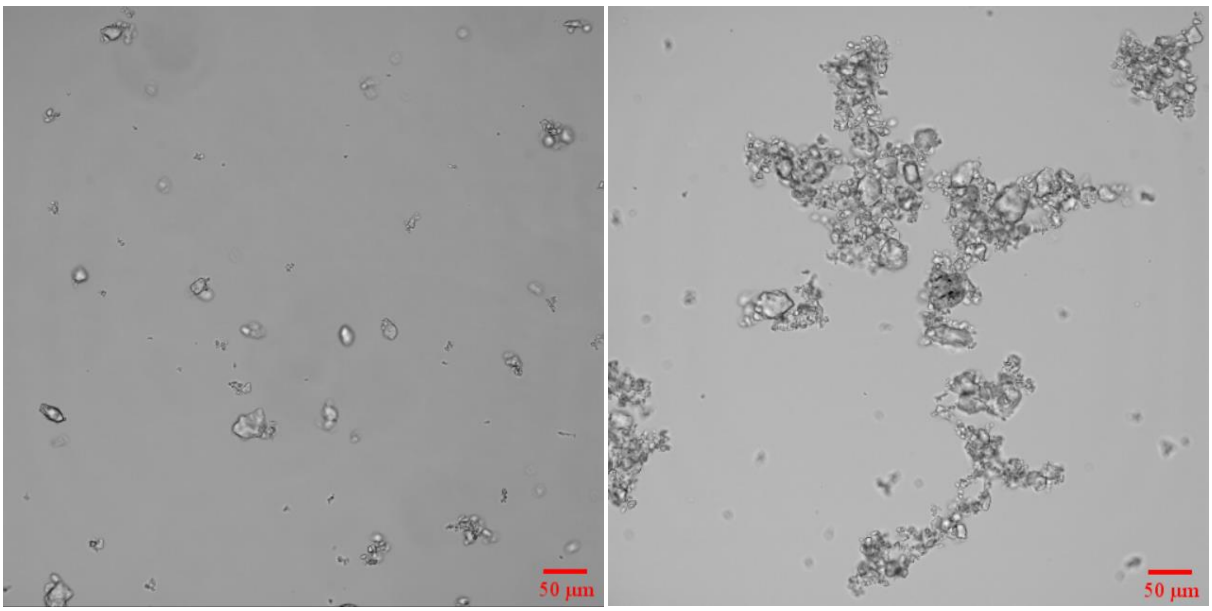

Figure 20: polyhalite suspended in silicon oil under a microscope with 20x magnification, both 2 minutes grinded. On the right a wider distribution of particle sizes can be found compared to the left.

The results are somewhat surprising due to the results of the microscopy analysis (see section 5.1). Here it was found that the mean size of the P4 particles have been decreased due to grinding, but that the grinding for a longer time didn't influence the size at all. There is a chance however that the grinding time did decrease the P4 particle size without directly noticing with microscopy. During these analyses, it was worth noting that the particle size did also depend on their location. The particles that clogged together were a mix of very big particles (around 40 micron) and quite small ones of a few micron. However, not all particles did clog together. When there was an open space, mostly small particles were visible, while clogged particles did contain a larger variety of particle sizes. An example can be found in Figure 20**.** Measuring the diameter of the P4 particles in the left picture will give a different result compared to the right picture.
It is therefore quite difficult to determine the mean size of the particles, because it depends on the area. Taking a microscopic picture of another location can change the mean size of the particles. Even when 600 particles are analyzed; each picture will contain a few thousand particles, so it is still a small amount that can be analyzed.

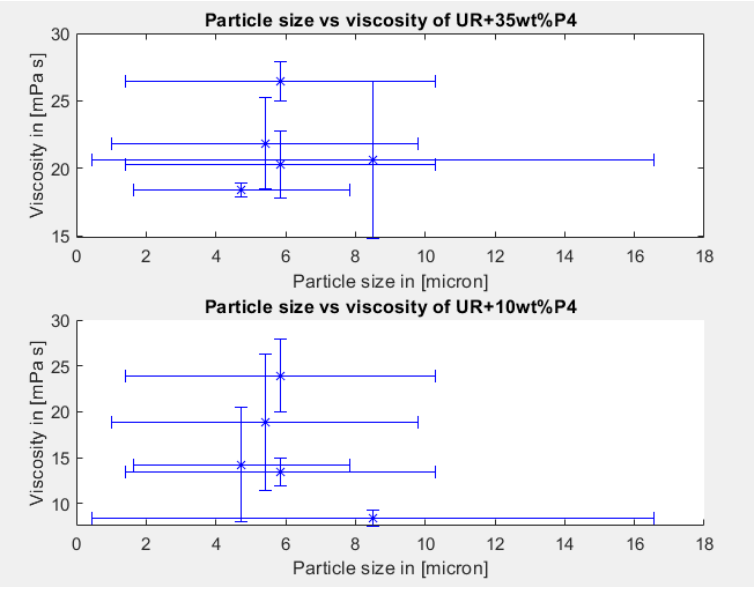

Figure 21: viscosity versus particle size, translated from P4 microscopy results.

As been mentioned before, the P4 microscopy measurements didn't show a big relationship between grinding times and particle size. However, the viscosity

measurements show the opposite. Therefore, also the viscosity of the samples has been plotted against the mean particle size with their standard deviations, see Figure 21**.** As can be seen in this figure, the standard deviations for particle sizes are quite large despite the large amount of particles that have been analyzed. There is not a clear relationship in this study between the particle size and the viscosity of the suspension. Between a particle size of 4 and 6 microns, it seems like the viscosity will increase with increasing particle size. However the errors are too large to interpret this as a clear relationship.

5.2.2 P4 concentration and viscosity

According to [34], there is a relationship between particle concentration and viscosity of the suspension. In this thesis, the relationship has been analyzed and compared with a standard model for viscosity. For calculating the viscosity of a suspension, the Ostwald-de Waele model has been used. According to [34], this model can describe the viscosity of a suspension rather well compared to other models. Now, the viscosity of the suspension can be predicted as follow:

$$\mu = K\dot{\gamma}^{n-1} \qquad (30)$$

Here, K is the relative consistency index in mPa s^n, and n is the flow behavior index. When n<1, the suspension or fluid will show shear thinning effects, while n>1 will show shear thickening. When n=1, the liquid shows pure Newtonian behavior.

During the measurements, no data has been acquired for a shear rate of 1 s^{-1}. It is however important to know the viscosity of the suspension at a shear rate of 1 s^{-1} in order to calculate our parameters to model the viscosity, so Matlab [68] has been used with the least squares procedure to fit the experimental data in a power-law form for our problem. This leads for the urea with 10wt% P4 to K=79.77 mPa s^n (with a 95% confidence interval between 69.85 and 89.69 mPa s^n) and n=0.4658 (with a 95% confidence interval between 0.4244 and 0.5071). The other sample containing urea and 35wt% P4 have the following parameters: K=67.9 (with a 95% confidence interval between 60.13 and 75.68 mPa s^n) and n=0.6292 (with a 95% confidence interval between 0.5929 and 0.6655). The value of the flow behavior index clearly indicates both the samples show shear thinning behavior. Take note however that this index is quite larger for the more dense suspension compared to the suspension containing less P4 particles. This will be analyzed later on in this article.

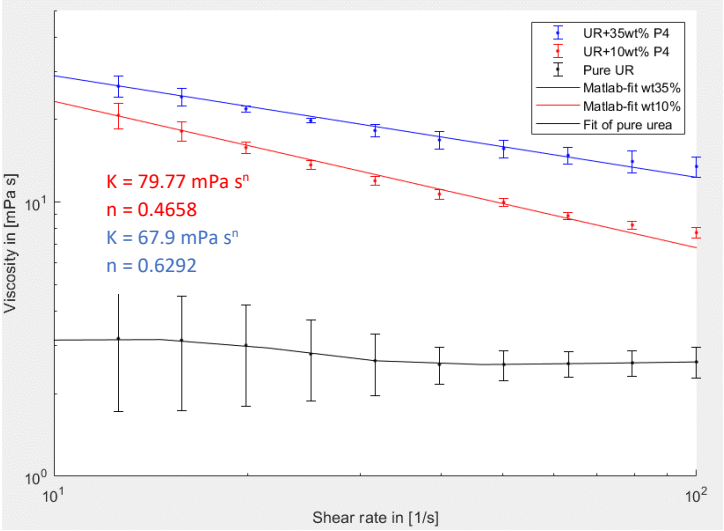

Figure 22: viscosity versus shear rates. Three samples have been plotted: pure urea, urea +10wt% P4 and urea +35wt% P4 at 140 °C. Parameters have been determined with Matlab.

The viscosity does follow the model quite well at lower shear rates. As can be seen in Figure 22, pure urea is a Newtonian fluid, which has a viscosity that doesn't have a dependance on the shear rate. At around a shear rate of 10 s^{-1}, it seems the viscosity is a bit higher, but that is probably due to the uncertainty in the measurements. According to [70], the dynamic viscosity can be calculated as follow for pure urea:

$$ln\,\mu = 6700/T - 15.311 \qquad (31)$$

Where T is the temperature of the liquid in Kelvin. In our case at a temperature of 140 degrees Celsius, we obtain a dynamic viscosity of 2.49 mPa s. This is quite close to our measured viscosity of around 2.55-2.61 mPa s at higher shear rates.

The measurements show a clear relation between the volume or weight fraction of suspended particles and the viscosity. The bigger the volume fraction of suspended particles, the higher the viscosity of the suspension. It now also shows clearly shear thinning effects: the higher the shear

rate, the lower the viscosity is. However, it is interesting to see that the sample containing a higher P4 concentration show less shear thinning effects compared to the sample with a lower concentration. Both the suspensions have an extrapolated viscosity of around ~70-80 mPa s, but the viscosity of the sample with 10wt% P4 drops slightly more at higher shear rates compared to the sample containing 35wt% P4. According to [34], the sample containing a higher volume fraction of particles should exhibit more shear thinning effects. This is due to a variable friction coefficient: there is a lot of particle-particle interactions, but the forces between the particles will break down at higher shear rates. This leads to lower viscosities at higher shear rates, which will approach the viscosity of suspensions containing a smaller volume fraction of particles [71], [72]. Now, it almost equally follow the same path or even show less shear thinning effects. The particle sizes of both suspensions are rather small, with a mean particle size of around 6 microns. According to the same research as *Konijn* [34], higher volume fractions of small particles in the suspension can even result to slightly more shear thickening effects (instead of thinning) in viscous fluids. The effect of particle concentration on the viscosity of the suspension is larger compared to particle sizes, but the influence of the particle size will dampen this effect slightly, resulting in a smaller shear thinning effect at higher particle concentrations. This effect can also slightly be seen in Figure 19. Here, the samples which are grinded more thoroughly show somewhat less shear thinning effects. According to [73], the effects of Brownian motion can only be neglected when the Pe>1000, which is the Peclet number. Here, the Peclet number is a dimensionless number which in this case represents the ratio of advection of particles by flow versus the molecular diffusion of particles by Brownian motion. This number can be calculated as follow [73]:

$$Pe = \frac{6\pi\mu_{\mathrm{liq}} a^3 \dot{\gamma}}{k_b T} > 10^3 \qquad (32)$$

Here, μ_{liq} is the viscosity of the pure liquid, a is the mean radius of the suspended particles, k_b is the Boltzmann constant, T the temperature of the suspension and $\dot{\gamma}$ the shear rate. In our cases, the Peclet number is 232 at a shear rate of 1 s^{-1}, which means Brownian motion will have an effect on the viscosity and cannot be neglected at low shear rates. These shear rates are however lower than the ones used in the experiments. *Van der Borght* [28] did observe some Brownian motion in the P4 particles at high temperatures. Take note this effect can only be taken into account at low shear rates between 1 s^{-1} and 4.3 s^{-1}, and means that we can neglect Brownian effects at the measured shear rates. Also the particle Reynolds number is important here. This can be determined with the following formula:

$$Re_j = \frac{\rho_{liq} d^2 \dot{\gamma}}{4\mu_{\mathrm{liq}}} < 10^{-3} \qquad (33)$$

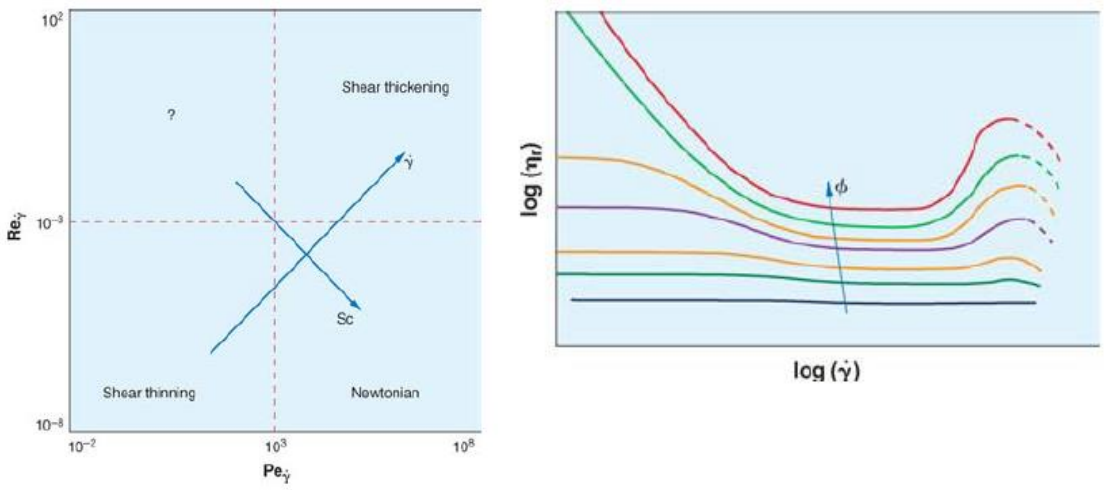

Figure 23: a schematic overview of non-Newtonian properties of suspensions. Increasing Pe and Re numbers can result in a suspension exhibiting shear-thickening or Newtonian behavior. On right graph the effect of this with increased volume fraction can be found [56].

With ρ_{liq} the density of the pure liquid and d the diameter of the suspended particles. When the Reynolds number is smaller than 10^{-3}, the suspension will show shear-thinning or Newtonian behavior. At larger values, it can show shear thickening effects, as can be seen in Figure 23**.** According to [73], all suspensions show a shear thinning behavior at low shear rates. However finally, at increasing shear rates, a Newtonian plateau will be reached, which will finally result in even shear thickening effects at higher shear rates, which can be seen Figure 23. This effect is slightly visible in Figure 22, mainly at the sample containing 35wt% P4. The suspension show clearly shear thinning behavior, while it seems like the plateau is going to be reached at a value above a shear rate of 100 s^{-1}.

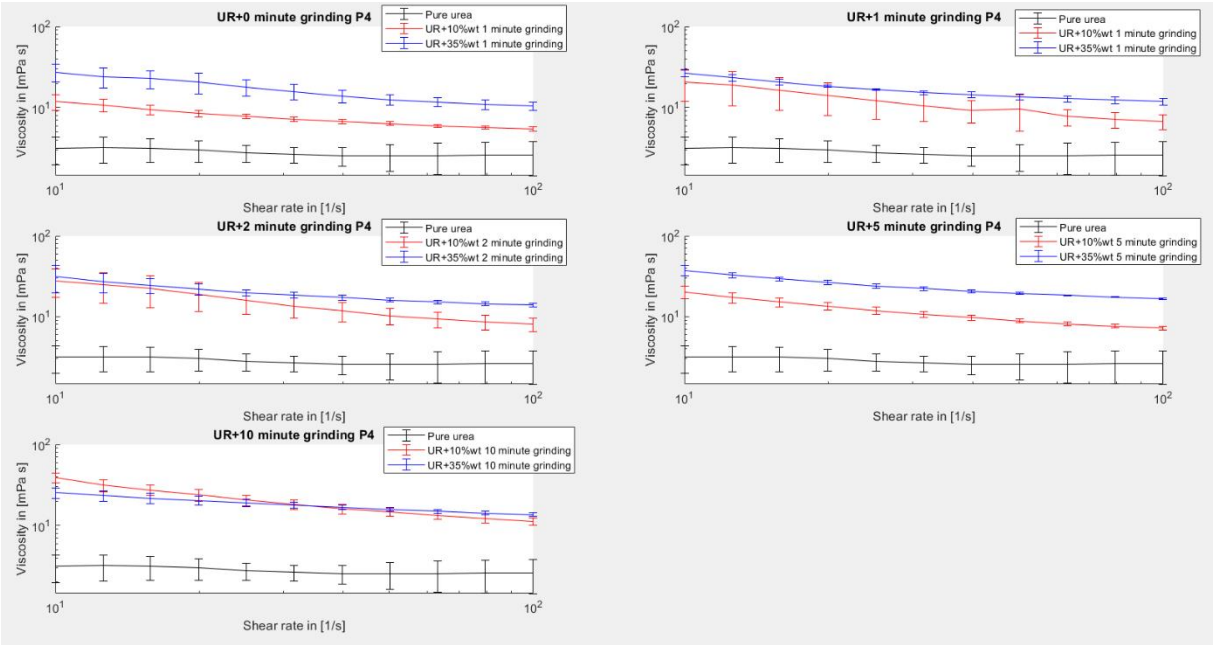

Figure 24: viscosity versus shear rates for the different samples at different grinding times. One could see grinding will increase the viscosity of both suspensions.

This is also the reason why the expected fit doesn't fit the graph in Figure 22 as expected. The expected viscosity at a shear rate of 1 s^{-1} is larger for the sample containing 10wt% P4 compared to the one containing 35wt%, which seems unlikely since particle concentration increases the viscosity of the suspension rather than decreases it. When ignoring the last measuring points, the relative consistency index calculated in Matlab [68] approaches each other but with rather big uncertainties. This is due to the way the data has been calculated in combination with the uncertainties in the measurements. For determining the mean value of each data point in the urea+10/35wt% P4, all measurements of the grinded and not-grinded samples have been taken into account. This leads to a small error. When looking at the data in Figure 24, the samples do follow a similar path, where the less concentrated sample will almost always have a lower viscosity than the concentrated sample with 35wt% P4. However, not everywhere. The viscosities will come closer to each other when the samples are more thoroughly grinded. At 10 minutes grinding, the viscosities of both the samples will be almost the same. In fact, the viscosity of the less concentrated sample will be exceeding the viscosity of the highly concentrated sample at lower shear rates. It would give more insight if the particle sizes of P4 can be determined more precisely.
It is also interesting to see that the viscosity drop at higher shear rates is becoming larger in the urea + 10wt% P4 sample at longer grinding times, but remains equal or even becomes smaller at longer grinding times in the concentrated sample, see Table 7**.** It seems like the samples which are grinded for 10 minutes are passed a sort of tipping point, where the low volume fraction sample will exhibit more shear thinning while the higher volume fraction sample will come close to its Newtonian plateau. It is expected that the particles are grinded to such a small size that Brownian motion cannot be neglected. This is expected to happen at the measured shear rate of 10 s^{-1} and 100 s^{-1} with an average particle diameter of 2 microns or smaller.

	Urea + 10wt% P4	Urea + 35wt% P4
0 minute grinded P4	6.41 mPa s	16.9 mPa s
1 minute grinded P4	13.8 mPa s	14.9 mPa s
2 minute grinded P4	19.9 mPa s	17.8 mPa s
5 minute grinded P4	13.1 mPa s	20.7 mPa s
10 minute grinded P4	27.7 mPa s	11.8 mPa s

Table 7: viscosity drop between a shear rate of 10 s^{-1} and 100 s^{-1}.

There are different models to estimate the viscosity of a suspension (at a shear rate of 1 s^{-1}). One such a way is by using the Eilers fit [74], which is an empirical model and uses the viscosity of the pure liquid, the volume fraction of the suspended particles and the maximum packing fraction of ϕ_m= 0.58-0.63 with a certain parameter B = 1.25 – 1.5:

$$\frac{\mu}{\mu_0} = \left[1 + \frac{B\phi}{1 - \frac{\phi}{\phi_m}}\right]^2 \qquad (34)$$

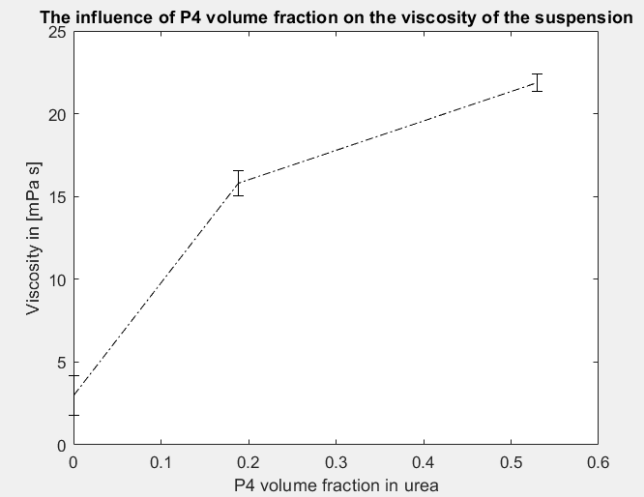

Figure 25: viscosity of the samples at a shear rate of 40/s versus volume fraction of P4.

Since the maximum packing fraction is not known, a range of the expected viscosity can be calculated at a shear rate of 1 s^{-1}. This is required for determining the consistency index K. For the urea + 35wt% P4 sample, this will lead to a viscosity of 74.2 – 286 mPa s, which is quite a large range. Therefore, it is assumed the maximum packing fraction will be around 0.63, since in that case the viscosity will be around 74.2 and 100 mPa s at 1 s^{-1} , which is in the extrapolated range. A maximum packing fraction of 0.63 corresponds to a sample containing 45wt% P4. This also means that in the current suspension, the maximum packing fraction is limited by close packing of the particles rather than the glass transition [65]. This formula however will give too low values for the urea + 10wt% P4 sample, since here the viscosity will be around 5.6 and 5.0 mPa s, which is at least half the value that has been found in the measurements with comparable particle concentrations. This is unexpected since the above mentioned model do give a good fit for other experiments [74]. Also other models like the MPQ-model, Mendoza and Krieger-Dougherty models [65] do give a good estimate of the viscosity of the highly concentrated suspension. Here, the viscosity at a shear rate of 1 s^{-1} which is equal to the K value in equation (30), will give a value of 96.5 - 97.8 mPa s^n for the concentrated suspension with the Mendoza model and the MPQ-model respectively. These parameters have also been found when the last measured points are neglected in Figure 22**,** which flattens the curve. With this calculated K from the above mentioned models, n=0.4933 – 0.4875 respectively, which is lower than the first estimate of n=0.6292. The n value however is still higher than the one of the more dilute sample, which is n=0.4658. However, the models don't provide a good fit for the urea+10wt% P4 samples, which estimates a too low value of K compared to measured data. It remains however unclear why the measured viscosity of the urea + 10wt% P4 sample is much higher than expected and why the models don't fit the measured data. The new fits with the investigated data can be found in Figure 26.

The viscosity versus the P4 volume fraction has been plotted for a shear rate of 40 s^{-1} in Figure 25**.** Here, it can be seen that the viscosity is increased the most at lower concentrations, and is much higher for the lower volume fraction than expected (which corresponds to the urea + 10wt% P4 sample). This also is an interesting result because at high volume fractions, it is expected that the viscosity of the sample (at a shear rate of 1 s^{-1}) will go to infinity, indicating that the viscosity will increase exponentially when increasing the volume fraction of the suspended particles.

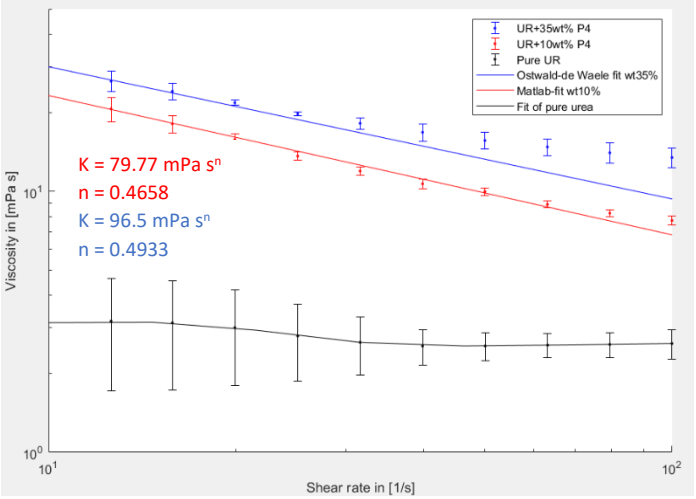

Figure 26: viscosity of the different samples at 140 °C. The Ostwald-de Waele fits have been configurated with the K-value found in the MPQ model.

5.3 Experimental setup

As been mentioned in the chapter 4, an experimental setup has been built in order to do some prilling experiments. First, this design will be tested and changed if necessary. After this, experiments to answer the questions related to the prills or prilling process can be answered.

5.3.1 Analysis of the setup

When undertaking some first tests, it was directly seen that at least two of the objectives could be reached for the design. It was successful at first try to melt the suspension at the end of the tube and some first prills could be made. However, it was in this trial not directly possible to form a jet: the prills that have been made originate from a dripping regime instead of a breaking-up jet. The formation of the droplets can be found in Figure 27 and Figure 31. Increasing the rotational velocity didn't resolve this: sometimes this even lead to a decrease in the dripping velocity. Also sometimes a bubble was formed, which indicates there was a lot of air in the screw, or the suspension was decomposing. The latter seemed most likely since urea decomposes already at its melting point and was observed more when the heater reached higher temperatures than desired. After taking apart the setup, the screw did only contain very small amounts of the suspension, with a bit of it sticking at the top of the screw. This indicates that the screw itself was unable to fill itself with the suspension. Therefore, a scraper was made and installed at the funnel, consisting of a metal wire which can be seen in Figure 29. Also more images can be found in Appendix E: Parts overview experimental setup. This resulted in a faster droplet formation. Now, when removing the tube during prilling, the screw did contain a lot of the powder. However, it was still impossible to form a jet. This is probably due to the size of the screw and tube. The outer diameter of the screw was ~5.5mm, but the empty space was only 1.7mm big. At one point, there will be a transition of the suspension between solid and liquid. The screw, which is relatively hot, will melt the urea. However, this process will require heat, and because the screw is not directly connected to the heater, it will locally cool down at the top of the screw because melting is an endothermic process, resulting in the attachment of the solid urea powder to the screw, which is really hard and difficult to remove, see Figure 28.

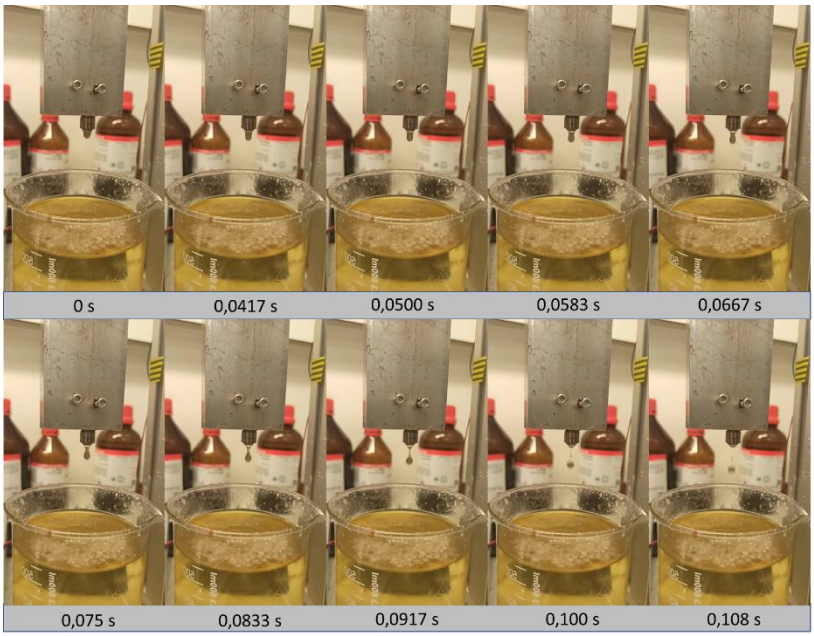

Figure 27: droplet formation of urea + 10wt% P4, filmed with 120 frames/s. Necking is clearly visible. The long thin thread will breakup into one droplet accompanied with a satellite droplet, which is visible in the last two frames.

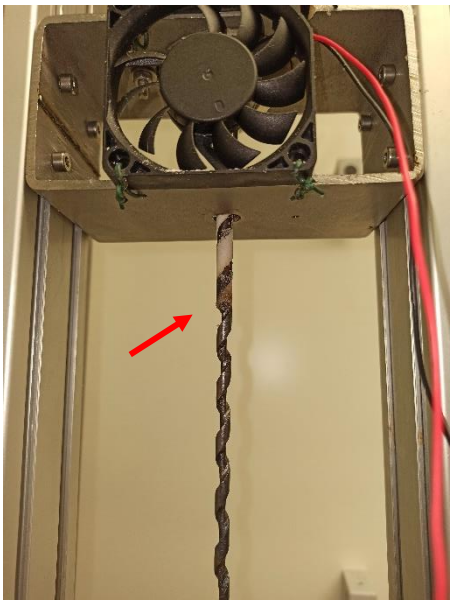

Figure 28: a hard lump at the red arrow has been formed on the screw just before it starts melting.

Therefore, more particles will melt and solidify there together, resulting in a bigger clump. Because the hole has just a height of 1.7mm, it will easily get stuck with the clumps, resulting in less throughput of the suspension through the tube and increasing friction with the wall when it is growing too big. See Figure 30 for an illustration.

Figure 29: the added scraper (green wire), in order to improve throughput of the powder.

Also another explanation arises here. During the design, a critical Weber number of 3.125 has been taken as reference to determine the correct prilling velocity. This dimensionless number requires the surface tension of the suspension to be determined accurately. However, since this property is unknown for the suspension, the surface tension of pure urea has been used, which is expected to be not the same. According to [75], the surface tension of suspensions is increased compared to its base fluid. The particles are slightly charged. When moving to the surface, the repulsive forces between the particles will increase the surface free energy. If it is assumed that the surface tension of the suspension is indeed higher, it means that with the current prilling velocity a smaller Weber number is obtained, hence resulting in a dripping regime. The Ohnesorge number (equation (6)) and Eötvös number (equation (8)) were determined to be 0.40 and 248 respectively when taking the surface tension from pure urea and the viscosity of the suspension at the extrapolated value of 1 s^{-1}, since it is expected that the shear rate inside a droplet will be close to zero. This means that with the current data gravitational forces will be much more dominant compared to surface tension forces. Inertial and surface tension forces will be more dominant as well compared to its viscous forces. However, more investigation on the surface tension of the urea-P4 suspension will be required to provide a more accurate analysis.

The prills will be formed out of a 1mm nozzle. First, a nozzle of 0.6mm has been tried, but this resulted in more clogging compared to a 1mm nozzle. When operating the device, one should pay attention to the temperature. When the temperature is fluctuating, the suspension will switch between melting and solidifying at the top of the screw, resulting in a quite hard substance when solidified. This sometimes prevent powder for reaching the end of the screw. Also, it was observed that at higher temperatures, prilling became much more easy resulting in a higher mass flow or droplets. This is due to the fact the viscosity of urea will decrease at higher temperatures, which can be calculated with equation (31)**.** When the suspension was for a longer time inside the heating tube, something notable happened: when prilled, the prills that were formed were a bit darker compared to the other prills. It is expected that this is due some oxidation reactions that happens with the steel screw. At high temperatures, some oxidation reactions will take place between urea and steel [76]. A ventilator was added in the design to prevent temperatures of 60 degrees Celsius or more to be reached inside the funnel. However, the tube was a bit shorter than designed, resulting in higher temperatures inside the funnel when prilling AN, since the distance between the funnel and the heater is now shorter. However, with urea this wasn't a problem, and can be easily solved by making the tube a bit longer. This tube is made of stainless steel, which has a bad heat conductance compared to normal steel or aluminium [57]. However, take note that when

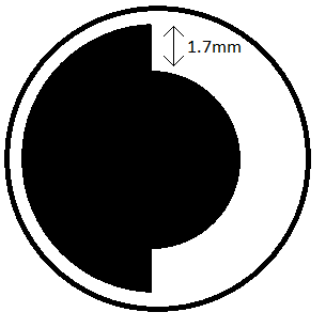

Figure 30: illustration of the screw (black) inside the tube, with the 1.7mm passage for the suspension to go through.

prilling for example ammoniumnitrate suspensions (which will require a higher temperature), the temperature at the funnel can become too high when prilling for a longer time.

Next to this, the first prills that were produced had a reddish color. After analyzing, a small clip holding the funnel and the prilling tube together was not the right material and was therefore rusting. When changing this part, the prills weren't red anymore.

5.3.2 Pressure drop

As has been mentioned above, the experimental setup was able to make prills, but not to form a jet. An analysis has been made in order to give more insight in the reason why. Data from the viscosity measurements has been used as well. First, the presence of the screw is neglected and therefore it has been assumed this is a standard pipeflow with a non-Newtonian fluid. The velocity that is required to form a jet can be derived from the critical Weber number and hence was used in the initial calculations in section 4 has been used to calculate the volume flow ($\dot{Q}$) in the tube:

$$\dot{Q} = \frac{U_b d_{tube}^2 \pi}{4} \qquad (35)$$

With U_b the bulk velocity of the suspension in the tube and d_{tube} the diameter of the tube. According to [77], the shear rate of a power-law fluid at the wall of the tube can be calculated as follow:

$$\dot{\gamma} = \frac{8\dot{Q}}{\pi d^3}\left(3 + \frac{1}{n}\right) \qquad (36)$$

With n is the flow behavior index. This value was obtained from the viscosity calculations and is 0.4933 for the urea+35wt% P4 suspension. This sample will be analyzed here since it is expected that this suspension will lead to the biggest pressure drop due to its highly viscous properties compared to pure urea.
Now the shear rate has been determined, there are three terms which determine the required pressure to prill: one is the pressure drop in the tube due to viscous friction, the other one is the pressure drop in the nozzle, also due to viscous friction and the last one is the pressure drop due to the change in velocity when the fluid is going through the nozzle with a smaller diameter. This formula will be as follow:

$$\Delta p = 4K\left(\frac{L}{d_{tube}}\dot{\gamma}_{tube}^n + \frac{t}{d_{noz}}\dot{\gamma}_{noz}^n\right) + \frac{1}{2}\rho_{susp}\left(U_{jet}^2 - U_b^2\right) \qquad (37)$$

With K as the relative consistency index, L the length of the tube, t the thickness of the nozzle and ρ_{susp} the total density of the suspension. For the investigated suspension, this will result in a pressure drop of 316 Pa compared to a pressure drop of 246 Pa of pure urea, which doesn't seem as one of the limiting factors to form a jet since this will result in a required torque of 0.015Nm compared to the holding torque of 0.5Nm of the steppermotor. Note that not all of the urea and suspension are molten, thus resulting in an extra friction force to overcome next to the pressure drop. Furthermore, the torque of the steppermotor will drop when rotating. It however is unclear what the torque-velocity curve is for the specific steppermotor that has been used.

Next to that however, the shear rates are quite different at the different locations. In the tube, the shear rate is 22.3 s^{-1} while in the nozzle the shear rate is 4830 s^{-1}. The nozzle has a diameter of 1mm in this case. This is really high compared to the regimes the viscosity measurements have been done.

It is expected that inside the nozzle, the suspension will show shear thickening effects. When calculating the particle Reynolds number with formula (33), it has been found that this Reynolds number is 0.0184 at the nozzle. The criteria to show shear thinning or Newtonian effects is when this number is smaller than 10^{-3}. The calculated particle Reynolds number is ten times larger than this, which means that the suspension will be in the shear thickening regime in the nozzle. Because the fluid is only accelerated there, the viscosity will be increased much, which is expected to be the reason why it is very difficult to form a jet out of this nozzle. It will probably help to decrease the thickness of the nozzle and increase the nozzle diameter, however, more research on the viscosity of the suspension at higher shear rates needs to be done to qualitatively determine how much these dimensions needs to be changed.

It also explains why the current design with the screw is unable to prill this suspension, but *Emma* [28] succeeded with a simple piston. When the required pressure is going up in the current design, at a certain point the screw won't be able to push the liquid downwards but will only mix the fluid at the bottom. The rest of the powder and half molten suspension will just stay in place in the screw or is even compressed because it can't move on further. This has also been observed. When the prilling device wasn't able to prill, the screw did contain very hard and compressed powder at the top of the screw. At the bottom, the screw didn't contain any liquid anymore because this just dripped out of it. In the meanwhile, this powder at the top would be compressed more and heated up a bit, which results in very hard clumps.
The reason why it was possible to form a jet in *van der Borght's* [28] setup was because of mass conservation. When the piston was pressed downwards, it could only go to one end and even it did still require some force, it would possible to form a jet. The screw can rotate as fast as it is possible, it won't be possible with the current one to form a jet because it can't build up much pressure. The liquid will just stay in place. However, if a screw is used with a small pitch, it may be possible to overcome this pressure, or the particle Reynolds number has to be decreased by decreasing the particle size. If the average particle size of P4 is decreased to $1/5^{th}$ of what has been measured it is possible to let the fluid remain in the shear thinning or Newtonian regime. However, this also has to

be researched because viscous suspensions will just show the opposite effect when decreasing particle sizes [34].

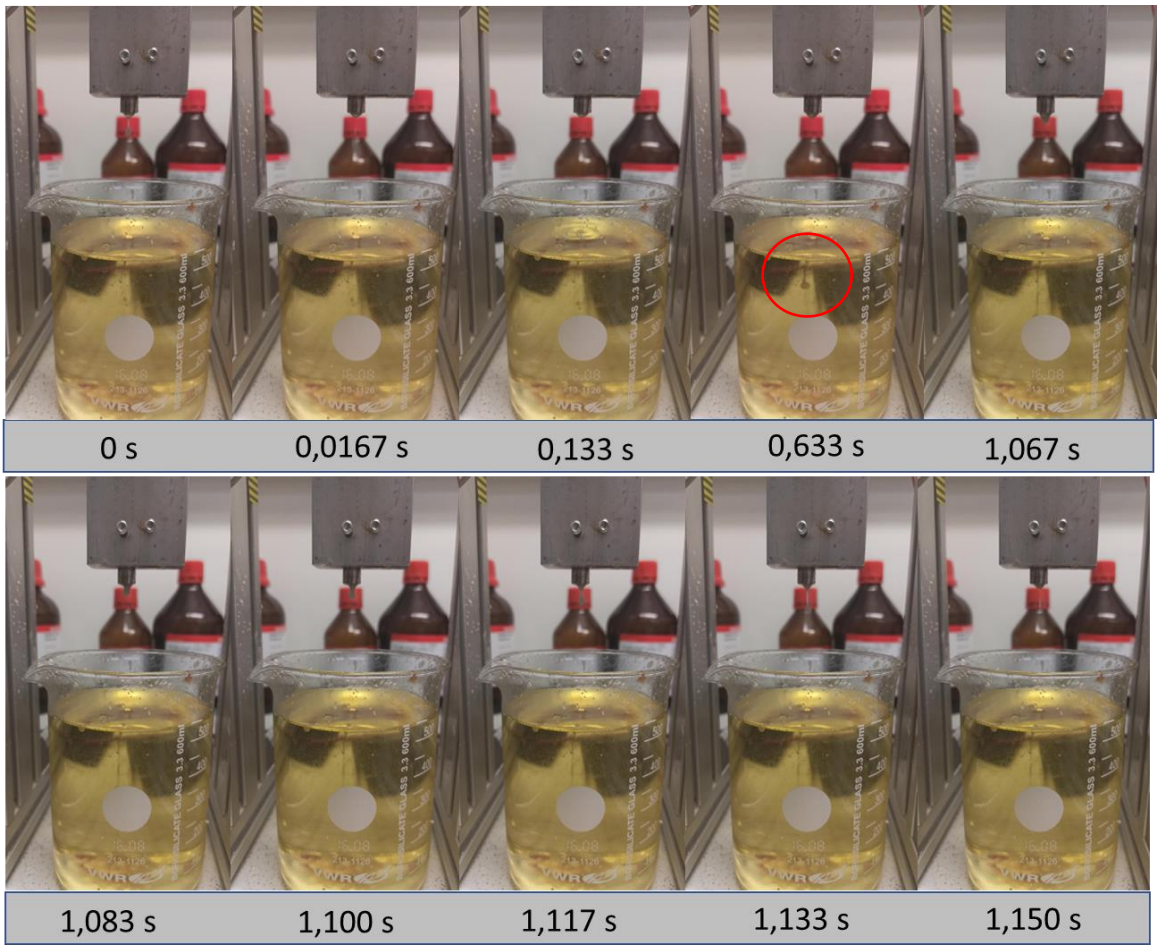

Figure 31: dripping regime of urea + 10wt% P4. In this case, a droplet is formed every ~1 second. Also here a thin filamentis formed, where the droplet will break up combined with the formation of a satellite droplet. In the fourth frame at the red circle, the droplet is visible in the oil, combined with a tail of hot oil.

5.4 Prills

The prills have been produced with the experimental setup which was designed for this thesis. These prills however have been formed in the dripping regime, which can lead to some other results. When the prills fall down, the distance to cool them completely is not large enough in the air, so the droplets will be collected in an oil bath to cool them. This was quite successful since the prills were almost all completely solidified when reaching the bottom of the bath. Take note however that the oil bath warms up when prilling for a longer time.

Also something noteworthy happened during prilling and collecting the prills in oil. First, the distance between the nozzle and oil was relatively high. The idea behind this was that the prill could cool as much as possible in the air, forming a small shell already resulting in a more spherical droplet and then cooled down as fast as possible in the oil. This was first no problem with the prills containing a suspension. But when switched back to pure urea, the droplets where deformed when hitting the oil, resulting in flat disks of urea, which can be seen in Figure 32. Here, the kinetic energy of the droplet is high enough to overcome the surface energy of the droplet that will hold the droplet together, resulting in a flat disk when the kinetic energy is absorbed into the droplet during impact. Data acquisition and calculations of the prills can be found in Appendix F.4 and Appendix F.5.

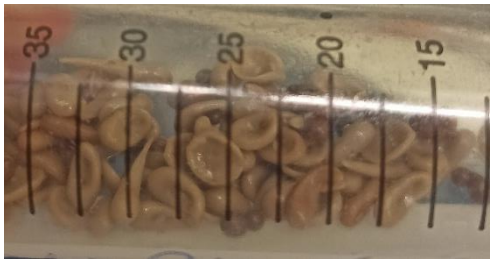

Figure 32: flat prills due to the impact with oil.

5.4.1 P4 distribution

The diameter or size of the prills have been determined by hand. A digital caliper has been used with an uncertainty of 0.01mm and a SAB 225i scale with an uncertainty of 0.01 mg. First, the prills where collected on a paper towel and were cleaned thoroughly. Since they were collected in oil, it was necessary to clean them since this can lead to big errors. With the measured size and mass of each prill, the expected concentration of P4 in each prill can be determined. This will give an indication how the P4 is distributed over the prills and therefore indicate the quality of each prill. It is necessary to have an equal distribution of P4 over the prills. When the prills are distributed over the land as fertilizer, it is required that each prill will deliver the same amount of minerals and nitrogen to the ground, since otherwise some plants will have some shortages of certain required elements and some a surplus, which is also not good.

There are a few samples of prills that have been analyzed. The prills were made in one run, with each sample close after each other, so the circumstances are quite similar. Three different concentrations of urea+P4 prills have been analyzed: one batch did contain only urea, a second one urea and 10wt% P4 and a third one urea and 35wt% P4. Next to this, prills of the latter two are also made with P4 that has been grinded for 10 minutes and which are not grinded at all. Each batch did contain about 40 to 42 prills, which were selected for their roundness. Not all prills were perfectly round, but to make calculations more precise, only prills that were round to the naked eye were selected, which made it able to assume that the prills where perfectly spherical. To determine if this method is suitable, first the pure urea prills have been analyzed, where an estimate of the density of each prill has been made and compared to the real density of them. In the current calculations, the density of the prills were only 8,5% higher than expected. The measuring error in size and mass will contribute to an error of about 1% in each prill. The other error is due to some oil that probably was still present on the prills. Therefore, the prills are cleaned more intensely, which reduced the error to 6.7%. This seemed acceptable for the current investigation.

Now it is time to analyze the results from the suspensions. Also here, the density was calculated, from which the P4 concentration could be obtained. First, the total P4 concentration of each batch of prills has been determined in Table 8**.**

	Measured P4 wt%	Standard deviation
10wt% P4 not grinded	11.4%	7.58%
10wt% P4 grinded	8.66%	6.34%
35wt% P4 not grinded	23.2%	10.1%
35wt% P4 grinded	29.6%	12.3%
10wt% P4	10.1%	7.10%
35wt% P4	26.5%	11.7%

Table 8: different suspensions with the expected wt% of P4.

As can be seen here, the measured and calculated P4 in the 10wt% samples are very close to what has been expected. However, the amount of P4 in the 35wt% samples are much lower than expected. There is a small explanation for that. During prilling, it was observed that some P4 was sticking at the funnel after prilling this specific sample. This was probably the reason why the concentration of P4 in the prills is much lower here. Also interesting to see is that the standard deviation for the more concentrated prills is higher compared to the prills containing less P4. This can also be the result of P4 sticking at the funnel, resulting in more prills containing a small bit of P4 and normal quantities.

Now some plots can be made, to analyze the distribution of the polyhalite over the prills.

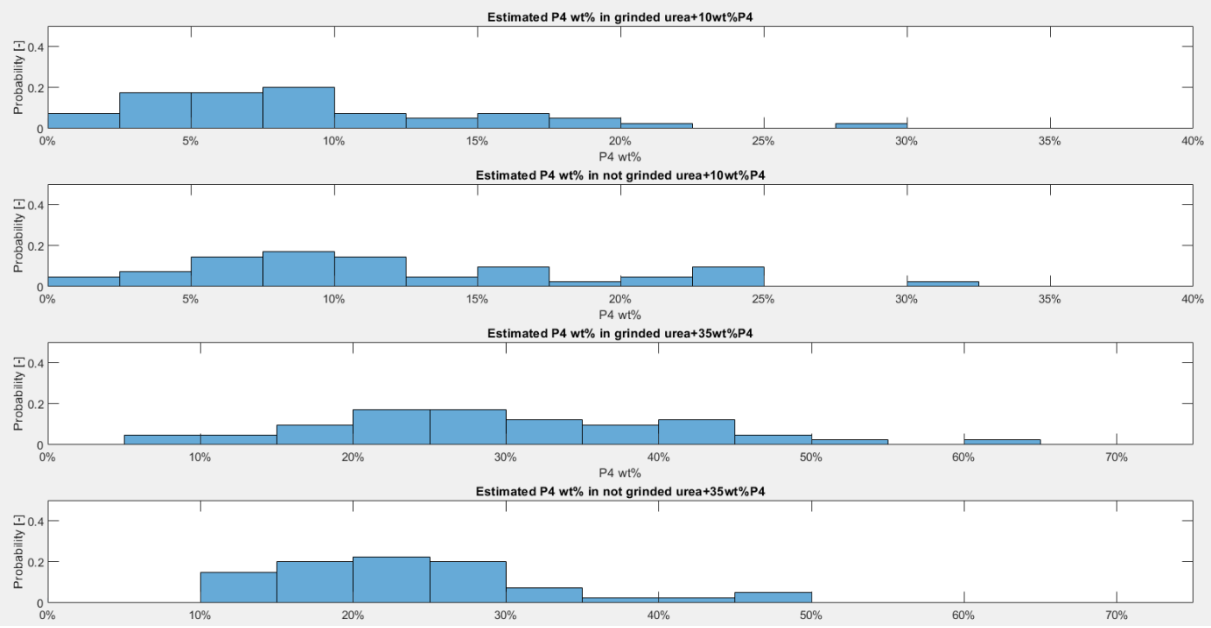

Figure 33: estimated wt% P4 of each prill.

As can be seen in Figure 33, the prills don't have a quite equal distribution of P4 over each prills. Some prills of the 10wt% batch don't even contain any measurable amount of P4, but some others can contain P4 up to 30%. Something similar is happening with the 35wt% batch. Only here all prills do contain some P4, varying from 5% to even ~60% P4 (which is equal to a volume fraction of 0.75). This seems too much, and since this was measured at only one prill, this is probably an error due to the presence of some oil that wasn't cleaned up. The grinded and not-grinded batch don't show much difference or other relationships.

Now the grinded and not-grinded batches are combined to give some insight in the total concentrations of P4 in the samples. The results of this can be found in Figure 34.

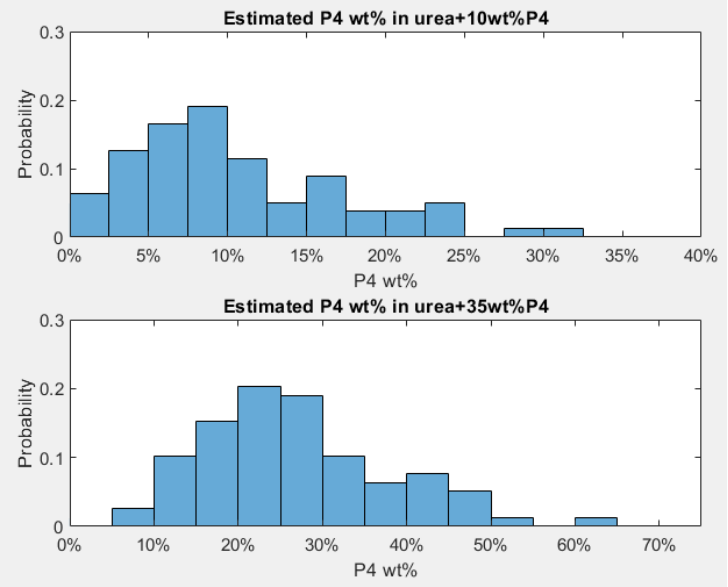

Figure 34: estimated P4 in each prill of different samples. Both the grinded and not-grinded batches are combined.

It is interesting to see that the peak of P4 concentrations in the samples are always below the target concentration. This is mostly visible in the 10wt% sample, where the peak of P4 is just below 10%, with however a mean P4 wt% of 10.1%. This is not really illogical since prills containing a higher concentration of P4 also influences the total result the most. For each prill that does contain let's say 30% of P4, there will be two prills containing no P4.

The reason there are some prills with a relatively high wt% of P4 is difficult to understand since a lot of factors are involved during this prilling process. P4 was added to urea when still a solid and then thoroughly mixed. Probably the high concentration of P4 in some prills are due to 2 factors. First, P4 was observed to be quite sticky with and without being submerged into silicon oil, and will clump together with other P4, which can be seen in the microscopy analysis as well. This will prevent spreading the P4 out equally and instead will form clumps that are prilled together, thus increasing the concentration of P4 in some prills and reducing it much in others. Next to this, it can also have something to do with the prilling equipment. As was mentioned in chapter 5.3, there wasn't enough pressure to press the molten suspension as a jet out of the nozzle. Instead, it will stay at the bottom of the nozzle for a while, dripping in the oil. During that moment, probably some sedimentation of the P4 particles will take place, which will lead to a less mixed suspension.

5.4.2 Microstructure

Some microscopic images of the prills have been obtained. Since measurements could only be done with an inverted microscope, there were some difficulties obtaining pictures since light would be required to shine up from below instead of down. To overcome this, the pictures have been made with UV light mixed with light from the surrounding. Next to that, the surfaces of the prills were not flat, so not all parts in the images are as sharp as desired. More microscopic images can be found in Appendix B: prills microscopy.

Figure 35 shows a microscopic image of the inside of a pure urea prill. The prill was cut through with a small knife. Here, some large grains are visible with a few black spots present. It is expected that those are small holes in the prill: the light can't reach the inside of the hole thus resulting in a black spot. It is not clear if the large rectangular grains are the result of cutting or are formed during cooling. The latter is a bit more convincing since it seems the grains are ordered in a circular pattern while cutting was just in one way. Cutting marks are present in the form of vertical lines. In the red box, some smaller grains are visible, ordered in a less structured way. Note that here there are less cutting marks visible, so this indicates that this is probably more brittle since it already broke apart when applying force.

Next to the inside of a prill, it is also interesting to see the outside of the prill, which is visible in Figure 37.

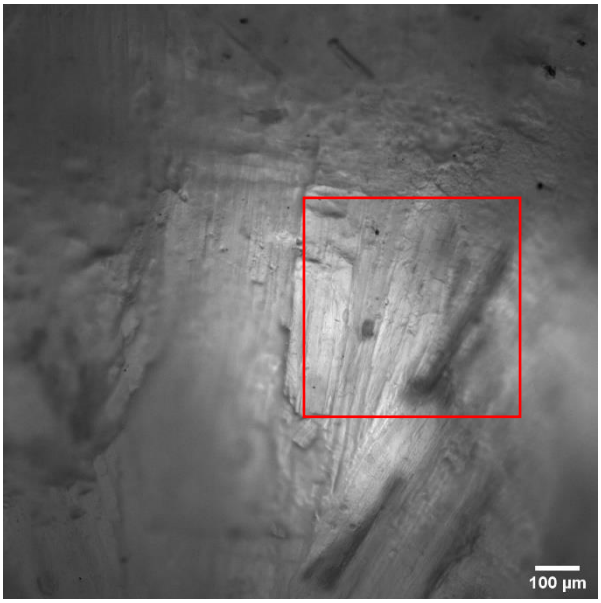

Figure 35: magnification of 10x of the inside of a pure urea prill.

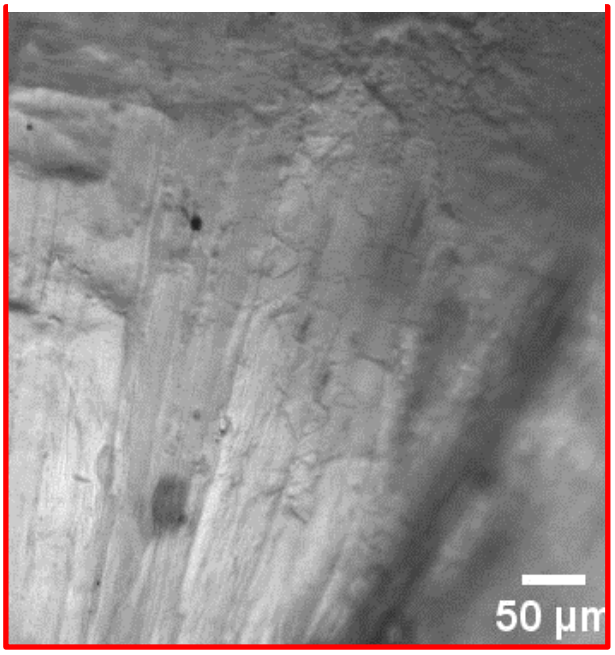

Figure 36: zoomed-in selection of the red square in Figure 30.

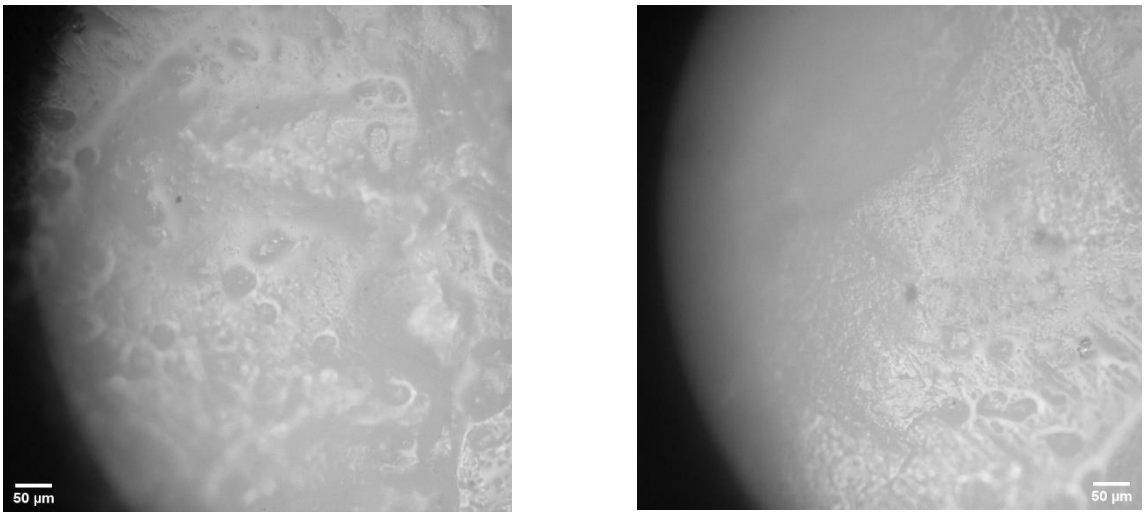

Figure 37: microsctructure of a pure urea prill on the outside (magnification 20x). Left some 'hills' are visible, right is a much finer structure.

Here, the structure looks quite different compared to the inside. Some parts do contain some 'hills' of urea and some 'craters' as is visible in the left image in Figure 37, but other structures that have been found do have a much finer structure, as can be seen in the right image in Figure 37. This is expected to be the result of different cooling rates, which is quite complex here since it depends on the location on the prill but is also influenced by the different ways of cooling. The prill is cooled both in the air as in oil. The first will result in a faster cooling rate compared to the latter. If some parts are already solidified in the air, it will give a different pattern than the location on the prill which was still liquid when reaching the oil.

Now also the other prills containing 10 and 35wt% P4 can be analyzed. Starting with the 10wt% in Figure 38, it is already difficult to observe the presence of P4 particles, since they have the same color as urea. However, some particles are visible since they have a different shape compared to their surroundings. The particles that are visible are relatively large since this image has been taken with a magnification of 10X. Also larger magnifications have been used to analyze the prills, but it remained difficult to see smaller P4 particles. In another investigation it would be interesting to see if P4 and urea can be separated, to give more insight in the amount of P4 that is present in the prills. More P4 can be observed with a 40x magnification, this would result in Figure 39**.** P4 is more clearly visible. It is interesting to see that in powder form, the P4 has the property to really stick together, but in this image it seems like the P4 particles have moved freely through

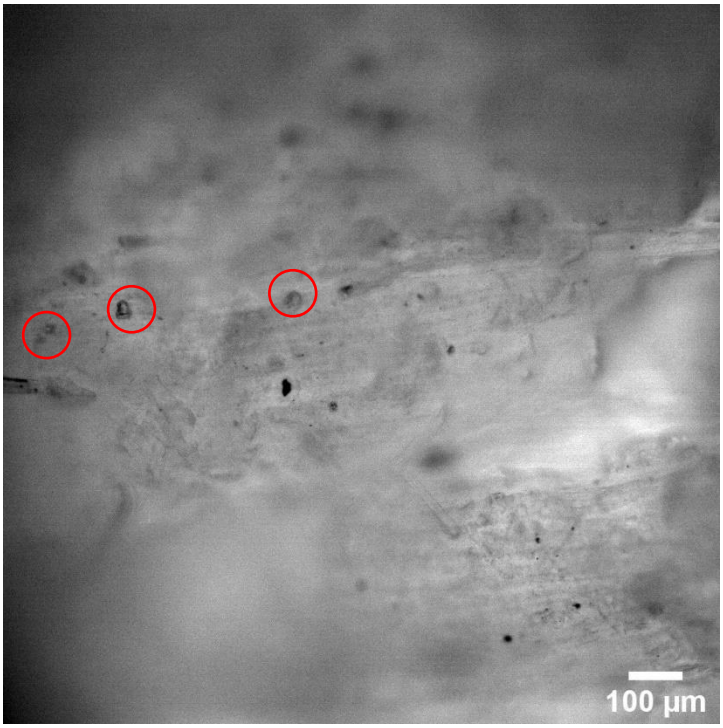

Figure 38: microscopic image of the inside of an urea +10wt% P4 prill. In the red circles some P4 is visible (10x magnification)

the liquid urea without clustering much together. Take note that although the P4 particles don't stick together, they are still found close together. Also in the 10wt% P4 prill, some small black cavities are present at the inside of the prill. They are however less visible at the outside of the prill, and doesn't seem to be affected by the presence of P4. The cavities can be formed due to two processes: the first one is that during cooling, urea is a bit decomposing resulting in small bubbles of gas, which are trapped in the droplet. Another explanation is that these cavities are the result of the cooling process, where the density of the solid is much higher compared than its liquid phase thus resulting in small holes.

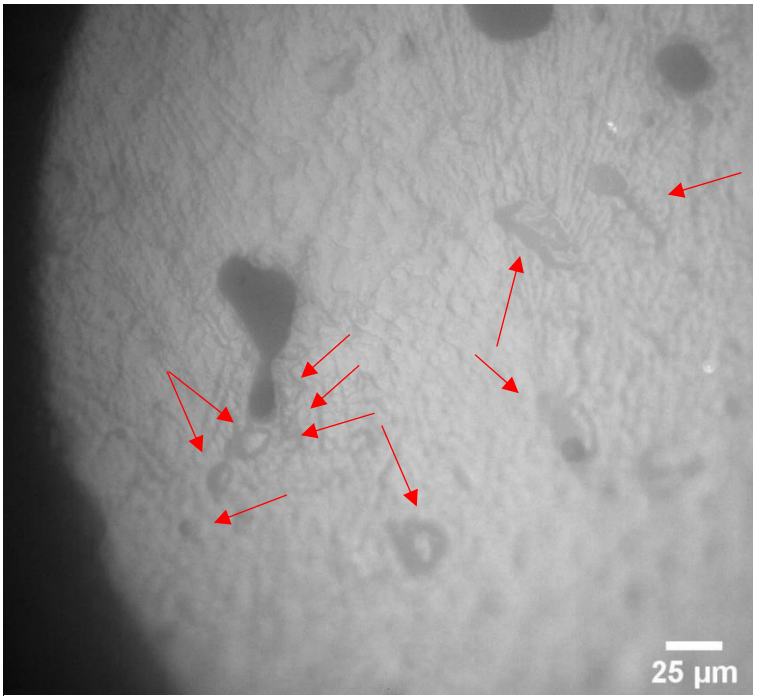

Figure 39: microscopic image of an urea +10wt% P4 prill (magnification of 40x). The arrows show some P4. Also some black cavities are visible here.

Finally, also prills containing 35wt% P4 have been analyzed as well. Since the prills were darker compared to the other prills, it was quite difficult to make the images sharp and search for P4 particles. It is expected that in Figure 40**,** the dark-grey spots are P4 particles, however this remains uncertain since it was impossible to make the image sharper. Otherwise, those are just some holes that are present on the other prills as well. The black cavities however are still present in the prills, but look much smaller compared to the other prills. Also no cutting marks are present here.

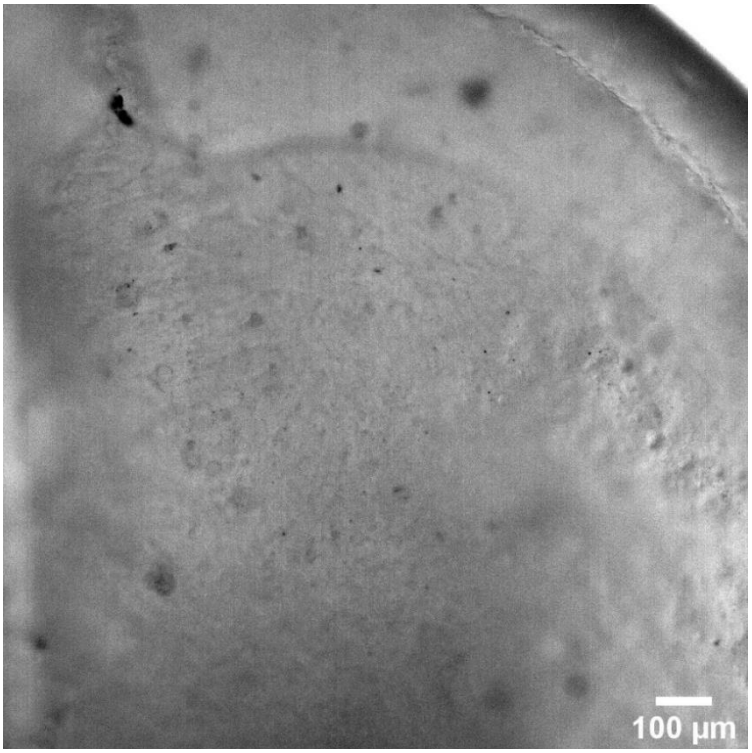

Figure 40: inside of a 35wt% P4 prill. The arrow show the shell of the prillMagnification: 10x.

When zooming in on another part of the same prill with a magnification of 40x, a border between shell and inside of the prill can be found, see Figure 41. Here, the right side is the inside of the prill, while the bottom left corner is the outer shell. The inside of the prill is not a sharp image because this part seems to be at a different height. This can indicate that the microstructure at the shell is somewhat different compared to the inside, but it can also just be an optical effect.
Since it was difficult to analyze other sides of this prill as well with the current magnification, it is difficult to normalize the observations here for the whole prill, but it is

noteworthy to say that here it is hard to detect P4 particles. It is still possible they are there, since it is difficult to detect due to the color of the prill, but it can be interesting for further research to analyze the locations where P4 is present and if there are spots where they aren't present at all.

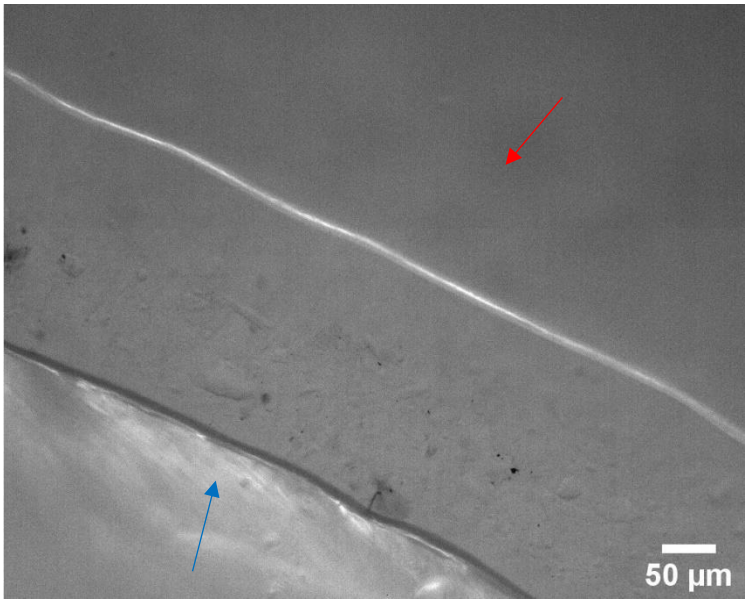

Figure 41: the distinctive shell of a 35wt% P4 prill. Magnification: 20x. The red-arrow is pointing at the inside of the prill, while the blue arrow show the outer-layer of the prill. The black spots are expected to be small cavities.

5.4.3 Prill size

The prills have been produced with a nozzle of 1mm diameter. With the desired jet breakup, the droplets are expected to have a diameter of around 1.9mm. This has been calculated with formula (16). Since the setup experienced the more chaotic (faucet) dripping regime, the droplets that have been formed have a more unpredictable diameter. Also, they are slightly larger than expected, which can be seen in Table 9**.**

	Mean prill diameter [mm]	Standard deviation [mm]	Roundness
Urea	3.25	0.565	0.941
Urea+10wt% P4	2.90	0.427	0.940
Urea+35wt% P4	2.87	0.443	0.935
Urea+10wt% P4 10 min grinded	3.31	0.519	0.946
Urea+35wt% P4 10 min grinded	3.12	0.580	0.933

Table 9: prill sizes & roundness of the different types of prills.

The diameters or sizes of the prills have been measured with ImageJ [62]. Pictures of the prills were taken and calibrated with a caliper. This can be seen in Appendix A: prills measurements. Now in ImageJ, the prills could be measured. The batches contained between 227 and 291 prills. Next to the diameter of the prills, also the roundness has been determined. As can be seen in the Table 9**,** all the prills have a very high roundness, thus indicating that the prills are quite spherical. This will validate the assumptions made in section 5.4.1. Since there are also some satellite droplets present, the data has been split. The data that is represented here only show the mean size, roundness and standard deviation of usable prills. Data from the satellites has been removed here, but will be analyzed later on in table Table 10. In order to do this, an assumption has been made while using Figure 42. It has been assumed that all satellite droplets have a diameter which is smaller than 1.75mm. Everything above it will be discussed as a main droplet or prill, everything below as a satellite. The formation of satellite droplets during the experiments can be seen in Figure 27.

As can be observed in Table 9, there is a weak relationship between P4 concentration and the diameter of the prills. When increasing the concentration of P4 in the suspension, it seems the mean diameter of the prills will drop slightly. In the not-grinded sample, the prill mean diameter will drop from 3.25mm to 2.87mm. This is also visible in the second batch where P4 has been grinded for 10 minutes. Here, the mean size also decreases with increasing P4 concentration. It is remarkable that the mean size of these prills are larger than the mean size of the not-grinded prills. This can be explained. According to [75], increasing particle size and concentration will also increase the surface tension of the suspension. Since an increase in surface tension will prevent droplets to grow more, the droplets will be much smaller when they fall down. It was unfortunately not possible to analyze the surface tension of the suspension with a goniometer, since the suspension has to be heated to too high temperatures, which the current goniometer can't reach. Next to that, the needle that is used here can be clogged due to the presence of the P4 particles. It is otherwise recommended to use the prilling setup with a camera and another nozzle to analyze this property in the future. Also, the grinded samples do contain much smaller P4 particles compared to the not grinded samples, hence decreasing the surface tension of the suspension, resulting in bigger droplets compared to the other suspensions. Take note however that the droplet size is also depending on the viscosity of the suspension. An increase in viscosity will result in larger droplets, see equation (16). Overall, it depends on the combination of both the viscosity and the surface tension. It is possible that the

surface tension is more sensitive to particle size than viscosity, but more research would be required for this.

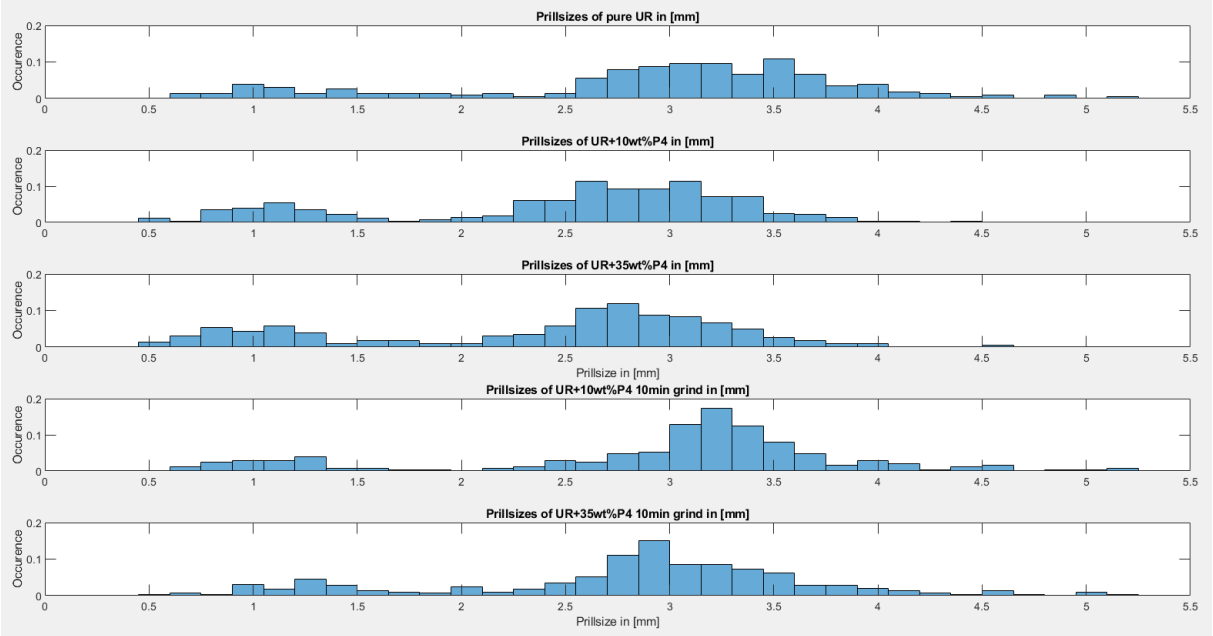

Figure 42: the measured prillsizes. Take note that the peaks at the left are satellite droplets.

Next to this, the prill size has also been plotted in Figure 42. It was difficult to collect all satellite droplets since they were small, but still they are visible when plotted. Therefore, they are also analyzed here. In Table 10, data can be found about the satellite droplets. According to this data, also the size of the satellite droplets is slightly reduced at higher P4 concentrations, but the effect seems less compared to the pure prills. Take a note that the prills have a diameter of about 3 times the nozzle size while the satellite droplets have a diameter which is almost equal to the nozzle diameter.

Also it seems like the amount of satellite droplets will increase at increased P4 concentration. When prilling urea, 15.7% of the analyzed batch did contain satellite droplets, while with the not-grinded samples there are much more satellite droplets present. Take note however that it was quite difficult to collect the satellite droplets, and not all prills were sharp enough on the images to analyze them, so these values have a big uncertainty. It also doesn't really fit well in other experiments. According to *McIlroy* [31], increasing the size or volume fraction of the particles will reduce the amount of satellite droplets. In this experiment, the opposite is happening. When increasing the volume fraction, more satellite droplets will form but when decreasing the particle size the amount of satellites will also be reduced. Therefore, it is expected that this result obtained in this thesis is influenced by the difficulties collecting satellite droplets.

	Prill diameter [mm]	Satellite droplet diameter [mm]	Amount of sat. droplets
Urea	3.25	1.16	15.7%
Urea+10wt% P4	2.90	1.10	21.4%
Urea+35wt% P4	2.87	1.05	27.8%
Urea+10wt% P4 10 min grinded	3.31	1.11	15.3%
Urea+35wt% P4 10 min grinded	3.12	1.22	15.5%

Table 10: diameter of the prills and satellite droplets.

6 Conclusion & Discussion

The objectives of this MSc research project were to investigate how high-quality fertilizer grains can be produced by analyzing how urea and ammonium nitrate suspensions containing polyhalite particles can be optimally prilled. An experimental setup was designed to assess how molten liquid jets of Urea with suspended polyhalite particles can be optimally prilled for producing high-quality fertilizer grains. For the experimental setup, the focus was mainly on how to heat, mix and pump the suspension through the prilling equipment. It is important to reach an equal heat and particle distribution without clogging the equipment, and produce monodisperse prills. The first can be visually observed during prilling: if the liquid suspension is flowing out of the system without solidifying directly, the heat distribution is good enough since the wall is kept at a constant maximum temperature. The latter can be observed during analyzing the P4 concentration in each prill, where it is desired to have the same concentration of P4 in each prill.

During the research, obtaining the size of P4 particles was rather important since this could explain the behavior that has been observed in other experiments. However, this was rather difficult to analyze, since the particles seem to clog together. This made it impossible to automatically determine all particle sizes in one image with computer programs. Therefore, all particles were measured by hand, which could unwillingly lead to errors: only the clearer particles could be measured. These are most times the somewhat larger particle, which explains why the effect of grinding does seem negligible in particle sizes. For analyzing P4 particles, it is recommended to try other fluids to submerge P4 in, where P4 will be less sticking together and to analyze if there is also much P4 clogging together in liquid urea, since this can explain the previous assumptions. However, the viscosity measurements do show that grinding did have an effect on the viscosity and hence on the particle size. It can be therefore interesting to investigate how to prevent clogging of these particles to more accurately obtain the sizes of the particles.
Next to that, other methods to decrease P4 particle size would be desirable. Grinding by hand is not consistent. This was also visible in the samples: the particles did have a large range of different sizes, between 0.5 micron to 40 micron. To adequately connect the viscosity measurements with particle sizes, it is recommended to obtain a more uniform distribution of particles with professionally grinding methods.

It can be seen however that our findings are comparable with literature. The grinded P4 particles resulted in a higher viscosity of the suspension compared to the not-grinded batches. This indicates that smaller P4 particles will increase the viscosity of the suspension. The higher the viscosity is however, the more force is required to prill the suspension. It was however interesting to see that this effect was larger on the less concentrated suspension; it even reached with grinding for ten minutes about the same apparent viscosity as the suspension with a larger mass fraction of particles. Therefore it is recommended for the prilling process of this suspension to obtain rather large P4 particles. One would expect that this will also increase however the amount of clogging in the nozzle. However up to now, clogging inside the nozzle was only observed when using a nozzle with a diameter of 0.6mm. The 1mm nozzle did not resulted in clogging. By increasing P4 sizes, it can be necessary to increase the nozzle size as well. The Mendoza and the MPQ-model were found to describe the viscosity of the 35wt% P4 sample rather well, but it didn't provide a satisfying explanation for the behavior of the 10wt% P4 sample, since the measured viscosity was too high according to models.

Visually, there was not much difference in the ability to prill between the 35wt% P4 suspension and the 10wt% P4 suspension. The difference however between pure urea and the suspensions was large. Forming droplets with the suspension was more difficult compared to pure urea. This probably

has something to do with the shear rate inside the nozzle. Here, the shear rate will reach about 5000 s^{-1}, which can lead to unexpected behavior such as shear thickening effects. This explains as well why the suspension is more difficult to prill since this effect will increase the viscosity significantly. It is expected that this also leads to inconsistent droplet formations, since the shear thickening effects will lead to an equilibrium where the suspension will be both slowed down as accelerating: the shear rate will also go up, which will result in a higher viscosity due to shear thickening effects. When the viscosity and thus shear stress is higher, the suspension will move slower through the nozzle resulting in a lower shear rate, which will be repeated. It is therefore recommended to investigate the viscosity of the suspension at very large shear rates of about 5000 s^{-1}. Increasing the diameter of the nozzle will also decrease this effect. This was however not possible to measure with the current experimental setup since this was designed for a nozzle between 0.5 and 1mm diameter. Larger nozzles would here require a larger heater.

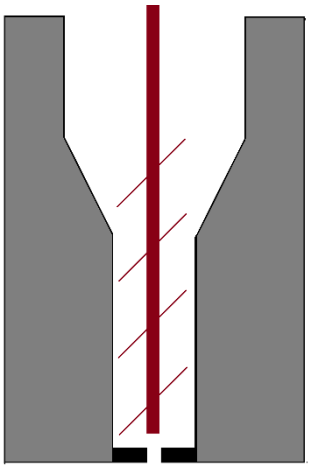

Figure 43: schematic overview for the upgraded setup, which needs a suspension that has been melted beforehand. The gray part will be the heater. This will let the tube, nozzle and funnel remain a constant temperature. The screw (in red) will push the suspension out of the nozzle. Note that here no sealing ring is required.

Unfortunately, the setup was unable to form a jet. This was due to a few effects. First of all, the diameter of the tube was too small. The screw wasn't heated, so when heating up the tube, some of the powder will melt at the top of the setup and some will stick to the cold screw, resulting in the formation of hard lumps. This decreased the throughput much of the design since the lumps prevented powder to move downwards. Increasing the size of the tube and screw will result in a larger gap, which will allow some urea to stick on before clogging. Another method to prevent this is by melting the suspension beforehand. This will prevent the formation of lumps sticking at the screw. This was however not possible with the current setup, since the suspension will solidify immediately when it is in contact with the funnel, which doesn't contain a heater in the current design. In a upgrade, it is possible to heat the funnel as well, which will make it possible to put the liquid suspension in it beforehand. This will also reduce the screw length since the suspension is already molten. To visualize this recommended upgrade, a schematic overview is given in Figure 43. Another reason why the setup wasn't able to form a jet, was because the pitch of the screw was too large. Decreasing this will push the powder forward, which will build up the pressure for the jet. Now due to the large pitch, when increasing the pressure, the liquid will just stay in their position.

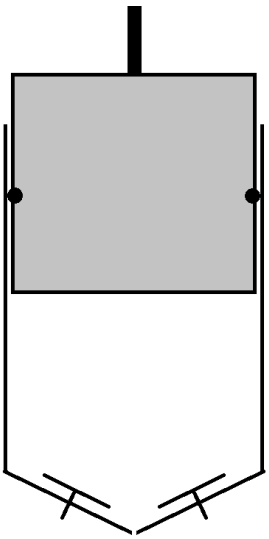

Figure 44: an example of the proposed prilling piston. At the bottom, two mixers will mix the suspension. However, the piston is unable to prill all the liquid out of the tube.

The idea behind building the setup containing a screw was to make the process semi-continuous. When succeeded, the setup would be able to constantly prill the suspension without the need to refill and wait for the material to be completely molten. This seemed however not possible with the current design. The setup could work if the suspension is melted beforehand and added to a heated funnel and tube. Otherwise only for experimental purposes, a simple prilling piston can be build. There is however a disadvantage with this method, since it is difficult to mix the suspension when heating up in a piston. It can be possible to add a mixing device in this setup, but

this will prevent prilling all the molten substance through the device. An example of such a device can be seen in Figure 44. Since the sealing-rings will experience axial movement of the piston, high temperatures and has to be resistant against urea fumes, a FFKM or FEPM O-ring or X-ring will be recommended [78]. Simple mixers with heat and urea resistant materials would be sufficient, only to prevent the sedimentation of P4. However, implementing mixers into the design would be quite difficult since it will lead to some open parts where the suspension can go through. Therefore, a smaller device without mixers would probably lead to higher chances for success, but this will decrease the monodisperse P4 distribution over the prills. Since this device contains more critical parts and is difficult to build compared to the screw-priller, it is recommended to first implement the recommended upgrades before changing to a new type of prilling device.

The setup was however able to make some prills by dripping the suspension in sunflower oil. The prills were collected and analyzed. It seemed like the 35wt% P4 suspension prills did not contain as much P4 as was measured beforehand. It is possible that some of the P4 powder was still sticking at the funnel when prilling the suspension, resulting in a lower concentration of P4 in the prills. The prills of both batches did not contain an equal amount of P4. The 10wt% P4 prills did contain between 0 and 30% P4 while the 35wt% P4 prills did vary between 5% and 60% P4. P4 has the property to clog together much. This will probably lead to some prills containing a lot of P4 which was clogged together beforehand and some prills containing almost no P4. When analyzing the prills under a microscope, sometimes some P4 was visible, but it remained rather difficult to detect, since the particles are rather small and have almost the same color as urea. Finally, a relationship between prill size and P4 concentration was found. By increasing the concentration of P4 in the suspension, the diameter of the prills dropped. However, the standard deviation of the prill sizes is larger than the difference between each sample, but this result was consistent in all the batches. In order to reach a monodisperse size distribution of the prills, it is recommended to use a steppermotor which can deliver higher torques: this will let the screw rotate smoothly and higher velocities can be reached, which are desirable for the formation of a jet.

Overall, this thesis will give more insight in the behavior of prilling suspensions, where the influence of particles on the viscosity and prill properties have been investigated. Unfortunately, the setup was unable to form jets. For future experiments, more information about the surface tension of the suspension would be required, and some changes would be necessary in the current design, where it is recommended to pre-melt the suspension. If this doesn’t lead to a jet, a simple piston would be also sufficient. Finally, it is also recommended for future experiments to analyze the physics in the regimes the prilling process takes in place, such as at high shear rates. This will give more insight in how to optimally prill suspensions, which will eventually lead to high quality prills.

Bibliography

[1] Unctas, GDS, and MDPB, “The 2008 Food Price Crisis: Rethinking Food Security Policies Anuradha Mittal UNITED NATIONS CONFERENCE ON TRADE AND DEVELOPMENT UNITED NATIONS,” 2008.

[2] X. Tian, B. A. Engel, H. Qian, E. Hua, S. Sun, and Y. Wang, “Will reaching the maximum achievable yield potential meet future global food demand?,” *J Clean Prod*, vol. 294, p. 126285, Apr. 2021, doi: 10.1016/j.jclepro.2021.126285.

[3] D. Nepstad *et al.*, “Road paving, fire regime feedbacks, and the future of Amazon forests,” *For Ecol Manage*, vol. 154, no. 3, pp. 395–407, Dec. 2001, doi: 10.1016/S0378-1127(01)00511-4.

[4] R. Licker *et al.*, “Mind the gap: how do climate and agricultural management explain the ‘yield gap’ of croplands around the world?,” *Global Ecology and Biogeography*, vol. 19, no. 6, pp. 769–782, Nov. 2010, doi: 10.1111/j.1466-8238.2010.00563.x.

[5] John H. Lienhard, “Three-field crop rotation,” *https://www.uh.edu/engines/epi26.htm*.

[6] R. Lines-Kelly, “Plant nutrients in the soil,” *Wollongbar Agricultural Institute, Australia*, 1992.

[7] T. Nieboer, “The differences between prilling and granulation,” *https://www.kreber.nl/knowledge-center/prilling-meaning-and-prill-definition* .

[8] J. Chen *et al.*, “Environmentally friendly fertilizers: A review of materials used and their effects on the environment,” *Science of The Total Environment*, vol. 613–614, pp. 829–839, Feb. 2018, doi: 10.1016/j.scitotenv.2017.09.186.

[9] C. O. Dimkpa, J. Fugice, U. Singh, and T. D. Lewis, “Development of fertilizers for enhanced nitrogen use efficiency – Trends and perspectives,” *Science of the Total Environment*, vol. 731. Elsevier B.V., Aug. 20, 2020. doi: 10.1016/j.scitotenv.2020.139113.

[10] Khalil and Makhol, “Granules of polyhalite and urea,” Apr. 01, 2021

[11] T. Nieboer, “Meaning of prilling,” *https://www.kreber.nl/knowledge-center/prilling-meaning-and-prill-definition* .

[12] C. M. van’t Land, *Industrial crystallization of melts*. Marcel Dekker, 2005.

[13] S. N. Saleh, S. M. Ahmed, D. Al-mosuli, and S. Barghi, “Basic design methodology for a prilling tower,” *Canadian Journal of Chemical Engineering*, vol. 93, no. 8, pp. 1403–1409, Aug. 2015, doi: 10.1002/cjce.22230.

[14] R.-J. Roe, “Wetting of fine wires and fibers by a liquid film,” *J Colloid Interface Sci*, vol. 50, no. 1, pp. 70–79, Jan. 1975, doi: 10.1016/0021-9797(75)90255-6.

[15] J. Eggers and E. Villermaux, “Physics of liquid jets,” *Reports on Progress in Physics*, vol. 71, no. 3, Mar. 2008, doi: 10.1088/0034-4885/71/3/036601.

[16] S. N. Saleh and S. Barghi, “Reduction of fine particle emission from a prilling tower using CFD simulation,” *Chemical Engineering Research and Design*, vol. 109, pp. 171–179, May 2016, doi: 10.1016/j.cherd.2016.01.017.

[17] A. O. Gezerman, “Mathematical modeling for prilling processes in ammonium nitrate production,” *Engineering Reports*, vol. 2, no. 6, Jun. 2020, doi: 10.1002/eng2.12173.

[18] W. Yuanf, B. Chuanping, and Z. YuxinM, “An Innovated Tower-fluidized Bed Prilling Process,” 2007.

[19] A. M. Ganan-Calvo *et al.*, “The natural breakup length of a steady capillary jet,” Aug. 2019, [Online]. Available: http://arxiv.org/abs/1908.10841

[20] C. J. Gurney, M. J. H. Simmons, V. L. Hawkins, and S. P. Decent, “The impact of multi-frequency and forced disturbances upon drop size distributions in prilling,” *Chem Eng Sci*, vol. 65, no. 11, pp. 3474–3484, 2010, doi: 10.1016/j.ces.2010.02.030.

[21] B. Ambravaneswaran, H. J. Subramani, S. D. Phillips, and O. A. Basaran, “Dripping-Jetting Transitions in a Dripping Faucet,” *Phys Rev Lett*, vol. 93, no. 3, p. 034501, Jul. 2004, doi: 10.1103/PhysRevLett.93.034501.

[22] R. M. Erb, D. Obrist, P. W. Chen, J. Studer, and A. R. Studart, “Predicting sizes of droplets made by microfluidic flow-induced dripping,” *Soft Matter*, vol. 7, no. 19, p. 8757, 2011, doi: 10.1039/c1sm06231j.

[23] I. Pavlenko *et al.*, “Effect of superimposed vibrations on droplet oscillation modes in prilling process,” *Processes*, vol. 8, no. 5, May 2020, doi: 10.3390/PR8050566.

[24] S. P. Decent, A. C. King, and I. M. Wallwork, “Free jets spun from a prilling tower,” 2002.

[25] A. P. Deshpande, J. M. Krishnan, and P. B. S. Kumar, *Rheology of complex fluids*. Springer New York, 2010. doi: 10.1007/978-1-4419-6494-6.

[26] P. Kundu, Cohen Ira, and Dowlin David, *Fluid Mechanics*, 6th ed. Academic Press, 2015.

[27] C. Macosko, R. Ewoldt, and G. McKinley, “Introduction to rheology fundamentals,” *Rheology: Principles, Measurements and Applications*, vol. 2nd Edition, no. DRAFT, 2021.

[28] E. van der Borght, “An investigation into the addition of polyhalite to nitrogen fertilizers,” 2021. [Online]. Available: http://repository.tudelft.nl/.

[29] J. Château and H. Lhuissier, “Breakup of a particulate suspension jet,” *Phys Rev Fluids*, vol. 4, no. 1, Jan. 2019, doi: 10.1103/PhysRevFluids.4.012001.

[30] M. S. van Deen, T. Bertrand, N. Vu, D. Quéré, E. Clément, and A. Lindner, “Particles accelerate the detachment of viscous liquids,” *Rheol Acta*, vol. 52, no. 5, pp. 403–412, May 2013, doi: 10.1007/s00397-013-0691-9.

[31] C. McIlroy and O. G. Harlen, “Modelling capillary break-up of particulate suspensions,” *Physics of Fluids*, vol. 26, no. 3, Mar. 2014, doi: 10.1063/1.4866789.

[32] B. Dubey, W. Case, and E. J. Windhab, “Processing of functional capsule powder particles based on multiple emulsions using a prilling process,” in *Process-Spray: Functional Particles Produced in Spray Processes*, Springer International Publishing, 2016, pp. 941–985. doi: 10.1007/978-3-319-32370-1_23.

[33] “Changing the Properties of Particles to Control Their Rheology,” 2015. [Online]. Available: https://www.azom.com/article.aspx?ArticleID=12304

[34] B. J. Konijn, O. B. J. Sanderink, and N. P. Kruyt, “Experimental study of the viscosity of suspensions: Effect of solid fraction, particle size and suspending liquid,” *Powder Technol*, vol. 266, pp. 61–69, 2014, doi: 10.1016/j.powtec.2014.05.044.

[35] V. Babrauskas and D. Leggett, “Thermal decomposition of ammonium nitrate,” *Fire Mater*, vol. 44, no. 2, pp. 250–268, Mar. 2020, doi: 10.1002/fam.2797.

[36] G. H. Bagheri, C. Bonadonna, I. Manzella, and P. Vonlanthen, “On the characterization of size and shape of irregular particles,” *Powder Technol*, vol. 270, no. Part A, pp. 141–153, Jan. 2015, doi: 10.1016/j.powtec.2014.10.015.

[37] E. P. Cox, “A Method of Assigning Numerical and Percentage Values to the Degree of Roundness of Sand Grains,” 1927. [Online]. Available: https://www.jstor.org/stable/1298056

[38] M. Skydanenko, V. Sklabinskyi, and S. Saleh, “CFD simulation of ammonium nitrate melt in a perforated rotating bucket,” in *Lecture Notes in Mechanical Engineering*, Pleiades Publishing, 2019, pp. 498–506. doi: 10.1007/978-3-319-93587-4_52.

[39] M. B. Hocking, “Ammonia, Nitric Acid and Their Derivatives,” in *Handbook of Chemical Technology and Pollution Control*, Elsevier, 2005, pp. 321–364. doi: 10.1016/B978-012088796-5/50014-4.

[40] M. G. Mason, “Ammonium Nitrate Vs Urea,” Western Australia, Perth, 1969. [Online]. Available: https://researchlibrary.agric.wa.gov.au/rqmsplant

[41] S. B. DuTeaux, “Texas City Disaster,” in *Encyclopedia of Toxicology*, Elsevier, 2014, pp. 519–520. doi: 10.1016/B978-0-12-386454-3.00086-5.

[42] S. Chaturvedi and P. N. Dave, “Review on Thermal Decomposition of Ammonium Nitrate,” *Journal of Energetic Materials*, vol. 31, no. 1, pp. 1–26, Jan. 2013, doi: 10.1080/07370652.2011.573523.

[43] D. H. Booth and V. C. Vinyardt, “DENSITY AND VISCOSITY OF AMMONIUM NITRATE, AMMONIUM NITRATE-POTASSIUM CHLORIDE AND AMMONIUM NITRATE-AMMONIUM PHOSPHATE MELTS.”

[44] D. R. Lide, *CRC Handbook of Chemistry and Physics*, 80th ed. Boca Raton, FL: CRC Press, 1999.

[45] D. S. Powlson and T. M. Addiscott, “NITROGEN IN SOILS | Nitrates,” in *Encyclopedia of Soils in the Environment*, Elsevier, 2005, pp. 21–31. doi: 10.1016/B0-12-348530-4/00905-X.

[46] C. J. Overdahl, G. W. Rehm, and H. L. Meredith, “Fertilizer Urea.”

[47] S. Tischer, M. Börnhorst, J. Amsler, G. Schoch, and O. Deutschmann, “Thermodynamics and reaction mechanism of urea decomposition,” *Physical Chemistry Chemical Physics*, vol. 21, no. 30, pp. 16785–16797, 2019, doi: 10.1039/c9cp01529a.

[48] P. M. Schaber, J. Colson, S. Higgins, D. Thielen, B. Anspach, and J. Brauer, “Thermal decomposition (pyrolysis) of urea in an open reaction vessel,” *Thermochim Acta*, vol. 424, no. 1–2, pp. 131–142, Dec. 2004, doi: 10.1016/j.tca.2004.05.018.

[49] A. Mehrez, A. H. H. Ali, W. K. Zahra, S. Ookawara, and M. Suzuki, “Study on Heat and Mass Transfer During Urea Prilling Process,” *International Journal of Chemical Engineering and Applications*, pp. 347–353, 2012, doi: 10.7763/ijcea.2012.v3.216.

[50] Y. E. Kamis, H. B. Eral, and W. P. Breugem, “Active control of jet breakup and droplet formation using temperature modulation,” *Phys Rev Fluids*, vol. 6, no. 10, Oct. 2021, doi: 10.1103/PhysRevFluids.6.103903.

[51] U. Yermiyahu, I. Zipori, I. Faingold, L. Yusopov, N. Faust, and A. Bar-Tal, “Polyhalite as a multi nutrient fertilizer-potassium, magnesium, calcium and sulfate,” *Isr J Plant Sci*, vol. 64, no. 3–4, pp. 145–157, 2017, doi: 10.1163/22238980-06401001.

[52] H. Xu, X. Guo, and J. Bai, “Thermal behavior of polyhalite: a high-temperature synchrotron XRD study,” *Phys Chem Miner*, vol. 44, no. 2, pp. 125–135, Feb. 2017, doi: 10.1007/s00269-016-0842-5.

[53] G. Wollmann, D. Freyer, and W. Voigt, “Polyhalite and its analogous triple salts,” *Monatshefte für Chemie - Chemical Monthly*, vol. 139, no. 7, pp. 739–745, Jul. 2008, doi: 10.1007/s00706-007-0835-7.

[54] M. Moss and G. M. Haseman, “Thermal conductivity of polyhalite and anhydrite from the site of the proposed waste isolation pilot plant,” 1981.

[55] N. M. U. Kerr McGee Mine, “Polyhalite,” *https://www.mindat.org/photo-784531.html*.

[56] C. Clanet and J. C. Lasheras, “Transition from dripping to jetting,” *J Fluid Mech*, vol. 383, pp. 307–326, Mar. 1999, doi: 10.1017/S0022112098004066.

[57] A.F. Mills, *Basic Heat and Mass Transfer*, 2nd ed. Essex: Pearson Education Limited, 2014.

[58] K. Pietrak and T. S. W. Wi´sniewski, “Journal of Power Technologies 95 (1) (2015) 14-24 A review of models for effective thermal conductivity of composite materials.”

[59] “Ansys Academic Research Mechanical.”

[60] Hau Tian, “Physics of electrorheological fluids,” 2005, pp. 235–340. doi: 10.1016/S1383-7303(05)80021-3.

[61] F. Mokobi, “Inverted Microscope- Definition, Principle, Parts, Labeled Diagram, Uses, Worksheet,” *https://microbenotes.com/inverted-microscope/*, Apr. 10, 2022.

[62] C. A. Schneider, W. S. Rasband, and K. W. Eliceiri, “NIH Image to ImageJ: 25 years of image analysis,” *Nat Methods*, vol. 9, no. 7, pp. 671–675, Jul. 2012, doi: 10.1038/nmeth.2089.

[63] O. R. Walton, “Review of adhesion fundamentals for micron-scale particles,” *KONA Powder and Particle Journal*, vol. 26, no. March, pp. 129–141, 2008, doi: 10.14356/kona.2008012.

[64] B. J. Konijn, O. B. J. Sanderink, and N. P. Kruyt, “Experimental study of the viscosity of suspensions: Effect of solid fraction, particle size and suspending liquid,” *Powder Technol*, vol. 266, pp. 61–69, 2014, doi: 10.1016/j.powtec.2014.05.044.

[65] H. M. Shewan and J. R. Stokes, “Analytically predicting the viscosity of hard sphere suspensions from the particle size distribution,” *J Nonnewton Fluid Mech*, vol. 222, pp. 72–81, Aug. 2014, doi: 10.1016/j.jnnfm.2014.09.002.

[66] P. Sollich, F. Lequeux, P. Hébraud, and M. E. Cates, “Rheology of Soft Glassy Materials,” *Phys Rev Lett*, vol. 78, no. 10, pp. 2020–2023, Mar. 1997, doi: 10.1103/PhysRevLett.78.2020.

[67] I. N. McCave, “Settling Velocity,” *Encyclopedia of Geology*, 2005.

[68] “MATLAB.” The MathWorks Inc., Natick, Massachusetts, 2022.

[69] “Transient, Three-Dimensional, Multiphase Pipe and Annular Flow,” 2012.

[70] J. H. Meessen, “Urea”, doi: 10.1002/14356007.a27.

[71] A. Hill, “Understanding the Links Between Rheology and Particle Parameters,” *https://www.americanlaboratory.com/913-Technical-Articles/35729-understanding-the-Links-Between-Rheology-and-Particle-Parameters/*, 2006.

[72] L. Lobry, E. Lemaire, F. Blanc, S. Gallier, and F. Peters, “Shear thinning in non-Brownian suspensions explained by variable friction between particles.” [Online]. Available: https://hal.archives-ouvertes.fr/hal-01765759v2

[73] J. J. Stickel and R. L. Powell, “Fluid mechanics and rheology of dense suspensions,” *Annual Review of Fluid Mechanics*, vol. 37. pp. 129–149, 2005. doi: 10.1146/annurev.fluid.36.050802.122132.

[74] F. Picano, W. P. Breugem, D. Mitra, and L. Brandt, “Shear thickening in non-Brownian suspensions: An excluded volume effect,” *Phys Rev Lett*, vol. 111, no. 9, Aug. 2013, doi: 10.1103/PhysRevLett.111.098302.

[75] D. Mei, Y. Fang, Z. Zhang, D. Guo, Z. Chen, and C. Sun, “Analysis of surface tension for nano-fuels containing disparate types of suspended nanoparticles,” *Powder Technol*, vol. 388, pp. 526–536, Aug. 2021, doi: 10.1016/j.powtec.2021.05.002.

[76] A. Galakhova *et al.*, “Corrosion of Stainless Steel by Urea at High Temperature,” *Corrosion and Materials Degradation*, vol. 2, no. 3, pp. 461–473, Aug. 2021, doi: 10.3390/cmd2030024.

[77] Malvern Instruments Limited, “Processing non-Newtonian products: Determining the pressure drop for a power law fluid along a straight circular pipe,” 2016. Accessed: Jul. 19, 2022. [Online]. Available: https://www.pharmaceutical-business-review.com/

[78] ERIKS, “Rubber materialen en compounds,” *https://eriks.nl/nl/producten/afdichtings-rubbertechniek/rubber-polymeren-compounds/*.

[79] C. Cramer, P. Fischer, and E. J. Windhab, “Drop formation in a co-flowing ambient fluid,” *Chem Eng Sci*, vol. 59, no. 15, pp. 3045–3058, Aug. 2004, doi: 10.1016/j.ces.2004.04.006.

[80] Q. Lehua, J. Xiaoshan, L. Jun, H. Xianghui, and L. Hejun, “Dominant Factors of Metal Jet Breakup in Micro Droplet Deposition Manufacturing Technique,” *Chinese Journal of Aeronautics*, vol. 23, no. 4, pp. 495–500, Aug. 2010, doi: 10.1016/S1000-9361(09)60246-6.

[81] A. Mehrez, A. H. H. Ali, W. K. Zahra, S. Ookawara, and M. Suzuki, “Study on Heat and Mass Transfer During Urea Prilling Process,” *International Journal of Chemical Engineering and Applications*, pp. 347–353, 2012, doi: 10.7763/ijcea.2012.v3.216.

[82] “Urea 46% N Prills,” *http://www.globalstocktrades.com/product/urea-46-n-prills/*.

Appendix A: prills measurements

The prills are measured as follow: the images which can be found above are loaded in ImageJ. Then, the program is calibrated. The distance between the two measuring points of the caliper will be measured in pixels, and translated into mm since the distance between the caliper measuring points are known (1.48 or 1.49mm). This will be measured about ten times for each image. The mean of these measurements will give the correct translation of the amount of mm per pixel. Now, we simply can draw measuring lines over each prill by hand with ImageJ. Also, the roundness can now be obtained by drawing points on the edges of each prill. ImageJ will automatically calculate the roundness with the Cox roundness method.

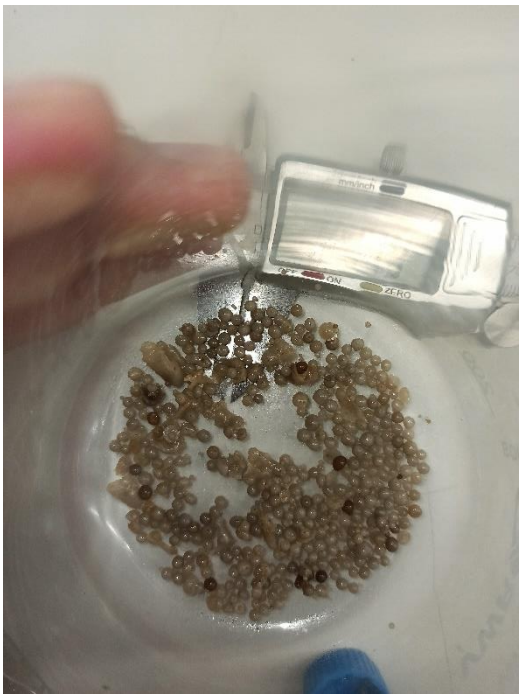

Figure 45: urea + 35wt% P4 prills, not grinded

Figure 46: pure urea prills

Figure 47: urea + 35wt% P4 prills, 10 minutes grinded

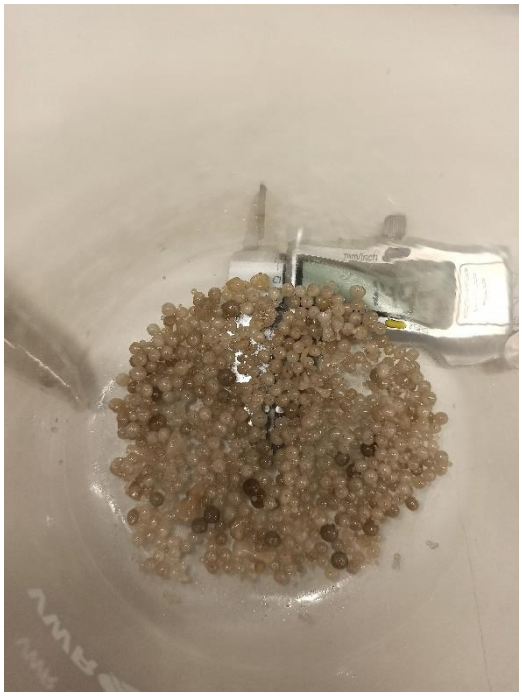

Figure 48: urea + 10wt% P4 prills, not grinded

Figure 49: urea + 10wt% prills, 10 minutes grinded

Appendix B: prills microscopy

Since the microscope that was used here was a inverted microscope, it was difficult to obtain images from the prills since they don't let light through. However, when using background light and UV light, it was possible to get some images. The images that are collected can be found below. More images of pure urea prills have been obtained compared to the suspensions since they have a white color, making observations more clear compared to the greyish prills containing P4.

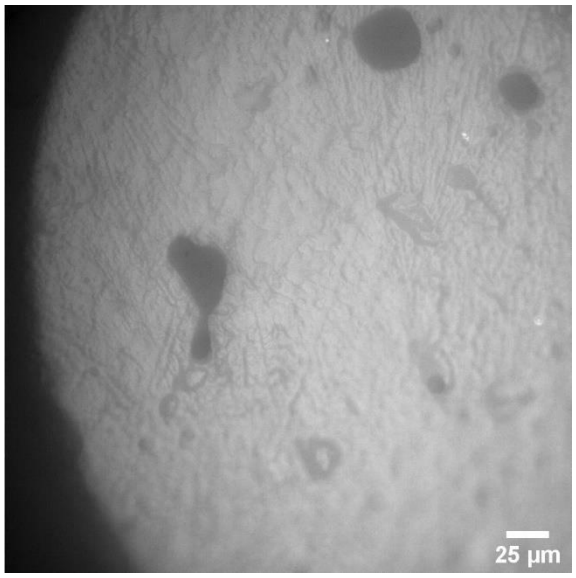

Figure 50: urea + 10wt% P4 prill at the shell, magnification: 40x.

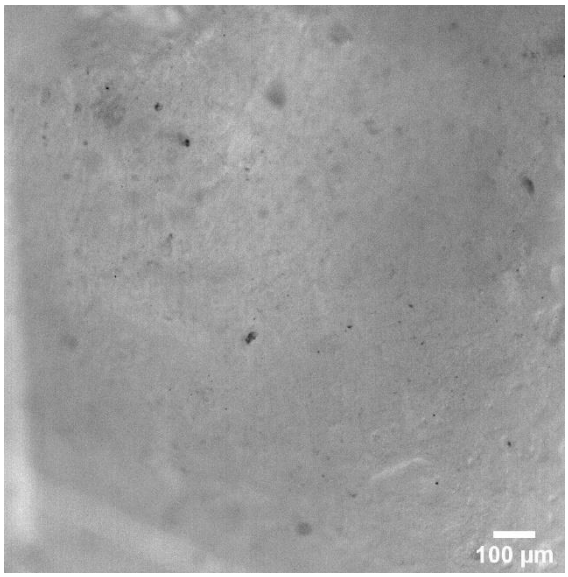

Figure 51: urea + 35wt% P4 prill, inside, magnification: 10x.

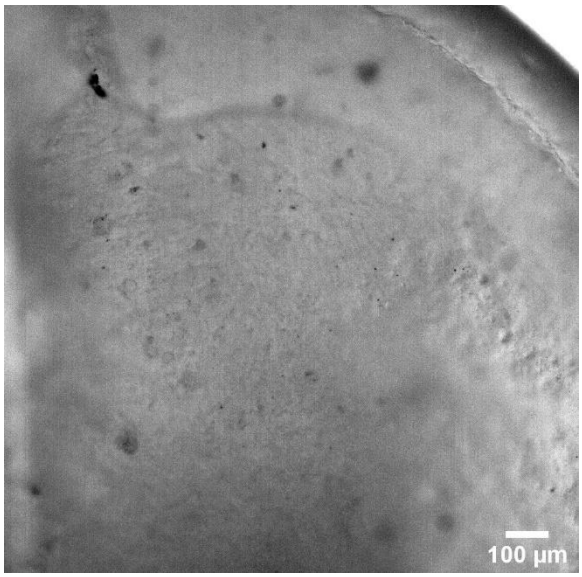

Figure 52: urea + 35wt% P4 prill, inside, magnification: 10x.

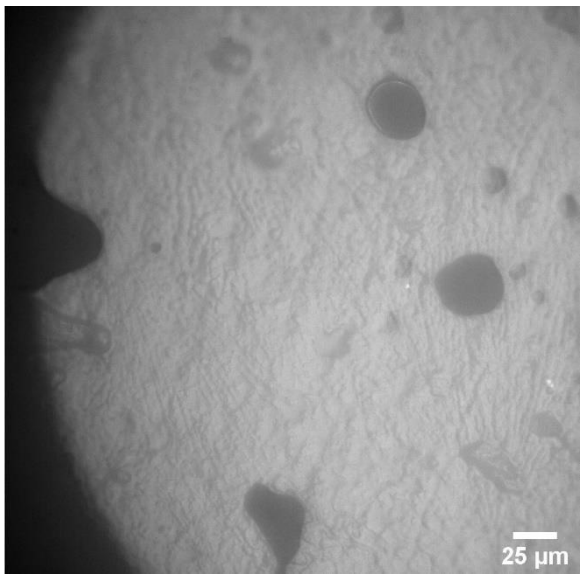

Figure 53: urea + 10wt% P4 prill at the shell, magnification: 40x.

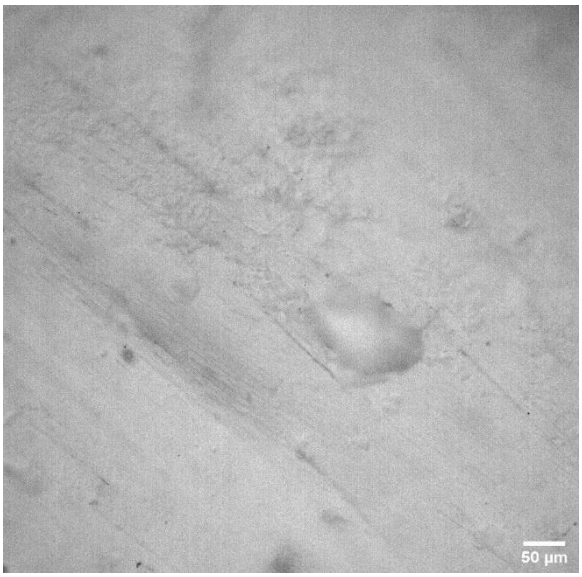

Figure 54: pure urea prill, inside. Magnification: 20x.

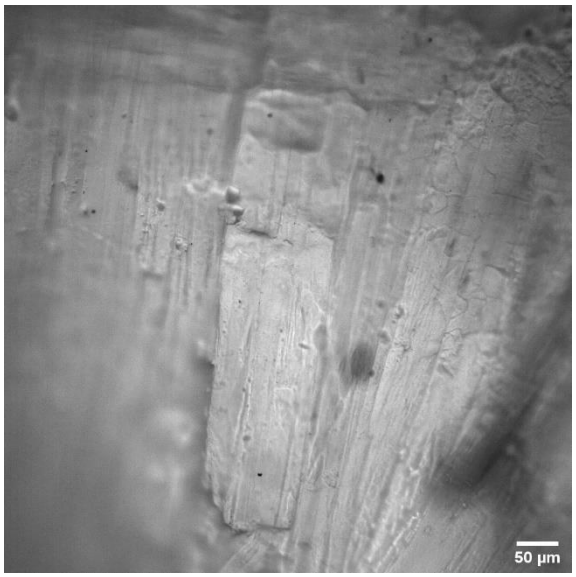

Figure 55: pure urea prill, inside. Magnification: 20x.

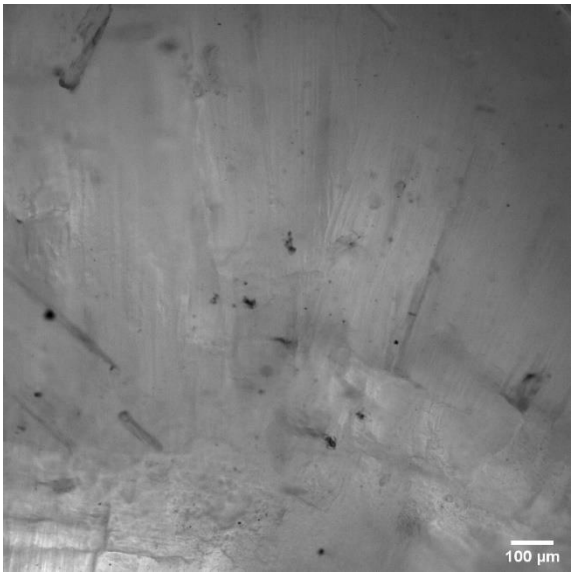

Figure 56: pure urea prill, inside. Magnification: 10x.

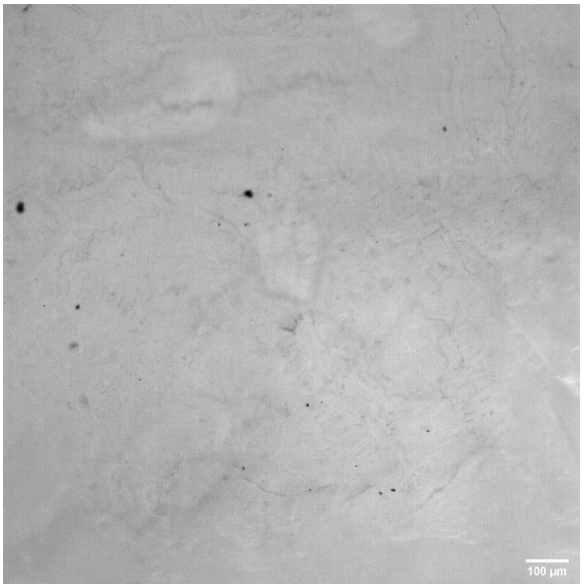

Figure 57: pure urea prill, inside. Magnification: 10x.

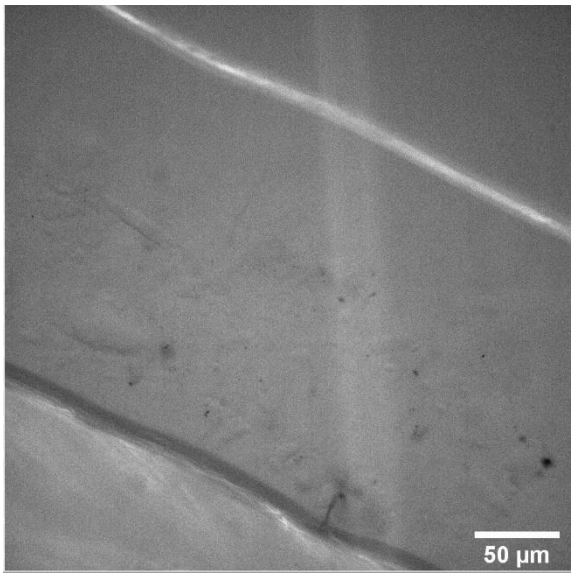

Figure 58: urea + 35wt% P4 prill at the inside. Magnification: 40x.

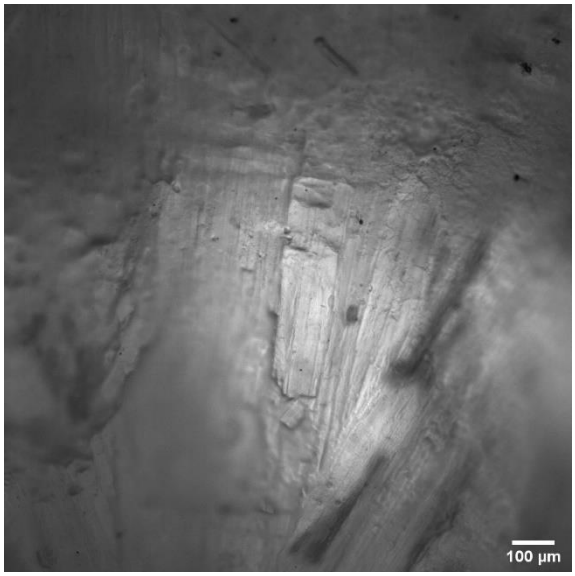

Figure 59: pure urea prill, inside. Magnification: 10x.

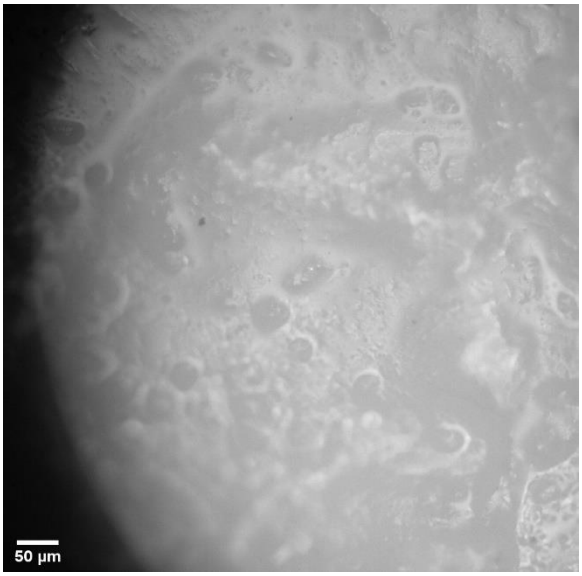

Figure 60: pure urea prill at the shell. Magnification: 20x.

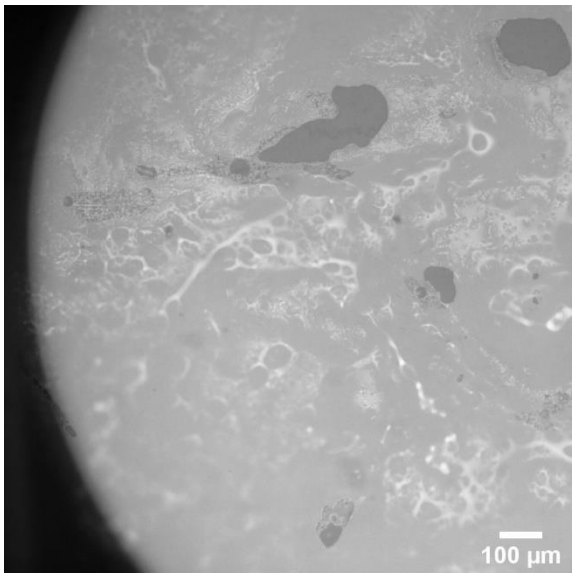

Figure 61: pure urea prill, at the shell. Magnification: 10x.

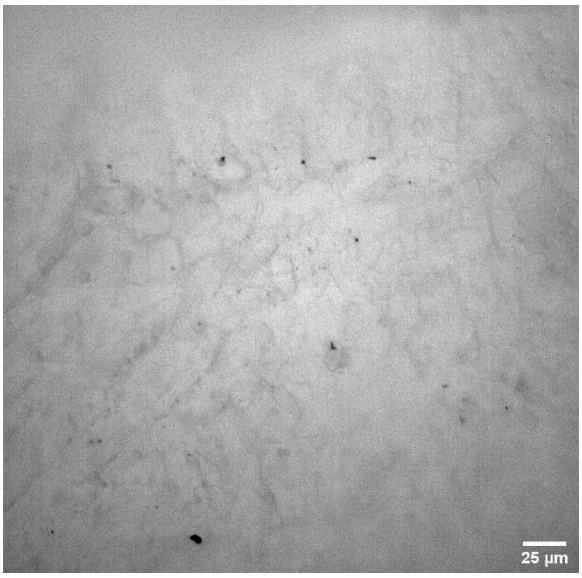

Figure 62: urea + 10wt% P4 prill, inside. Magnification: 40x.

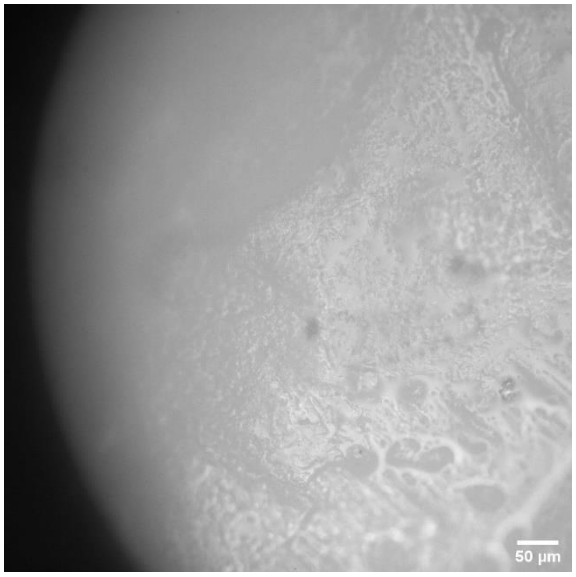

Figure 63: pure urea prill at the shell. Magnification: 20x.

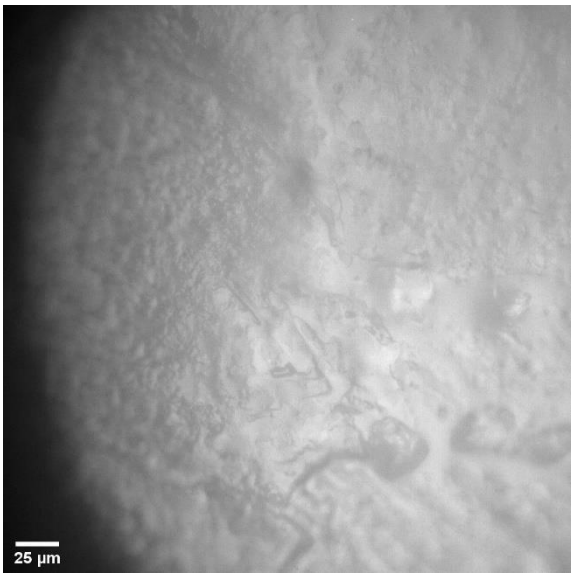

Figure 64: pure urea prill at the shell. Magnification: 40x.

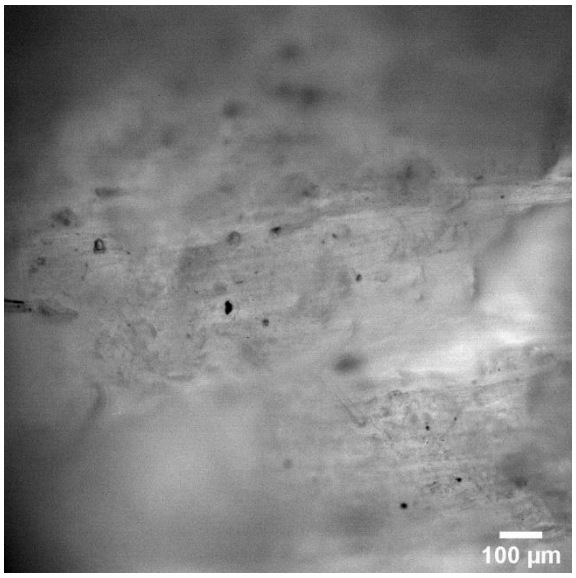

Figure 65: urea + 10wt% P4 prill, inside. Magnification: 10x.

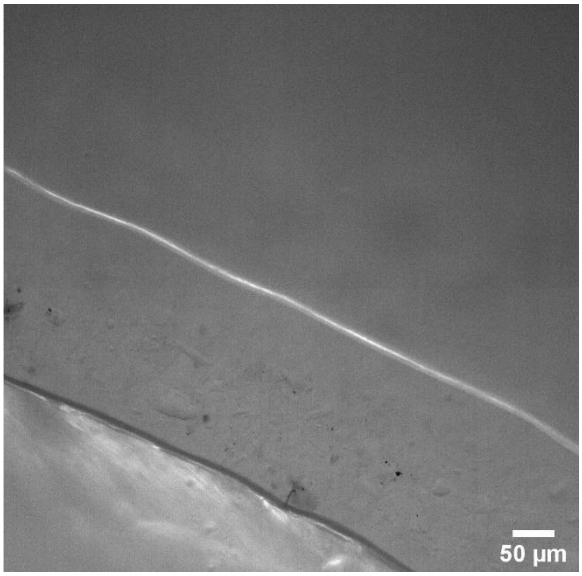

Figure 66: urea + 35wt% P4 prill at the inside. Magnification: 20x.

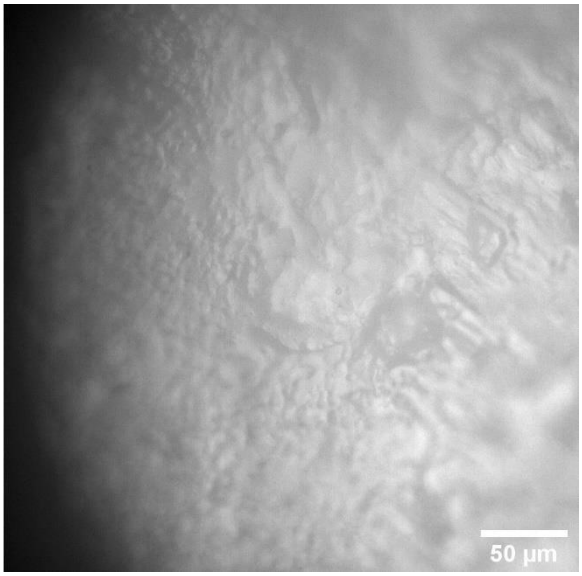

Figure 67: pure urea prill at the shell. Magnification: 40x.

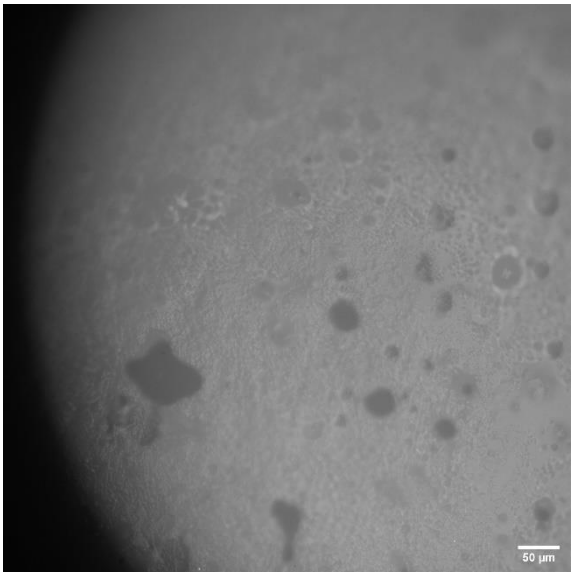

Figure 68: urea + 10wt% P4 at the shell. Magnification: 20x.

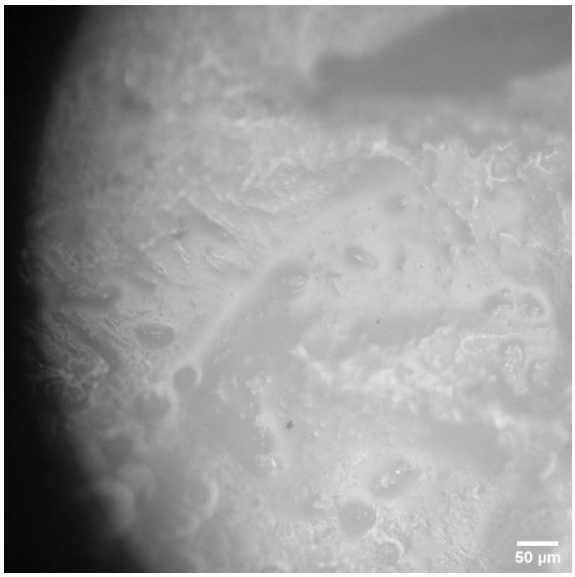

Figure 69: pure urea prill at the shell. Magnification: 20x.

Appendix C: P4 microscopy

Different images of P4 completely immersed in silicon oil are obtained with an inverted microscope. Often for the analyses, one image per batch did contain enough particles to analyze the size and shape; sometimes a larger magnification was required to more precisely determine the size of the particles. However, more images have been obtained.

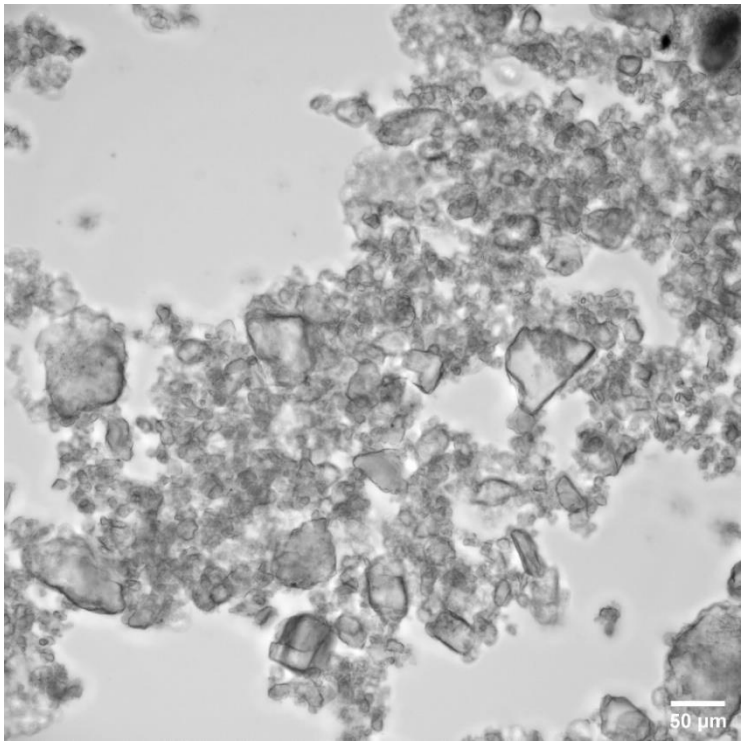

Figure 70: not grinded P4, magnification: 20x.

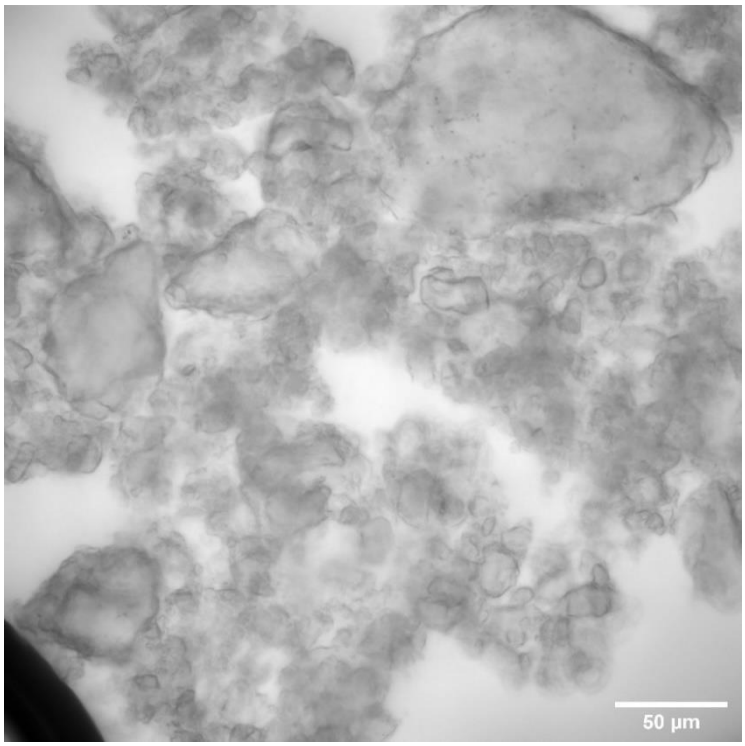

Figure 71: not grinded P4, magnification: 40x.

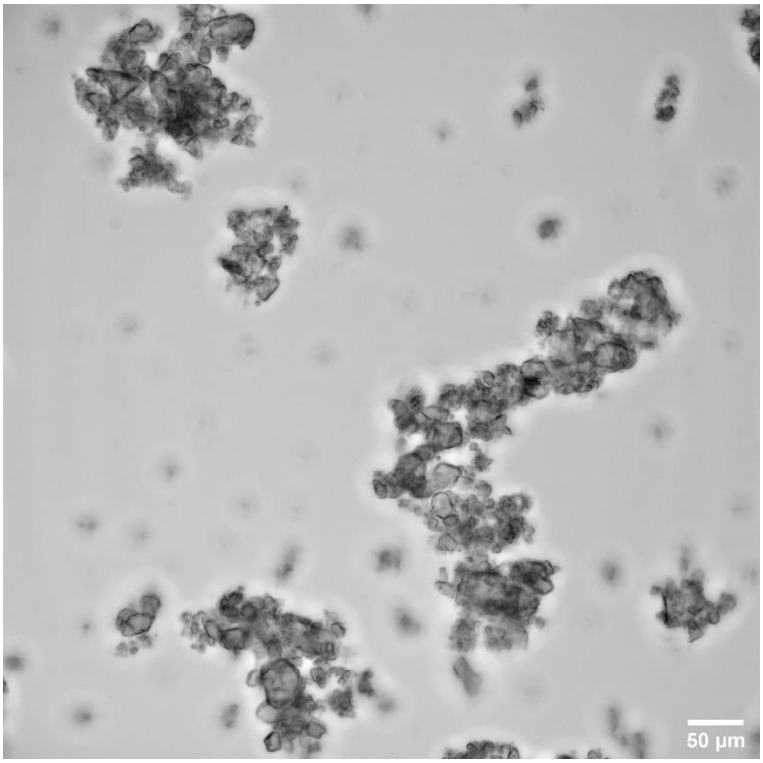

Figure 72: P4 grinded for 10 minutes, magnification: 20x.

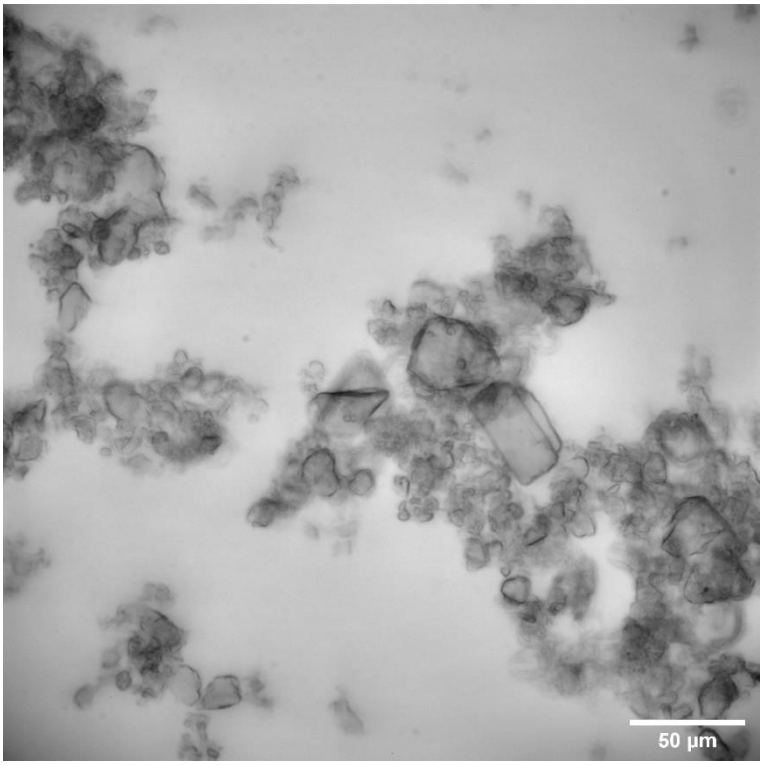

Figure 73: P4 grinded for 10 minutes, magnification: 40x.

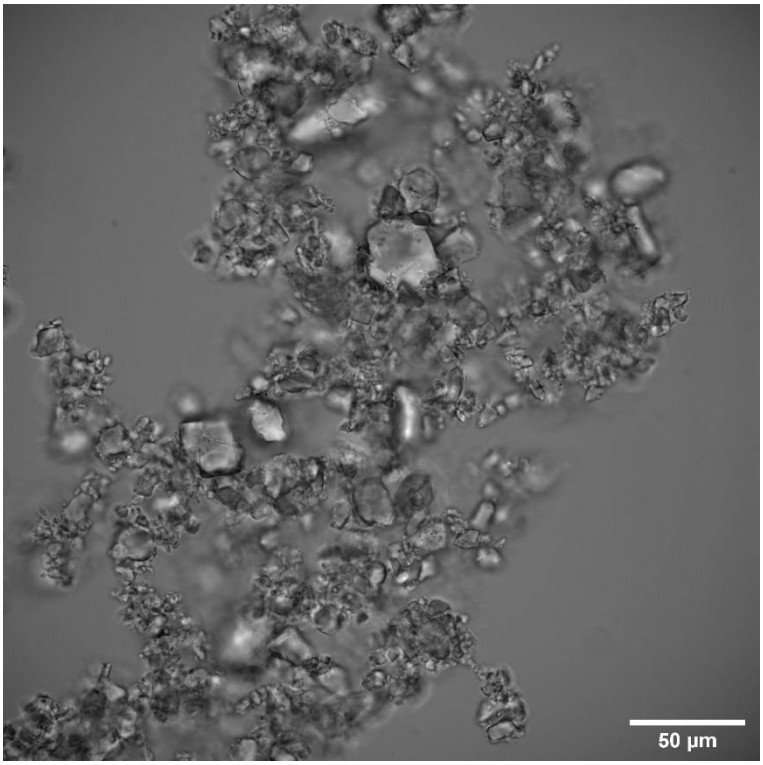

Figure 74: P4 grinded for 5 minutes, magnification: 40x.

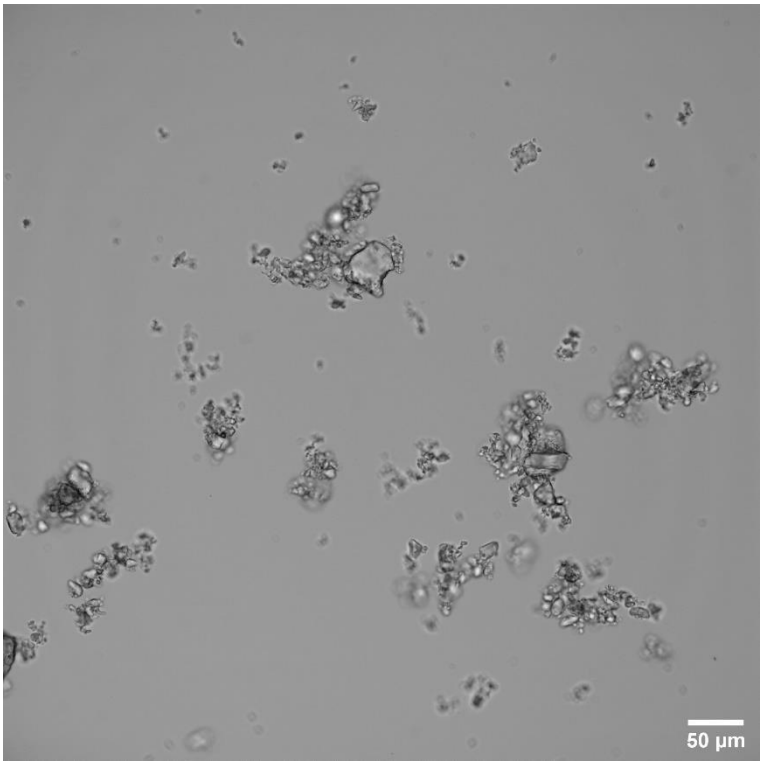

Figure 75: P4 grinded for 5 minutes, magnification: 20x.

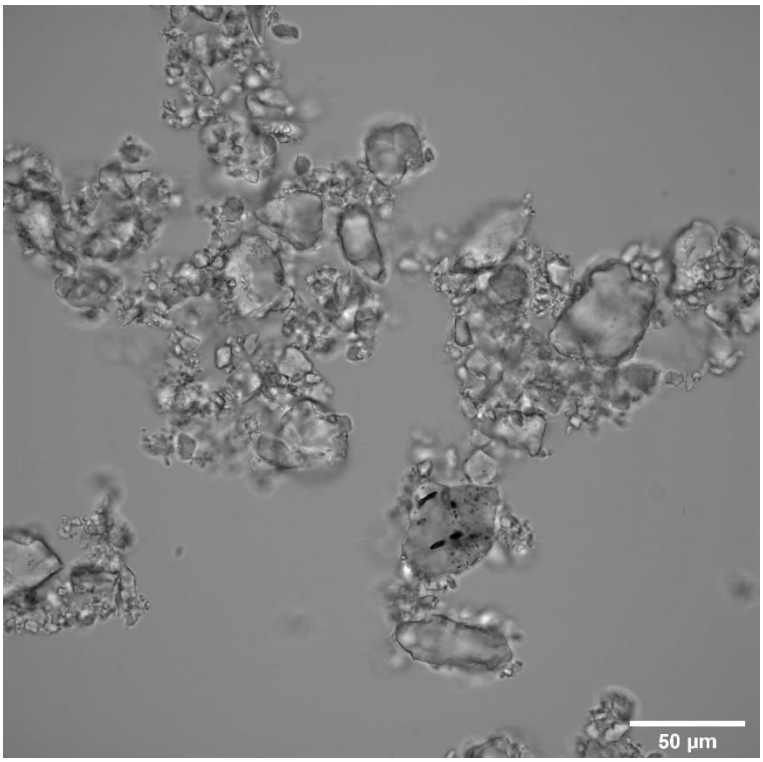

Figure 76: P4 grinded for 2 minutes, magnification: 40x.

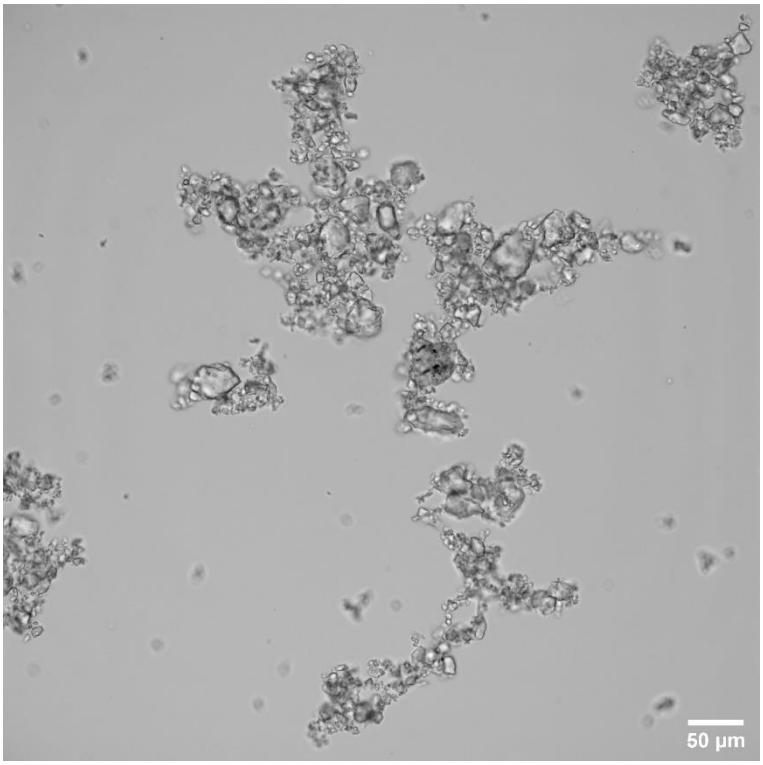

Figure 77: P4 grinded for 2 minutes, magnification: 20x.

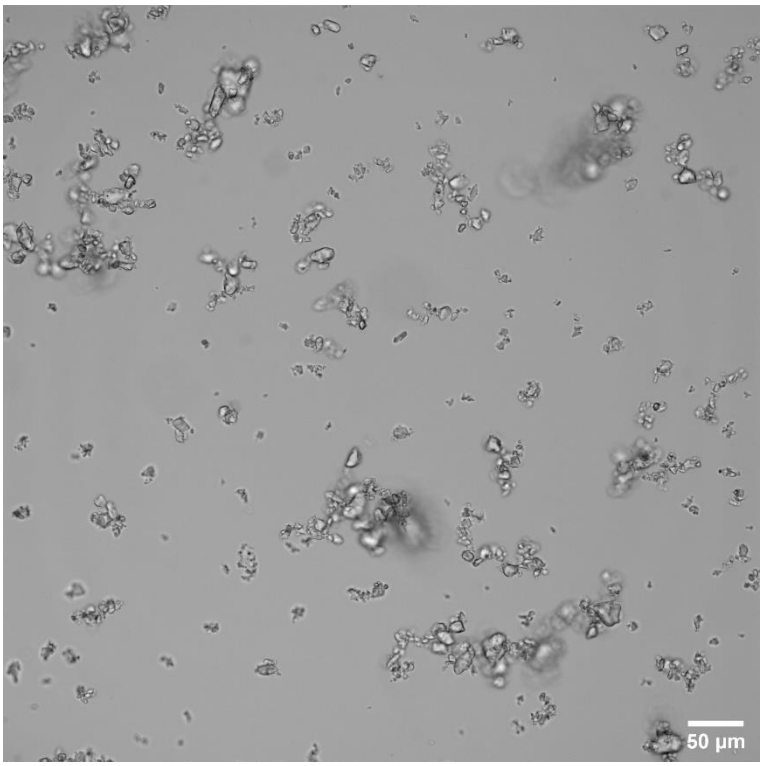

Figure 78: P4 grinded for 1 minute, magnification: 20x.

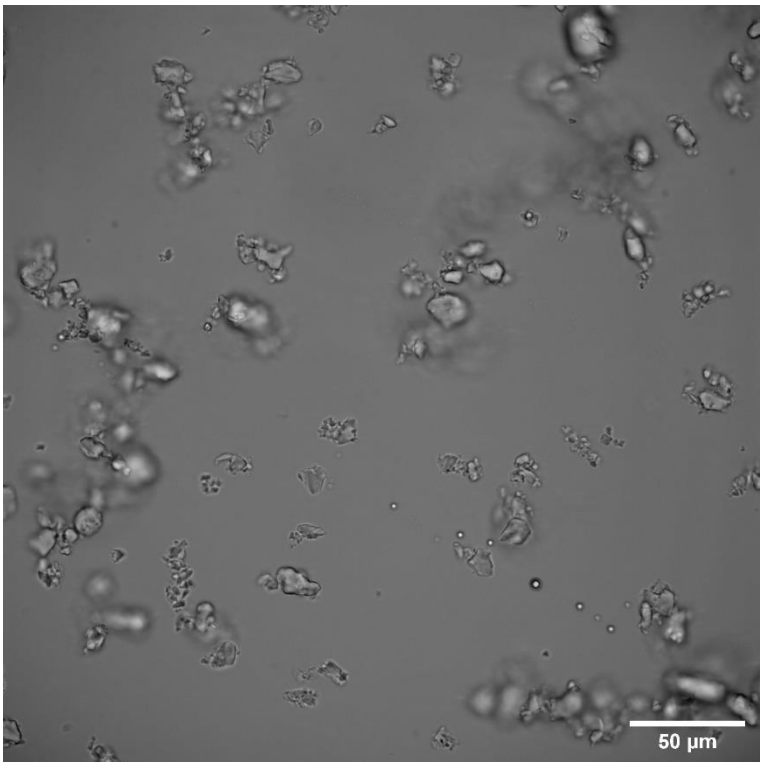

Figure 79: P4 grinded for 1 minute, magnification: 40x.

Appendix D: Experimental setup

Here, some images of the experimental setup will be shown.

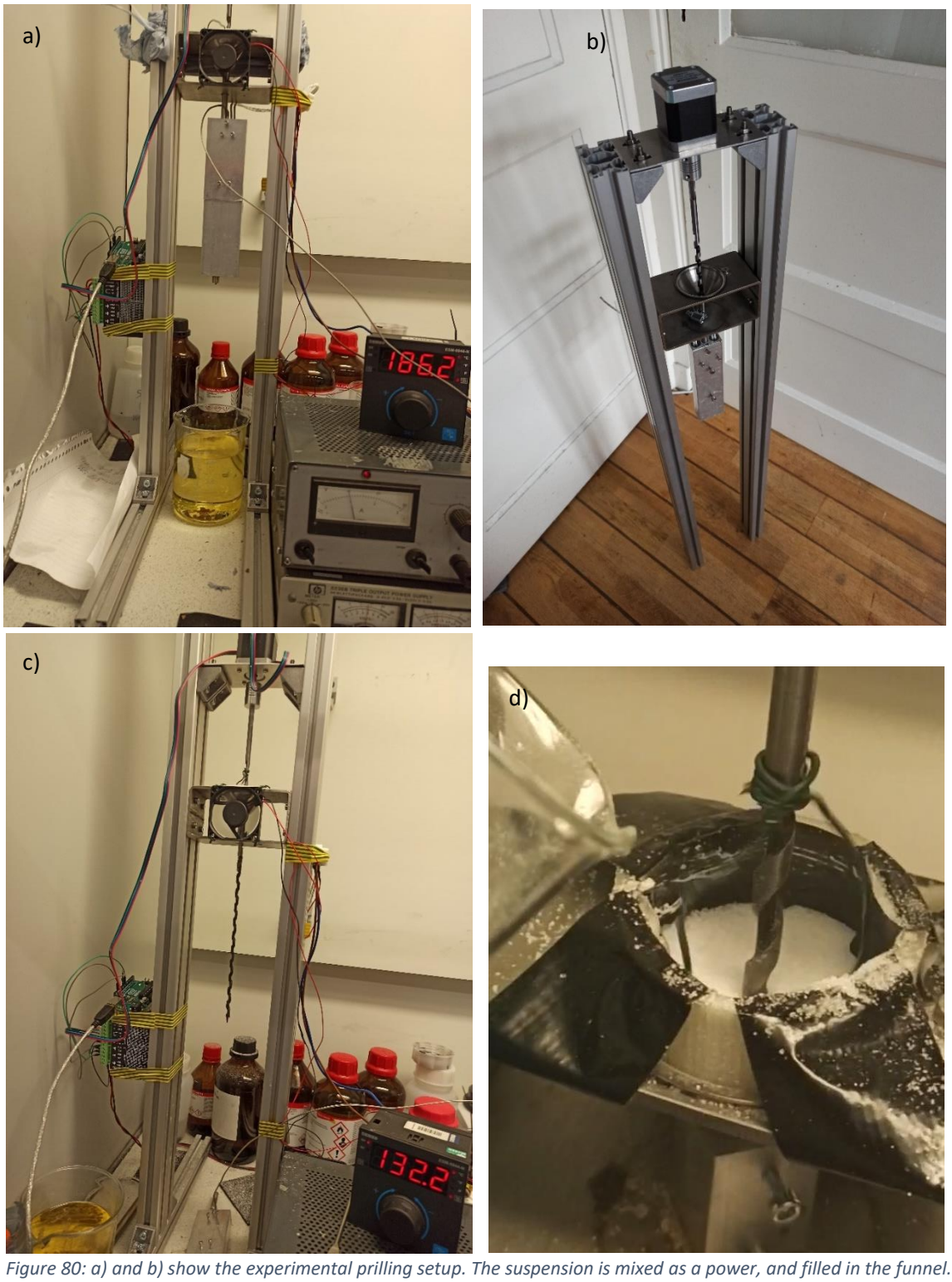

Figure 80: a) and b) show the experimental prilling setup. The suspension is mixed as a power, and filled in the funnel. The screw will transport the material down through a heater, which will melt the suspension. When it is melted, the screw will press the molten substance through a nozzle at the bottom, where it will form droplets. c) shows the screw which is inside the heating element and d) shows the improvised scraper.

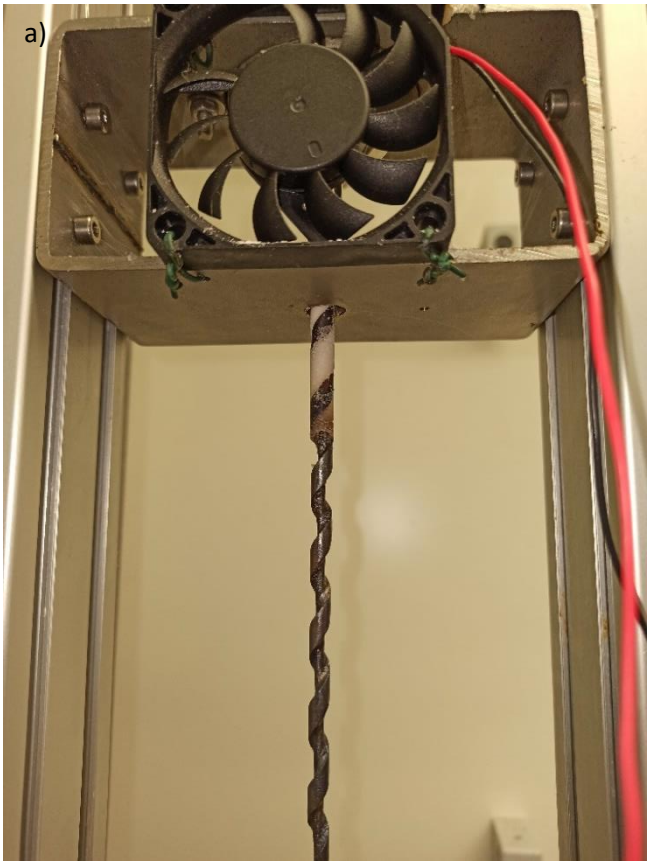

Figure 81: in a) and b), the part in the screw that is clogged is shown. Around this point, there is enough heat to partly melt the material, but since the screw is cold, it will attach to there. This will lead to a hard lump, where powder won't go through.

Appendix E: Parts overview experimental setup

Link	Amount	Product	Dimensions in mm	Price
https://www.boorkopen.nl/slangenboor-6-mm-320-mm-lang.html	1	Slangenboor 6mm (screw)	320x6	4,88
https://www.bol.com/nl/nl/p/rvs-mini-trechter-kitchen-craft/9200000059547001/?Referrer=&gclid=CjwKCAjwo8-SBhAlEiwAopc9W0yRFEtsPSPS_LDAmaBby51MbC4qDaiJYeGBFdTopGe28UIUao96mRoC614QAvD_BwE	1	Trechter (funnel)	55x27,5 +8x27,5	12,77
https://www.123-3d.nl/123-3D-Aluminium-profiel-3060-extrusion-lengte-1-m-123-3D-huismerk-i2464-t14577.html	2	3060 profiel (3060 profile)	30x60x1000	45
https://www.123-3d.nl/123-3D-Flexibele-motor-koppeling-5-mm-5-mm-i340-t3045.html	1	Flexibele koppeling (motor attachment)	5-5mm	5,5
https://nl.rs-online.com/web/p/heating-elements/8606940	2	Heating element 400W		46,56
https://www.123-3d.nl/123-3D-Aluminium-hoekverbinding-3030-inclusief-bevestigingsmateriaal-123-3D-huismerk-i2332-t14577.html	4	Hoekverbinding (corner)		14
https://www.123-3d.nl/123-3D-NEMA17-stappenmotor-1-8-graden-per-stap-47-mm-lang-5-0-kg-cm-SL42S247A-i2210-t14804.html	1	Nema17 motor		14,5
https://metaalshopper.nl/rvs-massief-10?selected=1248631-352,1249643,1251634,1249635&amount=1	1	RVS rondstaf 10mm	350mm	6,82
https://metaalshopper.nl/aluminium-plaat-1-5-mm?selected=105766-120-60,105766-120-60,109950&amount=1	1	Aluminium plaat 1,5mm	60x120x1.5	2,17
https://metaalshopper.nl/aluminium-strip-40x20?selected=233905-170,234918,234946,234949&amount=1	1	Aluminium blok	40x170x20	5,87
https://www.hornbach.nl/shop/KAISERTHAL-Ronde-buis-8x1-mm-RVS-onbehandeld-100-cm/4249598/artikel.html	1	RVS buis 8mm		10

https://www.123-3d.nl/123-3D-Glijmoer-M4-t-b-v-aluminium-3030-profiel-20-stuks-123-3D-huismerk-i2405-t14577.html	1	Glijmoer M4 (pakje van 20, , maar 8 nodig)		5,5
https://nl.rs-online.com/web/p/axial-fans/7897860	1	Ventilator (fan)		13,18
https://metaalshopper.nl/brute-rvs-koker-120x60x3?selected=2107356-60,2108379,2108879,2108390,2108395&amount=1	1	Vierkante RVS koker	120x60x3	6,81
	8	M4 bout	M4x12	
	1	M6 bout	M6x10	
	1	M6 moer		
	6	M3 bouten	M3x10	
Totaal (incl. btw)				**193,56**
Totaal (excl. btw)				**159,97**

Appendix F: Matlab scripts

F.1 Calculations for experimental setup performance.

```
%%%%%%%%%%%%%%%%%%%%
%Change parameters below
close all;
clear all;

d_noz   =       1e-3;               %nozzle diameter
U       =       0.48;               %prilling velocity in m/s
wt      =       0.35;               % wt% of P4
Twall   =       148;                %wall temperature
Qheat   =       1*400;              %Power of heating elements (2 elements)

Vdot    =       35.7;               %Fan air speed of cooling in m3/h

d_heat  =       6e-3;               %Heated tube diameter
H       =       200e-3;             %Height of heating part
t       =       1e-3;
s       =       16.5e-3;            %pitch (spoed) of screw
A_s     =       pi*d_heat^2/4*1/4;  %Area of screw. Half of it can be filled with powder, other half is
material of screw.

Dfun_max    = 55e-3-7e-3;       %maximum diameter of funnel in m
dfun_min    = 8e-3;             %minimum diameter of funnel
H_fun       = 25e-3;            %height of funnel



A_noz   = pi*d_noz^2/4;
A_heat  = pi*(d_heat+2*t)*H;
A_in    = pi*d_heat^2/4;
A_heat_in    = pi*d_heat*H;

for i=1;
g       = 9.81;                     %Gravitational acceleration
Ti      = 298.15;                   %initial temperature in [K]
To      = 143+273.15;               %outlet temperature of urea in [K] (=melting point)
Tw      = Twall+273;
%To     = 179+273;                  %outlet temperature of AN
Tm          = 133+273;              %melting temperature of urea in Kelvin
%Tm         = 169+73;               %Of AN
cp_s        = 1748;                 %J/kg/K, solid urea. Van 't Land
cp_l        = 2250;                 %J/kg/K, liquid urea.
Cp_p4       = 890;
rho_s       = 1335;                 %kg/m^3, solid urea. Van 't Land
rho_l       = 1247;
rho_c       = 0.865;                %kg/m3, density of continuous phase, here air
rho_p4      = 2790;                 %Density of polyhalite
rho_sus_l   = (1-wt)*rho_l+wt*rho_p4;
rho_sus_s   = (1-wt)*rho_s+wt*rho_p4;
%mAN        = 80.04e-3;             %molecular mass AN
murea       = 60.06e-3;             %molecular mass of urea
dh_fusion   = 224457;               %J/kg Energy required to melt urea
%dh_fusion  = 13.5e3/mAN;           %Of AN
k_w         = 20;                   %Conductivity of steel, W/m k
k_p4        = 1.4;                  %Conductivity of polyhalite
c_steel     = 500;
c_fg        = 700;                  %Fiberglass
rho_w       = 8000;
alpha_steel = 17.3e-6;              %Thermal expansion coefficient m/(m 76elsius)
p_atm       = 1.013e5;              %atmospheric pressure in Pa

     %Critical Weber number

%rhoAN       = 1.72e-3*(100^3);     %density of solid AN
%rho_l       = rhoAN;
%cp_l        = 1509;                %cp value of AN
%cp_s = cp_l
gamma       = 4*U/(0.5*d_noz);                  %shear rate
```

```
mu_pure     = 3.018e-3;                              %Pa s at T=135 Celsius, to 2.81e-3 at T=150 celsius
mu_sus      = 102.33*gamma^(-0.517)/1000;            %viscosity in nozzle of suspension
mu_sus_stat = 102.33e-3;                             %static viscosity suspension
mu_air      = 1.825e-5;
rho_air     = 1.204;
k_air       = 0.02514;
cp_air      = 1007;
Pr_air      = 0.69;                         %Prandt number of air
sigma       = 66.3e-3;                        %surfac tension of Urea at 135 celsius.

%mu_pure    = 7e-3;                           %of AN

k_l         = 0.83;                           %Heat conductance of liquid urea W/(m K)
k_s         = 1.19;                           %"of solid urea. W/(m K)
alpha_s     = k_s/(rho_s*cp_s);
alpha_l     = k_l/(rho_l*cp_l);

k_sus_s     = (1-wt)*k_s+wt*k_p4;
k_sus_l     = (1-wt)*k_l+wt*k_p4;
cp_sus_s    = (1-wt)*cp_s+wt*cp_p4;
cp_sus_l    = (1-wt)*cp_l+wt*cp_p4;
end
Rmin_fun    = dfun_min/2;                     %Minimum radius of funnel
Rmax_fun    = dfun_max/2;

V_fun       = pi*(Rmin_fun^2*H_fun+Rmin_fun*H_fun*(Rmax_fun-Rmin_fun)+1/3*(Rmax_fun-Rmin_fun)^2*H_fun);
%Volume of funnel
m_sus       = rho_sus_l*V_fun;

We_crit     = 6.25/2;
dp          = 1.88*(1+3*mu_sus/sqrt(rho_sus_l*sigma*d_noz))^(1/6)*d_noz;
%diameter of droplet

U_rec       = sqrt(We_crit*sigma/(rho_sus_l*d_noz/2));  %Recommended prilling velocity
mdot        = U*rho_sus_l*A_noz;
Qdot        = (1-wt)*mdot*(cp_l*(To-Tm)+dh_fusion+cp_s*(Tm-Ti))+wt*mdot*cp_p4*(To-Ti); %total energy in
joule to heat up.
Tmin_prill  = m_sus/mdot;

Ub          = U/A_in*A_noz;
omega       = Ub/s;         %rotational velocity in round/s

hc          = Qheat/A_heat_in/(To-Ti);  %heat transfer coefficient
Bi          = hc*d_heat/2/k_s;      %Biot number
t_flow      = H/Ub;
alpha       = k_sus_s/(rho_sus_s*cp_sus_s);
Fo          = alpha*t_flow/((d_heat/2)^2);
%T_end       = To+erfc(/sqrt(4*alpha*t_flow))*(Ti-To);
%%%%%%For calculations below, see page 182-185 of heat transfer book

Matrix         = [0.0398 0.07919 0.1182 0.1568 0.1951 0.3807 0.7552 1.037 1.32 1.577 2.558 3.641 4.198
4.531 4.75 5.235 5.411 5.501 5.556 5.669 5.784; 1.0051 1.010 1.015 1.02 1.025 1.049 1.094 1.135 1.173
1.208 1.338 1.47 1.526 1.553 1.568 1.593 1.598 1.6 1.601 1.602 1.602];
Biotrow        = [0.02 0.04 0.06 0.08 0.1 0.2 0.4 0.6 0.8 1 2 4 6 8 10 20 30 40 50 100 inf];


for I = 1:numel(Biotrow);
    if Biotrow(i)> Bi
        break
    end
end

Position= [i-1,i];

lambdal2    = Matrix(1,Position(1)) + (Matrix(1,Position(1))-
Matrix(1,Position(2)))/(Biotrow(Position(1))-Biotrow(Position(2)))*(Biotrow(Position(2))-Bi);
Al          = Matrix(2,Position(1)) + (Matrix(2,Position(1))-
Matrix(2,Position(2)))/(Biotrow(Position(1))-Biotrow(Position(2)))*(Biotrow(Position(2))-Bi);

T_end       = Al*exp(-lambdal2*Fo)*(Ti-Tw)+Tw;

Uair        = Vdot/(60^2)/(60e-3*60e-3); %Air velocity of cooling in m/s
%hcair       = 12.12-1.16*Uair+11.6*sqrt(Uair); %Air heat transfer coefficient in W/m2 degC;
https://www.engineeringtoolbox.com/convective-heat-transfer-d_430.html
```

```
Re_air      = rho_air*Uair*(d_heat+2*t)/mu_air;
Nu_air      = 0.3+0.62*sqrt(Re_air)*Pr_air^(1/3)/((1+(0.4/Pr_air)^(2/3))^0.25);

hcair = Nu_air*k_air/((d_heat+2*t));

m_s = rho_sus_l*s*A_s;        %Massa displacement in tube after turning 1 round (2*pi)
f   = mdot/m_s;               %rounds per second


%%%%%%%%%%%%%%%%%%%%%%%%%%%%%%%%%%%%%%%%%%%%%%%%
%Beyond this point, experiments were conducted and results will be used for
%further calculations
 mu_351 = 20.4e-3; %Viscosity of 10wt%p4+Ur, 35wt%P4 and pure urea
 mu_101 = 15.5e-3;
 mu_352 = 13.48e-3; %Viscosity of 10wt%p4+Ur, 35wt%P4 and pure urea
 mu_102 = 7.73^e-3;
 mu_ur = 3.1^e-3;


 %Let op, onderstaande formules zijn niet zelf berekend maar via
 %http://www.homepages.ucl.ac.uk/~uceseug/Fluids2/Notes_Viscosity.pdf.
 %Controleer of dit klopt.
 Rho35 = rho_sus_l;
 rho10 = 0.1*rho_p4+0.9*rho_l;

gamma1 = 4*Ub/(0.5*d_heat); %Shear rate in tube, controleer of dit klopt
gamma2 = 4*U/(0.5*d_noz);  %Shear rate in nozzle

Q1 = Ub*d_heat^2*pi/4;
K1 = 96.5e-3; %Index of 35wt% P4 suspension
K2 = 79.77e-3; %Index of 10wt% P4 susp

n1 = 0.4933;
n2 = 0.4658;

gamma351 = Q1/(pi*(d_heat/2)^3)*(3+1/n1); %Shear rate in pipe of 35wt%
gamma352 = Q1/(pi*(d_noz/2)^3)*(3+1/n1); %Shear rate in nozzle of 35wt%
gamma101 = Q1/(pi*(d_heat/2)^3)*(3+1/n2); %Shear rate in pipe of 35wt%
gamma102 = Q1/(pi*(d_noz/2)^3)*(3+1/n2); %Shear rate in nozzle of 35wt%

tau_351 = mu_351*gamma351; %shear stress
tau_101 = mu_101*gamma101;
tau_ur1 = mu_ur*gamma1;

tau_352 = mu_352*gamma352; %shear stress in nozzle
tau_102 = mu_102*gamma102;
tau_ur2 = mu_ur*gamma2;

Re35 = rho35*Ub*d_heat/mu_351;
Re10 = rho10*Ub*d_heat/mu_101;
Reur = rho_l*Ub*d_heat/mu_ur;

f35 = 64/Re35; %Friction factor, page 367 Fluid mechanics book
f10 = 64/Re10;
fur = 64/Reur;

hf35 = 32*mu_351*H*Ub/(rho35*g*d_heat^2);
hf10 = 32*mu_101*H*Ub/(rho10*g*d_heat^2);
hfur = 32*mu_ur*H*Ub/(rho_l*g*d_heat^2);


dp35 = 4*K1*H/d_heat*(gamma351)^n1+4*K1*2e-3/d_noz*(gamma352)^n1+0.5*rho35*(U^2-Ub^2); %dp in heated
tube + dp in nozzle with thickness=2mm (both due to viscosity) + dp of different Uin and Uout
dp10 = 4*K2*H/d_heat*(gamma101)^n2+4*K2*2e-3/d_noz*(gamma102)^n2+0.5*rho10*(U^2-Ub^2); %dp in heated
tube + dp in nozzle with thickness=2mm (both due to viscosity) + dp of different Uin and Uout
dpur = Q1*8*mu_ur*H/(pi*(d_heat/2)^4)+Q1*8*mu_ur*2e-3/(pi*(d_noz/2)^4)+0.5*rho_l*(U^2-Ub^2); %dp in
heated tube + dp in nozzle with thickness=2mm (both due to viscosity) + dp of different Uin and Uout

F35 = dp35*A_in;
F10 = dp10*A_in;
Fur = dpur*A_in;

Tnema17 = 0.5; %Holding torque of Nema17 motor in Nm
```

```
T35 = F35/tan(pi/4)*d_heat/2; %Required torque of UR+35wt%P4
T10 = F10/tan(pi/4)*d_heat/2;
Tur = Fur/tan(pi/4)*d_heat/2;

%%%%%%%%%%%%%%%%%%%%%%%%%%%%%%%%%%%%%%%%%%%%%%%%
%Display
disp('------------------------------------------------------------')
disp(['Droplet size                      ', num2str(round(dp*1000,2)), ' mm'])
disp(['Recommended prilling velocity     ', num2str(round(U_rec,2)), ' m/s'])
%disp(['Required heat                     ', num2str(ceil(Qdot)), ' Watt'])
disp(['Minimum prilling time             ', num2str(round(tmin_prill)), ' s'])
disp(['Outlet temperature                ', num2str(round(T_end-273.15)), ' degC'])
%disp(['Fourier number                    ', num2str(Fo)])
%disp(['Biot number                       ', num2str(Bi)])
%disp(['Heat transfer coefficient air     ', num2str(hcair), ' W/m2 K']);
disp(['Rotational velocity screw         ', num2str(f), ' Rps']);
disp(['Amount of required revolutions    ', num2str(tmin_prill/f), ' rev']);
disp('------------------------------------------------------------')
```

F.2 Data Processing of P4 sizes & shapes

```
%%%Size – roundness calculations
clear all;
close all;

%Import everything
%zero minutes
zerominar   = readmatrix('D:\Users\sande\Mijn Drive\Measurements\Microscope\P4 0 minute\Results – area-
roundness.csv');
zerominsiz  = readmatrix('D:\Users\sande\Mijn Drive\Measurements\Microscope\P4 0 minute\Results –
size.csv');
%1 minute
oneminsiz   = readmatrix('D:\Users\sande\Mijn Drive\Measurements\Microscope\Nieuwe metingen\1
minute\Results_Diameter.csv');
oneminar    = readmatrix('D:\Users\sande\Mijn Drive\Measurements\Microscope\Nieuwe metingen\1
minute\Results_roundness.csv');
%2 minutes
twominsiz   = readmatrix('D:\Users\sande\Mijn Drive\Measurements\Microscope\Nieuwe metingen\2
minutes\Results_length.csv');
twominar    = readmatrix('D:\Users\sande\Mijn Drive\Measurements\Microscope\Nieuwe metingen\2
minutes\Results_roundness.csv');
%5 minutes
fiveminar    = readmatrix('D:\Users\sande\Mijn Drive\Measurements\Microscope\Nieuwe metingen\5
minutes\Results_roundness.csv');
fiveminsiz   = readmatrix('D:\Users\sande\Mijn Drive\Measurements\Microscope\Nieuwe metingen\5
minutes\Results_length.csv');
%10 minutes
tenminar    = readmatrix('D:\Users\sande\Mijn Drive\Measurements\Microscope\Nieuwe metingen\10
minutes\Results_roundness.csv');
tenminsiz   = readmatrix('D:\Users\sande\Mijn Drive\Measurements\Microscope\Nieuwe metingen\10
minutes\Results_length.csv');

tenminar2  = readmatrix('D:\Users\sande\Mijn
Drive\Measurements\Microscope\Compare_nogrind_10min\Results_shape');
tenminsiz2 = readmatrix('D:\Users\sande\Mijn
Drive\Measurements\Microscope\Compare_nogrind_10min\Results_length');
%% Calculations

A = 0.25;
B = 40;
C = 20;
D = 1;
E = 0.5; %Binwidth
%zero minutes
zeroround = zerominar(2:end,8);
zerosiz = zerominsiz(2:end,11);

zeroroundness = mean(zeroround);
zerosize = mean(zerosiz);
zeromin = min(zerosiz);
zeromax = max(zerosiz);

figure(1);
subplot(5,1,1)
histogram(zeroround,B/2, 'Normalization','probability');
title('Roundness of P4 0 minutes grinding');

 ylim([0,A]);
 xlim([0,D]);

figure(2)
subplot(5,1,1)
H1 = histogram(zerosiz,B*3, 'Normalization','probability');
title('Size in micron of P4 0 minute grinding');
xlabel('P4 size in micron');
H1.BinWidth = E;

 ylim([0,A]);
 xlim([0,C]);

%one minute
oneround = oneminar(2:end,8);
onesiz = oneminsiz(2:end,11);
```

```
oneroundness = mean([oneround(1:34);oneround(36:end)]);
onesize = mean(onesiz);
onemin = min(onesiz);
onemax = max(onesiz);

figure(1);
subplot(5,1,2);
histogram(oneround,B/2, 'Normalization','probability');
title('Roundness of P4 1 minute grinding');


 ylim([0,A]);
 xlim([0,D]);

figure(2);
subplot(5,1,2)
H2 = histogram(onesiz,B, 'Normalization','probability');
title('Size in micron of P4 1 minute grinding');
xlabel('P4 size in micron');
H2.BinWidth = E;

 ylim([0,A]);
 xlim([0,C]);

%two minutes
tworound = twominar(2:end,8);
twosiz = twominsiz(2:end,11);

troroundness = mean(tworound);
twosize = mean(twosiz);
twomin = min(twosiz);
twomax = max(twosiz);

figure(1);
subplot(5,1,3)
histogram(tworound,B/2, 'Normalization','probability');
title('Roundness of P4 2 minute grinding');

 ylim([0,A]);
 xlim([0,D]);

figure(2)
subplot(5,1,3)

H3 = histogram(twosiz,B*2, 'Normalization','probability');
title('Size in micron of P4 2 minute grinding');
xlabel('P4 size in micron');
H3.BinWidth = E;

 ylim([0,A]);
 xlim([0,C]);

%five minutes
fiveround = fiveminar(2:end,8);
fivesiz = fiveminsiz(2:end,11);

fiveroundness = mean(fiveround);
fivesize = mean(fivesiz);
fivemin = min(fivesiz);
fivemax = max(fivesiz);

figure(1);
subplot(5,1,4)
histogram(fiveround,B/2, 'Normalization','probability');
title('Roundness of P4 5 minute grinding');
ylim([0,A]);
xlim([0,D]);

figure(2);
subplot(5,1,4)
H4 = histogram(fivesiz,B, 'Normalization','probability');
title('Size in micron of P4 5 minute grinding');
xlabel('P4 size in micron');
```

```
 ylim([0,A]);
 xlim([0,C]);
 H4.BinWidth = E;

%ten minutes
tenround = tenminar(2:end,9);
tensiz = tenminsiz(2:end,11);

tenroundness = mean(tenround);
tensize = mean(tensiz);
tenmin = min(tensiz);
tenmax = max(tensiz);



figure(1);
subplot(5,1,5)
histogram(tenround,B/2, 'Normalization','probability');
title('Roundness of P4 10 minute grinding');

 ylim([0,A]);
 xlim([0,D]);

figure(2)
subplot(5,1,5)
H5 = histogram(tensiz,B*2, 'Normalization','probability');
xlabel('P4 size in micron');
title('Size in micron of P4 10 minute grinding');
H5.BinWidth = E;

ylim([0,A]);
xlim([0,C]);

%10 minutes 2
tenround2 = tenminar2(2:end,8);
tensiz2 = tenminsiz2(2:end,11);

tenroundness2 = mean(tenround2);
tensize2 = mean(tensiz2);
tenmin2 = min(tensiz2);
tenmax2 = max(tensiz2);

std0 = std(zerosiz);
std1 = std(onesiz);
std2 = std(twosiz);
std5 = std(fivesiz);
std10 = std(tensiz2);

figure(1);
subplot(5,1,5)
histogram(tenround2,B/2, 'Normalization','probability');
title('Roundness of P4 10 minute grinding [2]');
 ylim([0,A]);
 xlim([0,D]);


figure(2)
subplot(5,1,5)
h102 = histogram(tensiz2,B, 'Normalization','probability');
 h102.BinWidth = E;
title('Size in micron of P4 10 minute grinding');
ylim([0,A]);
xlim([0,C]);
xlabel('P4 size in micron');

%%%%%%%%%%%%%%%%%%%%%%%%%%%%%%%%%%%%%%%%
disp('------------------------------------------------------------')
disp(['Mean size 0 minutes   ', num2str(zerosize), ' micron']);
disp(['Mean size 1 minutes   ', num2str(onesize), ' micron']);
disp(['Mean size 2 minutes   ', num2str(twosize), ' micron']);
disp(['Mean size 5 minutes   ', num2str(fivesize), ' micron']);
disp(['Mean size 10 minutes   ', num2str(tensize), ' micron']);
disp(['Mean size 10 minutes [2]   ', num2str(tensize2), ' micron']);
disp('….....');
```

```
disp(['STD size 0 minutes   ', num2str(std0), ' ']);
disp(['STD size 1 minutes   ', num2str(std1), ' ']);
disp(['STD size 2 minutes   ', num2str(std2), ' ']);
disp(['STD size 5 minutes   ', num2str(std5), ' ']);
disp(['STD size 10 minutes   ', num2str(std10), ' ']);

disp('…….');
disp(['Min size 0 minutes   ', num2str(zeromin), ' micron']);
disp(['Min size 1 minutes   ', num2str(onemin), ' micron']);
disp(['Min size 2 minutes   ', num2str(twomin), ' micron']);
disp(['Min size 5 minutes   ', num2str(fivemin), ' micron']);
disp(['Min size 10 minutes   ', num2str(tenmin), ' micron']);
disp(['Min size 10 minutes [2]   ', num2str(tenmin2), ' micron']);

disp('…….');
disp(['Max size 0 minutes   ', num2str(zeromax), ' micron']);
disp(['Max size 1 minutes   ', num2str(onemax), ' micron']);
disp(['Max size 2 minutes   ', num2str(twomax), ' micron']);
disp(['Max size 5 minutes   ', num2str(fivemax), ' micron']);
disp(['Max size 10 minutes   ', num2str(tenmax), ' micron']);
disp(['Max size 10 minutes [2]   ', num2str(tenmax2), ' micron']);

disp('…….');
disp(['Mean roundness 0 minutes   ', num2str(zeroroundness), ' ']);
disp(['Mean roundness 1 minutes   ', num2str((oneroundness)), ' ']);
disp(['Mean roundness 2 minutes   ', num2str((tworoundness)), ' ']);
disp(['Mean roundness 5 minutes   ', num2str((fiveroundness)), ' ']);
disp(['Mean roundness 10 minutes   ', num2str((tenroundness)), ' ']);
disp(['Mean roundness 10 minutes [2]   ', num2str((tenroundness2)), ' ']);

disp('…….');
disp(['STD roundness 0 minutes   ', num2str(std(zeroround)), ' ']);
disp(['STD roundness 1 minutes   ', num2str(std([oneround(1:34); oneround(36:end)])), ' ']);
disp(['STD roundness 2 minutes   ', num2str(std((tworound))), ' ']);
disp(['STD roundness 5 minutes   ', num2str(std((fiveround))), ' ']);
disp(['STD roundness 10 minutes   ', num2str(std((tenround))), ' ']);
disp(['STD roundness 10 minutes [2]   ', num2str(std((tenround2))), ' ']);

disp('------------------------------------------------------------')
```

F.3 Data processing of rheology measurements

```
close all;
clear all;

im = readmatrix('Urea data shear viscosity.xlsx');
imng = readmatrix('Notgrinded_Samples.xlsx');

%% im Urea+35wt% P4 10 minutes grinding
R35_101 = im(158:168,2);  %shear rate of urea 35wt% P4 sweep 2
S35_101 = im(158:168,4);  %viscosity of UR 35wt% P4 sweep 2

R35_1013 = im(171:181,2);  %shear rate of urea 35wt% P4 sweep 2
S35_1013 = im(171:181,4);  %viscosity of UR 35wt% P4 sweep 2

R35_102 = im(2:12,2);  %shear rate of urea 35wt% P4 10 minutes sweep 2
S35_102 = im(2:12,4);  %viscosity of UR 35wt% P4 10 minutes sweep 2

R35_1023 = im(15:25,2);  %shear rate of urea 35wt% P4 10 minutes sweep 2
S35_1023 = im(15:25,4);  %viscosity of UR 35wt% P4 10 minutes sweep 2


%% im Urea+35wt% P4 1 minute grinding

R35_12 = im(28:38,2);  %shear rate of urea 35wt% P4 1 minutes sweep 2
S35_12 = im(28:38,4);  %viscosity of UR 35wt% P4 1 minutes sweep 2

R35_123 = im(41:51,2);  %shear rate of urea 35wt% P4 1 minutes sweep 2
S35_123 = im(41:51,4);  %viscosity of UR 35wt% P4 1 minutes sweep 2

% R35_11 = im(,2);  %shear rate of urea 35wt% P4 1 minutes sweep 2
% S35_11 = im(,4);  %viscosity of UR 35wt% P4 1 minutes sweep 2
%
% R35_113 = im(,2);  %shear rate of urea 35wt% P4 1 minutes sweep 2
% S35_113 = im(,4);  %viscosity of UR 35wt% P4 1 minutes sweep 2

%% im Urea+35wt% P4 2 minute grinding

R35_21 = im(54:64,2);  %shear rate of urea 35wt% P4 1 minutes sweep 1
S35_21 = im(54:64,4);  %viscosity of UR 35wt% P4 1 minutes sweep 1

R35_213 = im(67:77,2);  %shear rate of urea 35wt% P4 1 minutes sweep 1 interval 3
S35_213 = im(67:77,4);  %viscosity of UR 35wt% P4 1 minutes sweep 1 interval 3

R35_22 = im(80:90,2);  %shear rate of urea 35wt% P4 1 minutes sweep 2
S35_22 = im(80:90,4);  %viscosity of UR 35wt% P4 1 minutes sweep 2

R35_223 = im(93:103,2);  %shear rate of urea 35wt% P4 1 minutes sweep 2 interval 3
S35_223 = im(93:103,4);  %viscosity of UR 35wt% P4 1 minutes sweep 2 interval 3

%% im Urea+35wt% P4 5 minute grinding

R35_51 = im(106:116,2);  %shear rate of urea 35wt% P4 5 minutes sweep 1
S35_51 = im(106:116,4);  %viscosity of UR 35wt% P4 5 minutes sweep 1

R35_513 = im(119:129,2);  %shear rate of urea 35wt% P4 5 minutes sweep 1 interval 3
S35_513 = im(119:129,4);  %viscosity of UR 35wt% P4 1 minutes sweep 1 interval 3

R35_52 = im(132:142,2);  %shear rate of urea 35wt% P4 5 minutes sweep 2
S35_52 = im(132:142,4);  %viscosity of UR 35wt% P4 5 minutes sweep 2

R35_523 = im(145:155,2);  %shear rate of urea 35wt% P4 5 minutes sweep 2 interval 3
S35_523 = im(145:155,4);  %viscosity of UR 35wt% P4 5 minutes sweep 2 interval 3

%% im Urea+35wt% P4 no grinding

 R35_01 = imng(1:11,2);  %shear rate of urea 35wt% P4 5 minutes sweep 1
 S35_01 = imng(1:11,4);  %viscosity of UR 35wt% P4 5 minutes sweep 1

 R35_013 = imng(14:24,2);  %shear rate of urea 35wt% P4 5 minutes sweep 1 interval 3
 S35_013 = imng(14:24,4);  %viscosity of UR 35wt% P4 1 minutes sweep 1 interval 3

 R35_02 = imng(27:37,2);  %shear rate of urea 35wt% P4 5 minutes sweep 2
 S35_02 = imng(27:37,4);  %viscosity of UR 35wt% P4 5 minutes sweep 2
```

```
 R35_023 = imng(40:50,2);  %shear rate of urea 35wt% P4 5 minutes sweep 2 interval 3
 S35_023 = imng(40:50,4);  %viscosity of UR 35wt% P4 5 minutes sweep 2 interval 3

%% END OF 35wt%
%Begin of 10 wt%

%%%%%%%%%%%%%%%%%%%%%%%%%%%%%%%%%%%%%%%%%%%%%%%%%%%%%%%%%%%%%%%%%%%%%%%%%%%%%%%%%%%%%%%%%%%%%%%
%%%%%%%%%%%%%%%%%%%%%%%%%%%%%%%%%%%%%%%%%%%%%%%%


%% im Urea+10wt% P4 10 minutes grinding
R10_101 = im(367:377,2);  %shear rate of urea 10wt% P4 sweep 2
S10_101 = im(367:377,4);  %viscosity of UR 10wt% P4 sweep 2

R10_1013 = im(380:390,2);  %shear rate of urea 10wt% P4 sweep 2
S10_1013 = im(380:390,4);  %viscosity of UR 10wt% P4 sweep 2

R10_102 = im(393:403,2);  %shear rate of urea 10wt% P4 10 minutes sweep 2
S10_102 = im(393:403,4);  %viscosity of UR 10wt% P4 10 minutes sweep 2

R10_1023 = im(406:416,2);  %shear rate of urea 10wt% P4 10 minutes sweep 2
S10_1023 = im(406:416,4);  %viscosity of UR 10wt% P4 10 minutes sweep 2


%% im Urea+10wt% P4 1 minute grinding

R10_11 = im(211:221,2);  %shear rate of urea 35wt% P4 1 minutes sweep 2
S10_11 = im(211:221,4);  %viscosity of UR 35wt% P4 1 minutes sweep 2

R10_113 = im(224:234,2);  %shear rate of urea 35wt% P4 1 minutes sweep 2
S10_113 = im(224:234,4);  %viscosity of UR 35wt% P4 1 minutes sweep 2

R10_12 = im(237:247,2);  %shear rate of urea 35wt% P4 1 minutes sweep 2
S10_12 = im(237:247,4);  %viscosity of UR 35wt% P4 1 minutes sweep 2

R10_123 = im(250:260,2);  %shear rate of urea 35wt% P4 1 minutes sweep 2
S10_123 = im(250:260,4);  %viscosity of UR 35wt% P4 1 minutes sweep 2

%% Urea+10wt% P4 no grinding
R10_01 = imng(53:63,2);
S10_01 = imng(53:63,4);

R10_013 = imng(66:76,2);
S10_013 = imng(66:76,4);

R10_02 = imng(79:89,2);
S10_02 = imng(79:89,4);

R10_023 = imng(92:102,2);
S10_023 = imng(92:102,4);
%% im Urea+10wt% P4 2 minute grinding

R10_21 = im(263:273,2);  %shear rate of urea 35wt% P4 1 minutes sweep 1
S10_21 = im(263:273,4);  %viscosity of UR 35wt% P4 1 minutes sweep 1

R10_213 = im(276:286,2);  %shear rate of urea 35wt% P4 1 minutes sweep 1 interval 3
S10_213 = im(276:286,4);  %viscosity of UR 35wt% P4 1 minutes sweep 1 interval 3

R10_22 = im(289:299,2);  %shear rate of urea 35wt% P4 1 minutes sweep 2
S10_22 = im(289:299,4);  %viscosity of UR 35wt% P4 1 minutes sweep 2

R10_223 = im(302:312,2);  %shear rate of urea 35wt% P4 1 minutes sweep 2 interval 3
S10_223 = im(302:312,4);  %viscosity of UR 35wt% P4 1 minutes sweep 2 interval 3

%% im Urea+10wt% P4 5 minute grinding

R10_52 = im(315:325,2);  %shear rate of urea 35wt% P4 5 minutes sweep 1
S10_52 = im(315:325,4);  %viscosity of UR 35wt% P4 5 minutes sweep 1

R10_523 = im(328:338,2);  %shear rate of urea 35wt% P4 5 minutes sweep 1 interval 3
S10_523 = im(328:338,4);  %viscosity of UR 35wt% P4 1 minutes sweep 1 interval 3

R10_51 = im(341:351,2);  %shear rate of urea 35wt% P4 5 minutes sweep 2
```

```
S10_51 = im(341:351,4);  %viscosity of UR 35wt% P4 5 minutes sweep 2

R10_513 = im(354:364,2);  %shear rate of urea 35wt% P4 5 minutes sweep 2 interval 3
S10_513 = im(354:364,4);  %viscosity of UR 35wt% P4 5 minutes sweep 2 interval 3

%% Pure urea

Rp_1 = im(419:429,2);  %shear rate of urea sweep 1
Sp_1 = im(419:429,4);  %viscosity of urea sweep 1

Rp_13 = im(432:442,2);  %shear rate of urea  sweep 1 interval 3
Sp_13 = im(432:442,4);  %viscosity of UR  sweep 1 interval 3

Rp_2 = im(445:455,2);  %shear rate of urea sweep 2
Sp_2 = im(445:455,4);  %viscosity of UR  sweep 2

Rp_23 = im(458:468,2);  %shear rate of urea  sweep 2 interval 3
Sp_23 = im(458:468,4);  %viscosity of UR sweep 2 interval 3

%%
%%%%%%%%%%%%%%%%%%%%%%%%%%%%%%%%%%%%%%%%%%%%%%%%%%%%%%%%%%%%%%%%%%%%%%%%%%%%%%%%%%%%%%%%%%%%%%%%%%%%%%%
%%%%%%%%%%%%%%%%%%%%%
%%%%%%%%%%%%%%%%%%%%
%%%%%%%%%%%%%%%%%%%%
% END IMPORT
%%%%%%%%%%%%%%%%%%%%
%%%%%%%%%%%%%%%%%%%%%%%%%%%%%%%%%%%%%%%%%%%%
%First, all data has to be placed in the right order, otherwise problems with mean calculations will
occur.


%% Urea 35wt% P4
for j=1:11
    RR35_123(12-j) = R35_123(j); %De volgorde van deze meting is anders dan bij de anderen. Dit om
consistent te houden.
    SS35_123(12-j) = S35_123(j);
end
clear j

R35 =   [R35_12 RR35_123' R35_21 R35_213 R35_22 R35_223 R35_51 R35_513 R35_52 R35_523 R35_101 R35_1013
R35_102 R35_1023 R35_01 R35_013 R35_02 R35_023];
S35 =   [S35_12 SS35_123' S35_21 S35_213 S35_22 S35_223 S35_51 S35_513 S35_52 S35_523 S35_101 S35_1013
S35_102 S35_1023 S35_01 S35_013 S35_02 S35_023];

R351 = [R35(:,1); R35(:,2)];
S351 = [S35(:,1); S35(:,2)];

R352 = [R35(:,3); R35(:,4); R35(:,5); R35(:,6)];
S352 = [S35(:,3); S35(:,4); S35(:,5); S35(:,6)];

R355 = [R35(:,7); R35(:,8); R35(:,9); R35(:,10)];
S355 = [S35(:,7); S35(:,8); S35(:,9); S35(:,10)];

R3510 = [R35(:,11); R35(:,12); R35(:,13); R35(:,14)];
S3510 = [S35(:,11); S35(:,12); S35(:,13); S35(:,14)];

R350 = [R35(:,15); R35(:,16); R35(:,17); R35(:,18)];
S350 = [S35(:,15); S35(:,16); S35(:,17); S35(:,18)];


R10 =   [R10_01 R10_013 R10_02 R10_023 R10_11 R10_113 R10_12 R10_123 R10_21 R10_213 R10_22 R10_223
R10_51 R10_513 R10_52 R10_523 R10_101 R10_1013 R10_102 R10_1023];
S10 =   [S10_01 S10_013 S10_02 S10_023 S10_11 S10_113 S10_12 S10_123 S10_21 S10_213 S10_22 S10_223
S10_51 S10_513 S10_52 S10_523 S10_101 S10_1013 S10_102 S10_1023];


R100 = [R10(:,1); R10(:,2); R10(:,3); R10(:,4)];
S100 = [S10(:,1); S10(:,2); S10(:,3); S10(:,4)];

R101 = [R10(:,5); R10(:,6); R10(:,7); R10(:,8)];
S101 = [S10(:,5); S10(:,6); S10(:,7); S10(:,8)];

R102 = [R10(:,9); R10(:,10); R10(:,11); R10(:,12)];
S102 = [S10(:,9); S10(:,10); S10(:,11); S10(:,12)];
```

```
R105 = [R10(:,13); R10(:,14); R10(:,15); R10(:,16)];
S105 = [S10(:,13); S10(:,14); S10(:,15); S10(:,16)];

R1010 = [R10(:,17); R10(:,18); R10(:,19); R10(:,20)];
S1010 = [S10(:,17); S10(:,18); S10(:,19); S10(:,20)];

%% Pure urea


Rpu =   [Rp_1 Rp_13 Rp_2 Rp_23];
Spu =   [Sp_1 Sp_13 Sp_2 Sp_23];

Rppu = [Rp_1; Rp_13; Rp_2; Rp_23];
Sppu = [Sp_1; Sp_13; Sp_2; Sp_23];


%%%%%%%%%%%%%%%%%%%%%%%%%Calculate mean
for j=1:11
    R100A(j) = mean([R10(j,1) R10(12-j,2) R10(j,3) R10(12-j,4)]);
    S100A(j) = mean([S10(j,1) S10(12-j,2) S10(j,3) S10(12-j,4)]);

    R101A(j) = mean([R10(j,5) R10(12-j,6) R10(j,7) R10(12-j,8)]);
    S101A(j) = mean([S10(j,5) S10(12-j,6) S10(j,7) S10(12-j,8)]);

    R102A(j) = mean([R10(j,9) R10(12-j,10) R10(j,11) R10(12-j,12)]);
    S102A(j) = mean([S10(j,9) S10(12-j,10) S10(j,11) S10(12-j,12)]);

    R105A(j) = mean([R10(j,13) R10(12-j,14) R10(j,15) R10(12-j,16)]);
    S105A(j) = mean([S10(j,13) S10(12-j,14) S10(j,15) S10(12-j,16)]);

    R1010A(j) = mean([R10(j,17) R10(12-j,18) R10(j,19) R10(12-j,20)]);
    S1010A(j) = mean([S10(j,17) S10(12-j,18) S10(j,19) S10(12-j,20)]);

    %wt35%

    R351A(j) = mean([R35(j,1) R35(12-j,2)]);
    S351A(j) = mean([S35(j,1) S35(12-j,2)]);

    R352A(j) = mean([R35(j,3) R35(12-j,4) R35(j,5) R35(12-j,6)]);
    S352A(j) = mean([S35(j,3) S35(12-j,4) S35(j,5) S35(12-j,6)]);

    R355A(j) = mean([R35(j,7) R35(12-j,8) R35(j,9) R35(12-j,10)]);
    S355A(j) = mean([S35(j,7) S35(12-j,8) S35(j,9) S35(12-j,10)]);

    R3510A(j) = mean([R35(j,11) R35(12-j,12) R35(j,13) R35(12-j,14)]);
    S3510A(j) = mean([S35(j,11) S35(12-j,12) S35(j,13) S35(12-j,14)]);

    R350A(j) = mean([R35(j,15) R35(12-j,16) R35(j,17) R35(12-j,18)]);
    S350A(j) = mean([S35(j,15) S35(12-j,16) S35(j,17) S35(12-j,18)]);


    %pure
    RpA(j) = mean([Rpu(j,1) Rpu(12-j,2) Rpu(j,3) Rpu(12-j,4)]);
    SpA(j) = mean([Spu(j,1) Spu(12-j) Spu(j,3) Spu(12-j,4)]);
end

%%%%%%%%%%%%%%%%%%%%%%%%%%%%%%%%%%%%%%%%%%%%%%%%%%%%%%%%%%%%%%%%%%%%%%%%%%%%%%%
%%Calculate Boxplots

for j=1:11
    R100B(j,:) = [R10(j,1) R10(12-j,2) R10(j,3) R10(12-j,4)];
    S100B(j,:) = ([S10(j,1) S10(12-j,2) S10(j,3) S10(12-j,4)]);

    R101B(j,:) = ([R10(j,5) R10(12-j,6) R10(j,7) R10(12-j,8)]);
    S101B(j,:) = ([S10(j,5) S10(12-j,6) S10(j,7) S10(12-j,8)]);

    R102B(j,:) = ([R10(j,9) R10(12-j,10) R10(j,11) R10(12-j,12)]);
    S102B(j,:) = ([S10(j,9) S10(12-j,10) S10(j,11) S10(12-j,12)]);

    R105B(j,:) = ([R10(j,13) R10(12-j,14) R10(j,15) R10(12-j,16)]);
    S105B(j,:) = ([S10(j,13) S10(12-j,14) S10(j,15) S10(12-j,16)]);

    R1010B(j,:) = ([R10(j,17) R10(12-j,18) R10(j,19) R10(12-j,20)]);
```

```
    S1010B(j,:) = ([S10(j,17) S10(12-j,18) S10(j,19) S10(12-j,20)]);

    %wt35%

    R351B(j,:) = ([R35(j,1) R35(12-j,2)]);
    S351B(j,:) = ([S35(j,1) S35(12-j,2)]);

    R352B(j,:) = ([R35(j,3) R35(12-j,4) R35(j,5) R35(12-j,6)]);
    S352B(j,:) = ([S35(j,3) S35(12-j,4) S35(j,5) S35(12-j,6)]);

    R355B(j,:) = ([R35(j,7) R35(12-j,8) R35(j,9) R35(12-j,10)]);
    S355B(j,:) = ([S35(j,7) S35(12-j,8) S35(j,9) S35(12-j,10)]);

    R3510B(j,:) = ([R35(j,11) R35(12-j,12) R35(j,13) R35(12-j,14)]);
    S3510B(j,:) = ([S35(j,11) S35(12-j,12) S35(j,13) S35(12-j,14)]);

    R350B(j,:) = ([R35(j,15) R35(12-j,16) R35(j,17) R35(12-j,18)]);
    S350B(j,:) = ([S35(j,15) S35(12-j,16) S35(j,17) S35(12-j,18)]);


    %pure
    RpB(j,:) = ([Rpu(j,1) Rpu(12-j,2) Rpu(j,3) Rpu(12-j,4)]);
    SpB(j,:) = ([Spu(j,1) Spu(12-j) Spu(j,3) Spu(12-j,4)]);

    %%%ERROR CALCULATION
upS100B(j) = max(S100B(j,:))-mean(S100B(j,:));
lowS100B(j) = mean(S100B(j,:))-min(S100B(j,:));
stdS100B(j) = std(S100B(j,:));

upS101B(j) = max(S101B(j,:))-mean(S101B(j,:));
lowS101B(j) = mean(S101B(j,:))-min(S101B(j,:));
stdS101B(j) = std(S101B(j,:));

upS102B(j) = max(S102B(j,:))-mean(S102B(j,:));
lowS102B(j) = mean(S102B(j,:))-min(S102B(j,:));
stdS102B(j) = std(S102B(j,:));

upS105B(j) = max(S105B(j,:))-mean(S105B(j,:));
lowS105B(j) = mean(S105B(j,:))-min(S105B(j,:));
stdS105B(j) = std(S105B(j,:));

upS1010B(j) = max(S1010B(j,:))-mean(S1010B(j,:));
lowS1010B(j) = mean(S1010B(j,:))-min(S1010B(j,:));
stdS1010B(j) = std(S1010B(j,:));
%wt35

upS350B(j) = max(S350B(j,:))-mean(S350B(j,:));
lowS350B(j) = mean(S350B(j,:))-min(S350B(j,:));
stdS350B(j) = std(S350B(j,:));

upS351B(j) = max(S351B(j,:))-mean(S351B(j,:));
lowS351B(j) = mean(S351B(j,:))-min(S351B(j,:));
stdS351B(j) = std(S351B(j,:));

upS352B(j) = max(S352B(j,:))-mean(S352B(j,:));
lowS352B(j) = mean(S352B(j,:))-min(S352B(j,:));
stdS352B(j) = std(S352B(j,:));

upS355B(j) = max(S355B(j,:))-mean(S355B(j,:));
lowS355B(j) = mean(S355B(j,:))-min(S355B(j,:));
stdS355B(j) = std(S355B(j,:));

upS3510B(j) = max(S3510B(j,:))-mean(S3510B(j,:));
lowS3510B(j) = mean(S3510B(j,:))-min(S3510B(j,:));
stdS3510B(j) = std(S3510B(j,:));

upSpB(j) = max(SpB(j,:))-mean(SpB(j,:));
lowSpB(j) = mean(SpB(j,:))-min(SpB(j,:));
stdSpB(j) = std(SpB(j,:));
end


% figure(8);
```

```
% hold on;
% plot(R100,S100,'y')
% plot(R101,S101,'k')
% plot(R102,S102,'r')
% plot(R105,S105,'g')
% plot(R1010,S1010,'b')
%     ylabel('Viscosity in [mPa s]');
%     xlabel('Shear rate in [1/s]');
%
% legend('10%wt 0 minute grinding','10%wt 1 minute grinding','10%wt 2 minutes grinding','10%wt 5
minutes grinding','10%wt 10 minutes grinding');

for j=1:11
    for i=1:10
        %10wt%
    RRA10(j,i) = R10(j,i*2-1);
    RRB10(j,i) = R10(j,i*2);

    SSA10(j,i) = S10(j,i*2-1);
    SSB10(j,i) = S10(j,i*2);

    end
    %10 wt%
    RA10(j) = mean(RRA10(j,:));
    RB10(j) = mean(RRB10(j,:));
    dRA10(j,:) = (RRA10(j,:));
    dRB10(j,:) = (RRB10(j,:));

    SA10(j) = mean(SSA10(j,:));
    SB10(j) = mean(SSB10(j,:));
    dSA10(j,:) = (SSA10(j,:));
    dSB10(j,:) = (SSB10(j,:));
end

clear i;
clear j;

for j=1:11
    for i=1:9

%35wt%
    RRA35(j,i) = R35(j,i*2-1);
    RRB35(j,i) = R35(j,i*2);


    SSA35(j,i) = S35(j,i*2-1);
    SSB35(j,i) = S35(j,i*2);
    end

     %35 wt%
    RA35(j) = mean(RRA35(j,:));
    RB35(j) = mean(RRB35(j,:));
    dRA35(j,:) = (RRA35(j,:));
    dRB35(j,:) = (RRB35(j,:));

    SA35(j) = mean(SSA35(j,:));
    SB35(j) = mean(SSB35(j,:));
    dSA35(j,:) = (SSA35(j,:));
    dSB35(j,:) = (SSB35(j,:));
end
clear i;
clear j;

for j=1:11
    for i=1:2
        %Pure urea
    RRApu(j,i) = Rpu(j,i*2-1);
    RRBpu(j,i) = Rpu(j,i*2);

    SSApu(j,i) = Spu(j,i*2-1);
    SSBpu(j,i) = Spu(j,i*2);

    end
    %Pure urea
```

```
    RApu(j) = mean(RRApu(j,:));
    RBpu(j) = mean(RRBpu(j,:));
    dRApu(j,:) = (RRApu(j,:));
    dRBpu(j,:) = (RRBpu(j,:));

    SApu(j) = mean(SSApu(j,:));
    SBpu(j) = mean(SSBpu(j,:));
    dSApu(j,:) = (SSApu(j,:));
    dSBpu(j,:) = (SSBpu(j,:));

end


for j=1:11
S35_fin(j) = mean([SA35(j) SB35(12-j)]);
R35_fin(j) = mean([RA35(j) RB35(12-j)]);
dS35_fin(j) = std([dSA35(j) dSB35(12-j)]);

S10_fin(j) = mean([SA10(j) SB10(12-j)]);
R10_fin(j) = mean([RA10(j) RB10(12-j)]);
dS10_fin(j) = std([dSA10(j) dSB10(12-j)]);

Spu_fin(j) = mean([SApu(j) SBpu(12-j)]);
Rpu_fin(j) = mean([RApu(j) RBpu(12-j)]);
dSpu_fin(j) = std([dSApu(j) dSBpu(12-j)]);
end

%%%%%Start extrapolating values to shear rate of 0/s
ex = logspace(0,2,13);

ex35 = interp1(R35_fin,S35_fin,ex,'spline','extrap');
ex10 = interp1(R10_fin,S10_fin,ex,'spline','extrap');
ex0 = interp1(Rpu_fin,Spu_fin,ex,'linear','extrap');

ex100 = interp1(R100A,S100A,ex,'spline','extrap');
ex101 = interp1(R101A,S101A,ex,'spline','extrap');
ex102 = interp1(R102A,S102A,ex,'spline','extrap');
ex105 = interp1(R105A,S105A,ex,'spline','extrap');
ex1010 = interp1(R1010A,S1010A,ex,'spline','extrap');

ex350 = interp1(R350A,S350A,ex,'spline','extrap');
ex351 = interp1(R351A,S351A,ex,'spline','extrap');
ex352 = interp1(R352A,S352A,ex,'spline','extrap');
ex355 = interp1(R355A,S355A,ex,'spline','extrap');
ex3510 = interp1(R3510A,S3510A,ex,'spline','extrap');
%%%%%End of extrapolating

    figure(1);
 hold on;

    %loglog(R35_fin,S35_fin,'b',R10_fin,S10_fin,'r',Rpu_fin,Spu_fin,'k');
errorbar(R35_fin,S35_fin,dS35_fin,'b');
errorbar(R10_fin,S10_fin,dS10_fin,'r');
errorbar(Rpu_fin,Spu_fin,dSpu_fin,'k');
    set(gca,'XScale','log', 'YScale','log');
    %loglog(R10_fin,S10_fin,'r');
    %loglog(Rpu_fin,Spu_fin,'k');
    %loglog(ex,ex10,'r.');
    %loglog(ex,ex35,'b.');
    %loglog(ex,ex0,'k.');

    ylabel('Viscosity in [mPa s]');
    xlabel('Shear rate in [1/s]');


    figure(2);
    subplot(2,1,1);
    loglog(R100A,S100A,'k.',R101A,S101A, 'k', R102A,S102A, 'r', R105A,S105A, 'g',R1010A,S1010A, 'b');
    legend('10%wt 0 minute grinding','10%wt 1 minute grinding','10%wt 2 minutes grinding','10%wt 5
minutes grinding','10%wt 10 minutes grinding');
%     ;
%     loglog(ex,ex100,'k--',ex,ex101, 'k*',ex,ex102, 'r*',ex,ex105, 'g*',ex,ex1010, 'b*');
    ylabel('Viscosity in [mPa s]');
    xlabel('Shear rate in [1/s]');
```

```
    subplot(2,1,2);
    loglog(R350A,S350A, 'k.', R351A,S351A, 'k', R352A,S352A, 'r', R355A,S355A, 'g',R3510A,S3510A, 'b')
    legend('35%wt not grinded','35%wt 1 minute grinding','35%wt 2 minutes grinding','35%wt 5 minutes
grinding','35%wt 10 minutes grinding');
    ylabel('Viscosity in [mPa s]');
    xlabel('Shear rate in [1/s]');

%     ;
%     loglog(ex,ex350,'k--',ex,ex351, 'k*',ex,ex352, 'r*',ex,ex355, 'g*',ex,ex3510, 'b*');
%
%%%%%%%%%%%Vergelijk verschillende percentages met elkaar

for j=1:11
    R1min(j) = mean([R101A(j); R351A(j)]);      %1minute
    S1min(j) = mean([S101A(j); S351A(j)]);

    R2min(j) = mean([R102A(j); R352A(j)]);
    S2min(j) = mean([S102A(j); S352A(j)]);

    R5min(j) = mean([R105A(j); R355A(j)]);
    S5min(j) = mean([S105A(j); S355A(j)]);

    R10min(j) = mean([R1010A(j); R3510A(j)]);
    S10min(j) = mean([S1010A(j); S3510A(j)]);

    R0min(j) = mean([R100A(j); R350A(j)]);
    S0min(j) = mean([S100A(j); S350A(j)]);

end
%%%%%Extrapolate
ex0min = interp1(R0min,S0min,ex,'spline','extrap');
ex1min = interp1(R1min,S1min,ex,'spline','extrap');
ex2min = interp1(R2min,S2min,ex,'spline','extrap');
ex5min = interp1(R5min,S5min,ex,'spline','extrap');
ex10min = interp1(R10min,S10min,ex,'spline','extrap');
%%%%%END


figure(3);

plot(R0min,S0min,'k.',R1min,S1min,'k',R2min,S2min,'r',R5min,S5min,'b',R10min,S10min,'g');
%set(gca,'YScale','log');

legend('Not grinded','1 minute grinding', '2 minutes grinding', '5 minutes grinding', '10 minutes
grinding');
    ylabel('Viscosity in [mPa s]');
    xlabel('Shear rate in [1/s]');
title('Comparison between grinded P4 in urea suspensions (combined 10wt% and 35wt%)');
%loglog(R1min,S1min,'k')
%loglog(R2min,S2min,'r')
%loglog(R5min,S5min,'b')
%loglog(R10min,S10min,'g')
set(gca, 'XScale', 'log', 'YScale', 'log');
% loglog(ex,ex0min,'k--',ex,ex1min,'k*',ex,ex2min,'r*', ex,ex5min, 'b*', ex,ex10min,'g*');

%%%%%%%%%%%%%%%%%%%%%%%%%%%%%%%%%%%%%%%%%%%%%%%%%%%%%%%%%%%%%%%%%%%%%%%%%%%%%%%
%%Calculate Einstein viscosity – check if correct

mu_p = mean(Spu_fin);

xa1 = 0.35;  %wt% of P4 in urea in sample 1 and 2
xa2 = 0.1;

rho_p4      = 2790; %density of P4
rho_s       = 1335; %density of urea
rho_l       = 1247; %density of liquid urea.

rhotot35 = xa1*rho_p4+(1-xa1)*rho_s;
rhotot10 = xa2*rho_p4+(1-xa2)*rho_s;
rho_max = 1/(0.63*(1/rho_p4-1/rho_s)+1/rho_s);

x1 = (1/rhotot35-1/rho_s)/(1/rho_p4-1/rho_s);
```

```
x2 = (1/rhotot10-1/rho_s)/(1/rho_p4-1/rho_s);
xamax = (rho_max-rho_s)/(rho_p4-rho_s);

mu_einstein10 = mu_p*(1+2.5*x2);
mu_einstein35 = mu_p*(1+2.5*x1);

%Ostwald-de Waele viscosity,
%https://www.cae.tntech.edu/~jbiernacki/CHE%204410%202018/HTL%20References/Viscosity%20of%20suspensions
.pdf
%page 6
%https://wiki.anton-paar.com/nl-en/the-influence-of-particles-on-suspension-
rheology/#:~:text=%CE%A6max%20is%20the%20maximum,shape%20(2.5%20for%20spheres).&text=Assuming%20spheric
al%20particles%2C%20the%20theoretical,stacking%20scheme%20(Figure%202).

%K10 = ex10(1);
%K35 = ex35(1);

%n35 = mean((log(S35_fin)-log(K35))./log(R35_fin)+1);
%n10 = mean((log(S10_fin)-log(K10))./log(R10_fin)+1);


fit35 = fit(R35_fin(1:end-4)',S35_fin(1:end-4)','power1');
fit10 = fit(R10_fin(1:end-4)',S10_fin(1:end-4)','power1');

K10 = 5.5097; %79.77; %
K35 = 96.5; %67.9; %

n10 = 1.2786; %0.4658; %
n35 = 0.4933; %0.6292; %

%XX = logspace(1,100,20);
XX = ex;
%Predict viscosity with Ostwald-de Waele viscosity
mu35OW = K35.*(XX).^(n35-1);
mu10OW = K10.*(XX).^(n10-1);



figure(1)
hold on;
loglog(XX,mu35OW,'b*',XX,mu10OW,'r*');
set(gca, 'XScale', 'log', 'YScale', 'log');
loglog(ex,ex0, 'k.')
legend('UR+35wt% P4','UR+10wt% P4',  'Pure UR','Ostwald-de Waele fit wt35%','Ostwald-de Waele fit
wt10%', 'Fit of pure urea')
xlim([10 100]);
%De viscosity met name bij wt10% verschilt flink tussen de extrapoleerde
%waardes en de Ostwald-de Waele bepaalde waardes. Zou door lage shear rate
%hier Brownian motion van invloed op zijn? Die is wel aanwezig volgens Emma
%bij T=140 graden Celsius. Viscosity of pure urea = 3.09 mPa at 140 degC.
hold off;


vis = [Spu_fin(4) S10_fin(4) S35_fin(4)];
co = [0 0.1882 0.5295];
R10_fin(4);
stdvis = [dSpu_fin(4) dS10_fin(4) dS35_fin(4)];

std35 = [stdS350B' stdS351B' stdS352B' stdS355B' stdS3510B']; %standard deviations of grinding graphs
std10 = [stdS100B' stdS101B' stdS102B' stdS105B' stdS1010B'];


%%%%%%%%%%%%%%%%%%%%%%%%%%%%%%%%%%%%%%%%%%%%%%%%%%%%%%%%%%%%%%%%%%%%%%%%%%%%%%%
%%%Mag Brownian motion gebruikt worden?

d = 5.85e-6 ; %5.85e-6; %Diameter particles.
kb = 1.38e-23; %Boltzmann constant
T = 140+273;

Pe = 3*pi*mu_p/1000*d^3*1/(4*kb*T);
Re = rho_l*d^2*1/(4*mu_p/1000);
% tr = t*k*T/(mu*a^3)
Sc = Pe/Re;
```

```
B = 1.5;
phi_m = 0.63;
mu_eiler35 = mu_p*(1+B*x1/(1-x1/phi_m))^2;
mu_eiler10 = mu_p*(1+B*x2/(1-x2/phi_m))^2;

figure(1);
figure(2);
figure(3);
figure(4);
errorbar(co,vis,stdvis,'k-.');
% hold on;
% errorbar([0 co(3)],[vis(1) vis(3)],[stdvis(1) stdvis(3)],'r')
xlabel('P4 volume fraction in urea');
ylabel('Viscosity in [mPa s]');
title('The influence of P4 volume fraction on the viscosity of the suspension')

figure(5);
subplot(2,1,1);
XXX = [0.01 1 2 5 10];
co1 = [S350A(4) S351A(4) S352A(4) S355A(4) S3510A(4)];
errorbar(XXX,co1,std35(4,:), 'r*');
xlabel('Grinding time in [minutes]')
ylabel('Viscosity in [mPa s]');
title('Grinding time vs viscosity of UR+35wt%P4');
hold on;
pfit = fit(XXX',co1', 'power1');
co1b = 21.52.*XXX.^0.01533;
plot(XXX,co1b);
hold off;


subplot(2,1,2);
hold on;
XXX = [0.01 1 2 5 10];
co2 = [S100A(4) S101A(4) S102A(4) S105A(4) S1010A(4)];
errorbar(XXX,co2,std10(4,:),'r*');
xlabel('Grinding time in [minutes]')
ylabel('Viscosity in [mPa s]');
title('Grinding time vs viscosity of UR+10wt%P4');
%pfit2 = polyfit(XXX,co2,3);
pfit2 = fit([XXX(1:3) XXX(4:5)]',[co2(1:3) co2(4:5)]','power1');
co2b = 14.99.*XXX.^0.1403;
plot(XXX,co2b)

%% plot figure 6
 figure(6);
 subplot(3,2,1)
 hold on;
 errorbar(Rpu_fin,Spu_fin,stdSpB, 'k');
 errorbar(R100A,S100A,stdS100B,'r');
 errorbar(R350A,S350A,stdS350B, 'b');
    legend('Pure urea','UR+10%wt 1 minute grinding','UR+35%wt 1 minute grinding');
    ylabel('Viscosity in [mPa s]');
    xlabel('Shear rate in [1/s]');
    title('UR+0 minute grinding P4');
set(gca, 'XScale', 'log', 'YScale', 'log');
ylim([0 100]);

%%%%plot 1 minute

 subplot(3,2,2)
 hold on;
 errorbar(Rpu_fin,Spu_fin,stdSpB, 'k');
 errorbar(R101A,S101A,stdS101B,'r');
 errorbar(R351A,S351A,stdS351B, 'b');

    legend('Pure urea','UR+10%wt 1 minute grinding','UR+35%wt 1 minute grinding');
    ylabel('Viscosity in [mPa s]');
    xlabel('Shear rate in [1/s]');
    title('UR+1 minute grinding P4');
set(gca, 'XScale', 'log', 'YScale', 'log');
ylim([0 100]);
%%%%plot 2 minute
```

```
 subplot(3,2,3)
 hold on;
 errorbar(Rpu_fin,Spu_fin,stdSpB, 'k');
 errorbar(R102A,S102A,stdS102B,'r');
 errorbar(R352A,S352A,stdS352B, 'b');

    legend('Pure urea','UR+10%wt 2 minute grinding','UR+35%wt 2 minute grinding');
    ylabel('Viscosity in [mPa s]');
    xlabel('Shear rate in [1/s]');
    title('UR+2 minute grinding P4');
set(gca, 'XScale', 'log', 'YScale', 'log');
ylim([0 100]);
%%%%plot 5 minute

 subplot(3,2,4)
 hold on;
 errorbar(Rpu_fin,Spu_fin,stdSpB, 'k');
 errorbar(R105A,S105A,stdS105B,'r');
 errorbar(R355A,S355A,stdS355B, 'b');

    legend('Pure urea','UR+10%wt 5 minute grinding','UR+35%wt 5 minute grinding');
    ylabel('Viscosity in [mPa s]');
    xlabel('Shear rate in [1/s]');
    title('UR+5 minute grinding P4');
set(gca, 'XScale', 'log', 'YScale', 'log');
ylim([0 100]);
%%%%plot 10 minute
 subplot(3,2,5)
 hold on;
 errorbar(Rpu_fin,Spu_fin,stdSpB, 'k');
 errorbar(R1010A,S1010A,stdS1010B,'r');
 errorbar(R3510A,S3510A,stdS3510B, 'b');

    legend('Pure urea','UR+10%wt 10 minute grinding','UR+35%wt 10 minute grinding');
    ylabel('Viscosity in [mPa s]');
    xlabel('Shear rate in [1/s]');
    title('UR+10 minute grinding P4');
set(gca, 'XScale', 'log', 'YScale', 'log');
ylim([0 100]);

%% Figure 7
figure(7);
subplot(2,1,1);
psize = [8.497 4.732 5.407 5.851 5.854];
co1 = [S350A(4) S351A(4) S352A(4) S355A(4) S3510A(4)];
pstd = [8.0462 3.1014 4.3809 4.4482 4.4289];
errorbar(psize,co1,std35(4,:),std35(4,:), pstd, pstd, 'b*');
xlabel('Particle size in [micron]')
ylabel('Viscosity in [mPa s]');
title('Particle size vs viscosity of UR+35wt%P4');


subplot(2,1,2);
hold on;
co2 = [S100A(4) S101A(4) S102A(4) S105A(4) S1010A(4)];
errorbar(psize,co2,std10(4,:),std10(4,:), pstd, pstd,'b*');
xlabel('Particle size in [micron]')
ylabel('Viscosity in [mPa s]');
title('Particle size vs viscosity of UR+10wt%P4');


%% calculate difference

D350 = S350A(1)-S350A(end);
D351 = S351A(1)-S351A(end);
D352 = S352A(1)-S352A(end);
D355 = S355A(1)-S355A(end);
D3510 = S3510A(1)-S3510A(end);

D100 = S100A(1)-S100A(end);
D101 = S101A(1)-S101A(end);
D102 = S102A(1)-S102A(end);
D105 = S105A(1)-S105A(end);
D1010 = S1010A(1)-S1010A(end);
```

```
disp(['Delta viscosity 0min grind 35wt%   ', num2str(D350), ' mPa s']);
disp(['Delta viscosity 1min grind 35wt%   ', num2str(D351), ' mPa s']);
disp(['Delta viscosity 2min grind 35wt%   ', num2str(D352), ' mPa s']);
disp(['Delta viscosity 5min grind 35wt%   ', num2str(D355), ' mPa s']);
disp(['Delta viscosity 10min grind 35wt%   ', num2str(D3510), ' mPa s']);
disp('.................')
disp(['Delta viscosity 0min grind 10wt%   ', num2str(D100), ' mPa s']);
disp(['Delta viscosity 1min grind 10wt%   ', num2str(D101), ' mPa s']);
disp(['Delta viscosity 2min grind 10wt%   ', num2str(D102), ' mPa s']);
disp(['Delta viscosity 5min grind 10wt%   ', num2str(D105), ' mPa s']);
disp(['Delta viscosity 10min grind 10wt%   ', num2str(D1010), ' mPa s']);
disp('_____________________________________________________________________')
```

F.4 Data processing of the prillsizes

```
close all;
clear all;

UR          = readmatrix('Results_pure_urea_sizefoto');
wt10ng      = readmatrix('Results_UR10wtP4_notgrinded');
wt35ng      = readmatrix('Results_P4wt35_notgrinded');
wt10gr      = readmatrix('Results_P4wt10_10minutes');
wt35gr      = readmatrix('Results_P4wt35_10minutes');

w10ng       = readmatrix('Results_Urea+P4wt10%_notgrinded_shape');
w10gr       = readmatrix('Results_P4wt10_10minutes_shape');
w35ng       = readmatrix('Results_Urea+P4wt35%_notgrinded_shape');
w35gr       = readmatrix('Results_P4wt35_10minutes_shape');
ur2         = readmatrix('Results_pure_urea_shape');

A = 10;
B = 0.15; %Binsize
C = 0.01; %Binsize

ro10ng = w10ng(2:end,8); %Roundness
ro10gr = w10gr(2:end,8);
ro35ng = w35ng(2:end,8);
ro35gr = w35gr(2:end,8);
rour   = ur2(2:end,8);

ci10ng = mean(w10ng(2:end,6));
ci10gr = mean(w10gr(2:end,6));
ci35ng = mean(w35ng(2:end,6));
ci35gr = mean(w35gr(2:end,6));
ciur   = mean(ur2(2:end,6));


D_ur        = UR(2:end,11); %Diameter
D_wt10ng  = wt10ng(2:end,11);
D_wt35ng  = wt35ng(2:end,11);
D_wt10gr  = wt10gr(2:end,11);
D_wt35gr  = wt35gr(2:end,11);

sat_ur      = length(find(UR(2:end,11)<1.75))/length(UR(2:end,11));   %Find amount of satellite
droplets
sat_wt10ng  = length(find(wt10ng(2:end,11)<1.75))/length(wt10ng(2:end,11));
sat_wt35ng  = length(find(wt35ng(2:end,11)<1.75))/length(wt35ng(2:end,11));
sat_wt10gr  = length(find(wt10gr(2:end,11)<1.75))/length(wt10gr(2:end,11));
sat_wt35gr  = length(find(wt35gr(2:end,11)<1.75))/length(wt35gr(2:end,11));

ur_mean       = mean(D_ur);         %Mean prillsize all prills
wt10ng_mean   = mean(D_wt10ng);
wt35ng_mean   = mean(D_wt35ng);
wt10gr_mean   = mean(D_wt10gr);
wt35gr_mean   = mean(D_wt35gr);

ur_mean1       = mean(D_ur(find(D_ur>1.75)));           %Mean prillsize without satellite droplets
wt10ng_mean1   = mean(D_wt10ng(find(D_wt10ng>1.75)));
wt35ng_mean1   = mean(D_wt35ng(find(D_wt35ng>1.75)));
wt10gr_mean1   = mean(D_wt10gr(find(D_wt10gr>1.75)));
wt35gr_mean1   = mean(D_wt35gr(find(D_wt35gr>1.75)));

ur_mean2       = mean(D_ur(find(D_ur<1.75)));           %Mean satellite droplet size
wt10ng_mean2   = mean(D_wt10ng(find(D_wt10ng<1.75)));
wt35ng_mean2   = mean(D_wt35ng(find(D_wt35ng<1.75)));
wt10gr_mean2   = mean(D_wt10gr(find(D_wt10gr<1.75)));
wt35gr_mean2   = mean(D_wt35gr(find(D_wt35gr<1.75)));

ur_max       = max(D_ur);
wt10ng_max   = max(D_wt10ng);
wt35ng_max   = max(D_wt35ng);
wt10gr_max   = max(D_wt10gr);
wt35gr_max   = max(D_wt35gr);

ur_min       = min(D_ur);
wt10ng_min   = min(D_wt10ng);
wt35ng_min   = min(D_wt35ng);
```

```
wt10gr_min    = min(D_wt10gr);
wt35gr_min    = min(D_wt35gr);

ur_std        = std(D_ur);
wt10ng_std    = std(D_wt10ng);
wt35ng_std    = std(D_wt35ng);
wt10gr_std    = std(D_wt10gr);
wt35gr_std    = std(D_wt35gr);

ur_std1        = std(D_ur(find(D_ur>1.75)));           %Mean prillsize without satellite droplets
wt10ng_std1    = std(D_wt10ng(find(D_wt10ng>1.75)));
wt35ng_std1    = std(D_wt35ng(find(D_wt35ng>1.75)));
wt10gr_std1    = std(D_wt10gr(find(D_wt10gr>1.75)));
wt35gr_std1    = std(D_wt35gr(find(D_wt35gr>1.75)));


figure(1);


subplot(5,1,1);
h1 = histogram(D_ur,A, 'Normalization','probability');
xlim([0,5.5]);
ylim([0,0.2]);
title('Prillsizes of pure UR in [mm]');
h1.BinWidth = B;
ylabel('Occurrence');

subplot(5,1,2);
h2 = histogram(D_wt10ng,A, 'Normalization','probability');
xlim([0,5.5]);
ylim([0,0.2]);
title('Prillsizes of UR+10wt%P4 in [mm]');
h2.BinWidth = B;
ylabel('Occurrence');

subplot(5,1,3);
h3 = histogram(D_wt35ng,A, 'Normalization','probability');
xlim([0,5.5]);
ylim([0,0.2]);
xlabel('Prillsize in [mm]');
title('Prillsizes of UR+35wt%P4 in [mm]');
h3.BinWidth = B;
ylabel('Occurrence');

subplot(5,1,4);
h4 = histogram(D_wt10gr,A, 'Normalization','probability');
xlim([0,5.5]);
ylim([0,0.2]);
title('Prillsizes of UR+10wt%P4 10min grind in [mm]');
h4.BinWidth = B;
ylabel('Occurrence');

subplot(5,1,5);
h5 = histogram(D_wt35gr,A, 'Normalization','probability');
xlim([0,5.5]);
ylim([0,0.2]);
xlabel('Prillsize in [mm]');
title('Prillsizes of UR+35wt%P4 10min grind in [mm]');
h5.BinWidth = B;
ylabel('Occurrence');

%%%%%Roundness plot
figure(2)
subplot(5,1,1);
hh1 = histogram(rour,A, 'Normalization','probability');
xlim([0.8,1]);
ylim([0,0.3]);
xlabel('Roundness');
title('Roundness of pure urea prills');
hh1.BinWidth = C;
ylabel('Occurrence');

subplot(5,1,2);
hh2 = histogram(ro10ng,A, 'Normalization','probability');
```

```
xlim([0.8,1]);
ylim([0,0.3]);
xlabel('Roundness');
title('Roundness of UR+10wt%P4 not grinded prills');
hh2.BinWidth = C;
ylabel('Occurrence');

subplot(5,1,3);
hh3 = histogram(ro35ng,A, 'Normalization','probability');
xlim([0.8,1]);
ylim([0,0.3]);
xlabel('Roundness');
title('Roundness of UR+35wt%P4 not grinded prills');
hh3.BinWidth = C;
ylabel('Occurrence');

subplot(5,1,4);
hh4 = histogram(ro10gr,A, 'Normalization','probability');
xlim([0.8,1]);
ylim([0,0.3]);
xlabel('Roundness');
title('Roundness of UR+10wt%P4 grinded prills');
hh4.BinWidth = C;
ylabel('Occurrence');

subplot(5,1,5);
hh5 = histogram(ro35gr,A, 'Normalization','probability');
xlim([0.8,1]);
ylim([0,0.3]);
xlabel('Roundness');
title('Roundness of UR+35wt%P4 grinded prills');
hh5.BinWidth = C;
ylabel('Occurrence');
%%%%%%%%%%%%%%%%%%%%%%%%PRINT%%%%%%%%%%%%%%%%%%%%
disp(['Mean pure urea    ', num2str(ur_mean), ' mm']);
disp(['Mean UR+10wt%P4   ', num2str(wt10ng_mean), ' mm']);
disp(['Mean UR+35wt%P4   ', num2str(wt35ng_mean), ' mm']);
disp(['Mean UR+10wt%P4 10min   ', num2str(wt10gr_mean), ' mm']);
disp(['Mean UR+35wt%P4 10min   ', num2str(wt35gr_mean), ' mm']);
disp('----------------');
disp(['Mean sat pure urea    ', num2str(ur_mean2), ' mm']);
disp(['Mean sat UR+10wt%P4   ', num2str(wt10ng_mean2), ' mm']);
disp(['Mean sat UR+35wt%P4   ', num2str(wt35ng_mean2), ' mm']);
disp(['Mean sat UR+10wt%P4 10min   ', num2str(wt10gr_mean2), ' mm']);
disp(['Mean sat UR+35wt%P4 10min   ', num2str(wt35gr_mean2), ' mm']);
disp('----------------');
disp(['Mean prill sat pure urea ', num2str(ur_mean1), ' mm']);
disp(['Mean prill UR+10wt%P4    ', num2str(wt10ng_mean1), ' mm']);
disp(['Mean prill UR+35wt%P4    ', num2str(wt35ng_mean1), ' mm']);
disp(['Mean prill UR+10wt%P4 10min   ', num2str(wt10gr_mean1), ' mm']);
disp(['Mean prill UR+35wt%P4 10min   ', num2str(wt35gr_mean1), ' mm']);
disp('----------------');
disp(['STD pure urea    ', num2str(ur_std), ' mm']);         %Standard Deviation
disp(['STD UR+10wt%P4   ', num2str(wt10ng_std), ' mm']);
disp(['STD UR+35wt%P4   ', num2str(wt35ng_std), ' mm']);
disp(['STD UR+10wt%P4 10min  ', num2str(wt10gr_std), ' mm']);
disp(['STD UR+35wt%P4 10min  ', num2str(wt35gr_std), ' mm']);
disp('----------------');
disp(['STD prill pure urea    ', num2str(ur_std1), ' mm']);         %Standard Deviation
disp(['STD prill UR+10wt%P4   ', num2str(wt10ng_std1), ' mm']);
disp(['STD prill UR+35wt%P4   ', num2str(wt35ng_std1), ' mm']);
disp(['STD prill UR+10wt%P4 10min  ', num2str(wt10gr_std1), ' mm']);
disp(['STD prill UR+35wt%P4 10min  ', num2str(wt35gr_std1), ' mm']);

disp('----------------');
disp(['Mean roundness pure urea    ', num2str(mean(rour)), ' ']);         %Standard Deviation
disp(['Mean roundness UR+10wt%P4   ', num2str(mean(ro10ng)), ' ']);
disp(['Mean roundness UR+35wt%P4   ', num2str(mean(ro35ng)), ' ']);
disp(['Mean roundness UR+10wt%P4 10min  ', num2str(mean(ro10gr)), ' ']);
disp(['Mean roundness UR+35wt%P4 10min  ', num2str(mean(ro35gr)), ' ']);
disp('----------------');
disp(['Mean circularity pure urea    ', num2str(ciur), ' ']);         %Standard Deviation
disp(['Mean circularity UR+10wt%P4   ', num2str(ci10ng), ' ']);
disp(['Mean circularity UR+35wt%P4   ', num2str(ci35ng), ' ']);
```

```
disp([‘Mean circularity UR+10wt%P4 10min  ‘, num2str(ci10gr), ‘ ‘]);
disp([‘Mean circularity UR+35wt%P4 10min  ‘, num2str(ci35gr), ‘ ‘]);
disp(‘----------------');
disp([‘Sat droplets urea         ‘, num2str(sat_ur*100), ‘% ‘]);         %Standard Deviation
disp([‘Sat droplets UR+10wt%P4   ‘, num2str(sat_wt10ng*100), ‘% ‘]);
disp([‘Sat droplets UR+35wt%P4   ‘, num2str(sat_wt35ng*100), ‘% ‘]);
disp([‘Sat droplets UR+10wt%P4 10min  ‘, num2str(sat_wt10gr*100), ‘% ‘]);
disp([‘Sat droplets UR+35wt%P4 10min  ‘, num2str(sat_wt35gr*100), ‘% ‘]);
disp(‘_____________________________________________’);
```

F.5 Data processing of the prillmass and P4 wt% estimate.

```
clear all;
close all;


ur          = readmatrix('Pure_urea.xlsx');
wt10_grind  = readmatrix('Urea+P4wt10%_10minutesground.xlsx');
wt35_grind  = readmatrix('Urea+P4wt35%_10minutesground');
wt10_ng   = readmatrix('Urea+P4wt10%_notgrinded.xlsx');
wt35_ng   = readmatrix('Urea+P4wt35%_notgrinded.xlsx');


A = 10;

rho_ur = ur(23:42,3);
diff_ur = ur(23:42,5);

rho_wt10grind = wt10_grind(:,3);
diff_wt10grind = wt10_grind(:,6);
wt10gr = wt10_grind(:,8);

rho_wt35grind = wt35_grind(:,3);
diff_wt35grind = wt35_grind(:,6);
wt35gr = wt35_grind(:,8);

%no grind
rho_wt10ng = wt10_ng(:,3);
diff_wt10ng = wt10_ng(:,6);
wt10ng = wt10_ng(:,8);

rho_wt35ng = wt35_ng(:,3);
diff_wt35ng = wt35_ng(:,6);
wt35ng = wt35_ng(:,8);

%total
wt35 = [wt35ng(2:end); wt35gr(2:end)];
wt10 = [wt10ng(2:end); wt10gr(2:end)];

%average wt% P4
P4_wt10ng = wt10_ng(10,12);
P4_wt35ng = wt35_ng(10,12);
P4_wt10gr = wt10_grind(10,12);
P4_wt35gr = wt35_grind(10,12);

%%%%%%%%PLOT mass difference
figure;
subplot(5,1,1);
ha = histogram(diff_ur*100,A, 'Normalization','probability');
xlim([-30 25]);
ylim([0 0.35]);
xtickformat('percentage')
title('Difference measured density vs expected density of pure urea')
ylabel('Probability');
xlabel('Difference between measured-expected in rho%');
ha.BinWidth = 2.5;

subplot(5,1,2);
hb =histogram(diff_wt10grind*100,A, 'Normalization','probability');
xlim([-30 25]);
ylim([0 0.35]);
xtickformat('percentage')
title('Difference measured density vs expected density of grinded urea+wt10%P4')
ylabel('Probability');
xlabel('Difference between measured-expected in rho%');
hb.BinWidth = 2.5;

subplot(5,1,3);
hc =histogram(diff_wt10ng*100,A, 'Normalization','probability');
xlim([-30 25]);
ylim([0 0.35]);
xtickformat('percentage')
title('Difference measured density vs expected density of not grinded urea+wt10%P4')
ylabel('Probability');
```

```
xlabel('Difference between measured-expected in rho%');
hc.BinWidth = 2.5;

subplot(5,1,4);
hd =histogram(diff_wt35grind*100,A, 'Normalization','probability');
xlim([-30 25]);
ylim([0 0.35]);
xtickformat('percentage')
title('Difference measured density vs expected density of grinded urea+wt35%P4')
ylabel('Probability');
xlabel('Difference between measured-expected in rho%');
hd.BinWidth = 2.5;

subplot(5,1,5);
he =histogram(diff_wt35ng*100,A, 'Normalization','probability');
xlim([-30 25]);
ylim([0 0.35]);
xtickformat('percentage')
title('Difference measured density vs expected density of not grinded urea+wt35%P4')
ylabel('Probability');
xlabel('Difference between measured-expected in rho%');
he.BinWidth = 2.5;
%%%%%%%%PLOT WT% estimate of P4

figure;
subplot(4,1,1);
h1 = histogram(wt10gr*100, 'Normalization','probability');
xlim([0 40]);
ylim([0 0.5]);
xtickformat('percentage')
title('Estimated P4 wt% in grinded urea+10wt%P4')
ylabel('Probability');
xlabel('P4 wt%');
h1.BinWidth = 2.5;


subplot(4,1,2);
h3 = histogram(wt10ng*100, 'Normalization','probability');
xlim([0 40]);
ylim([0 0.5]);
xtickformat('percentage')
title('Estimated P4 wt% in not grinded urea+10wt%P4')
ylabel('Probability');
xlabel('P4 wt%');
h3.BinWidth = 2.5;

subplot(4,1,3);
h2 = histogram(wt35gr*100, 'Normalization','probability');
xlim([0 75]);
ylim([0 0.5]);
xtickformat('percentage')
title('Estimated P4 wt% in grinded urea+35wt%P4')
ylabel('Probability');
xlabel('P4 wt%');
h2.BinWidth = 5;

subplot(4,1,4);
h4 = histogram(wt35ng*100, 'Normalization','probability');
xlim([0 75]);
ylim([0 0.5]);
xtickformat('percentage')
title('Estimated P4 wt% in not grinded urea+35wt%P4')
ylabel('Probability');
xlabel('P4 wt%');
h4.BinWidth = 5;

figure;
subplot(2,1,1);
H = histogram(wt10*100, 'Normalization','probability');
xlim([0 40]);
ylim([0 0.3]);
xtickformat('percentage')
title('Estimated P4 wt% in urea+10wt%P4')
ylabel('Probability');
```

```
xlabel('P4 wt%');
H.BinWidth = 2.5;

subplot(2,1,2);
H2 = histogram(wt35*100, 'Normalization','probability');
xlim([0 75]);
ylim([0 0.3]);
xtickformat('percentage')
title('Estimated P4 wt% in urea+35wt%P4')
ylabel('Probability');
xlabel('P4 wt%');
H2.BinWidth = 5;



%%%%%%%Display results

disp(['wt% of P4 in UR+10wt% not grinded  ', num2str(P4_wt10ng*100), '%']);
disp(['wt% of P4 in UR+10wt% grind     ', num2str(P4_wt10gr*100), '%']);
disp(['wt% of P4 in UR+35wt% not grinded  ', num2str(P4_wt35ng*100), '%']);
disp(['wt% of P4 in UR+35wt% grind     ', num2str(P4_wt35gr*100), '%']);
disp('-------');
disp(['wt% of P4 in UR+10wt%      ', num2str(mean(wt10)*100), '%']);
disp(['wt% of P4 in UR+35wt%      ', num2str(mean(wt35)*100), '%']);
disp('-------');
disp(['STD wt% of P4 in UR+10wt%      ', num2str(std(wt10)*100), '%']);
disp(['STD wt% of P4 in UR+35wt%      ', num2str(std(wt35)*100), '%']);
disp('_____________________________
```

Appendix G: Arduino script

```
/*
 * Stepper controller
 * Written to use with an arduino Nano.
 * TU Delft 3ME | G.Mulder
 */
// ======================================================================
// SETTINGS
// ======================================================================
float rev_sec =2; //     rev/sec max 50000 pulses
float revolutions = 4000  ; // set nr of revolutions

float steps_rev = 400.00;
float set_speed = steps_rev * rev_sec;
float acceleration = 200.00;
float max_speed = steps_rev * rev_sec;
float distance = (revolutions) * (steps_rev);
int incomingCharacter;

// ======================================================================
// INCLUDES
// ======================================================================
#include <AccelStepper.h>



// ============================================================
// DEFINES
// ============================================================
AccelStepper Stepper1(1, 8,9); //pin8=step, pin9=dir
int counter = 0;

void setup(){
  Serial.begin(9600); //start talking with the computer. 9600 just tells the rate.
  digitalWrite(10, HIGH);
}

// ============================================================
// LOOP
// ============================================================
void loop() {
  Stepper1.setSpeed(set_speed);
//  Stepper1.runToPosition();
  handleSerial();
}

// ============================================================
```

```
// STEPPER RUN
// ============================================================
void stepperRun(){
   Stepper1.setMinPulseWidth(20);
   Stepper1.setMaxSpeed(max_speed);
   Stepper1.setAcceleration(acceleration);
   Stepper1.move(distance);
   Stepper1.setSpeed(set_speed);
    Stepper1.runToPosition();
//    Stepper1.stop();
}

// ============================================================
// STEPPER STOP
// ============================================================
void stepperStop(){
   Stepper1.move(100);
}



// ============================================================
// HANDLE SERIAL INPUTS
// ============================================================
void handleSerial(){
     while (Serial.available() > 0) {
     int incomingCharacter = Serial.read();

     switch (incomingCharacter) {
     case 'a':
      stepperRun();
      Serial.println('a');
     break;

     case 'b':
      stepperStop();
      Serial.println('b');
     break;
   }
  }
}
```